NATIONAL OCEANOGRAPHY CENTRE, SOUTHAMPTON

INTERNAL DOCUMENT No. 1

Airflow distortion at instrument sites on the RV *Tangaroa*

B I Moat & M J Yelland

2005

James Rennell Division for Ocean Circulation and Climate
National Oceanography Centre, Southampton
University of Southampton, Waterfront Campus
European Way
Southampton
Hants SO14 3ZH
UK

Tel: +44 (0)23 8059 7739
Fax: +44 (0)23 8059 6204
Email: ben.moat@noc.soton.ac.uk

DOCUMENT DATA SHEET

AUTHOR

MOAT, B I & YELLAND, M J

PUBLICATION DATE

2005

TITLE

Airflow distortion at instrument sites on the RV *Tangaroa*.

REFERENCE

Southampton, UK: National Oceanography Centre, Southampton, 90pp.
(National Oceanography Centre Southampton Internal Document, No. 1) (Unpublished manuscript)

ABSTRACT

Accurate wind speed measurements from anemometers on research ships are required to obtain high quality air-sea flux measurements. However, the measurements can be biased by the distortion of the airflow over the ship, i.e. the wind speed can either be accelerated or decelerated by the presence of the ship. The computational fluid dynamics software VECTIS is used here to numerically simulate the airflow over the RV *Tangaroa*. The airflow distortion at ten anemometer sites has been quantified for a wind speed of 10 ms^{-1} blowing a) directly over the bows of the ship, b) from ±15 degrees and c) ±30 degrees off the bow. The wind speed errors ranged from decelerations of about 5 % at well-exposed bow locations to decelerations of close to 70 % in the turbulent wake region downwind of the ship's superstructure. Three anemometers located above the bridge top experienced wind speed increases of between 4 % and 16 % of the free stream, or undistorted, wind speed.

KEYWORDS

airflow distortion, CFD, computational fluid dynamics, RV *Tangaroa*, wind speed measurement

ISSUING ORGANISATION

National Oceanography Centre, Southampton
University of Southampton, Waterfront Campus
European Way
Southampton SO14 3ZH
UK

Airflow distortion at instrument sites on the RV Tangaroa

AIRFLOW DISTORTION AT INSTRUMENT SITES ON THE RV TANGAROA

B. I. Moat and M. J. Yelland

July 2005

1. INTRODUCTION

Ship based wind speed measurements made from anemometers can be biased by the distortion of the airflow by the presence of the ship's hull and superstructure. The computational fluid dynamics (CFD) package VECTIS (Ricardo, 2003) was used to simulate the flow of air over the RV *Tangaroa* and the wind speed bias at a number of anemometer sites was calculated. The instrument sites examined are those used during a cruise in the South Pacific (Popinet et al., 2004). Three instruments were located in positions that are used as permanent sampling sites. The remaining instruments were deliberately located in areas of high velocity gradients to provide in situ wind speed data that can be used for CFD model validation. The flow distortion at these instrument sites is examined and the wind speed errors produced.

Steady state solutions of the airflow over the ship were obtained using the Reynolds Averaged Navier-Stokes solver VECTIS. The code was run with the RNG $k \sim \varepsilon$ (Yakot et al., 1992) turbulence closure model. Three relative wind directions were modelled; flows directly over the bow (Section 2), 15° off the port bow (Section 3) and 30° off the port bow (Section 4). Effective anemometer positions were created to enable the velocity errors for winds at 15° and 30° off the starboard bow to be calculated from the two VECTIS simulations of the airflow over the port bow (Moat and Yelland, 1997). These results are included in Sections 3 and 4. All the results are summarised and discussed in Section 5. The upstream wind speed was specified as a 10 ms^{-1} uniform profile. All the surfaces of the ship's geometry and the sea surface were assigned with zero roughness, i.e. a slip boundary. All results presented in this report were normalized by the free stream wind speed at a large distance abeam of the anemometer location.

2. THE WIND SPEED ERROR FOR FLOWS AT 0° (HEAD TO WIND)

2.1 Introduction

The modelled geometry of the RV *Tangaroa* and the instrument sites are shown in Figure 1. The ship geometry was enclosed in the centre of a computational domain, or wind tunnel, 600 m in length (-300 m < x < 300 m), 300 m wide (-150 m < y < 150 m) and 150 m high (0 m < z < 150 m). The flow in the tunnel was examined to confirm that free stream conditions existed at the sides and ends of the tunnel, i.e. that the presence of the ship did not cause a significant blockage of the flow to these regions. Whilst the computational solver was running the velocities at 8 locations were monitored, 7 abeam of the ship in free stream flow and one at the Campbell 1 3D prop anemometer location. The data from these points show the solution had converged after approximately 12000 time steps with the velocities at the monitoring points constant to the 4th significant figure. The locations of the monitoring points are shown schematically in Figure 2, and Figure 3 shows the velocity data for the last 250 time steps. Once the model had converged a post-processing file was written for the extraction of the data throughout the computational volume. Illustrations of the output can be found in the Appendix and a detailed description of the data extraction procedure can be found in Moat et al. (1996).

The flow in the tunnel was examined to confirm that free stream conditions existed at the sides and ends of the tunnel, i.e. that the presence of the ship did not cause a significant blockage of the flow. Figure 4a shows the variation in the velocity along the tunnel at x=±300 m, at heights of 10, 20, 30 and 50 m on a plane at y=125 m, i.e. towards one side of the tunnel. The central section is shown in greater detail in Figure 4b, with the velocity data shown directly abeam of the ship on a plane at y=125 m and x=±50 m. The changes in velocity with height on this plane along the length of the ship are less than 0.02 ms^{-1}. This equates to less than ±0.1 % in the final calculation of the wind speed error and shows that the blockage in the tunnel is minimal. However, since the changes are not zero, the free stream velocity for a particular instrument site is estimated using the vertical profile of velocity at 125 m directly abeam of the instrument site, rather than the profiles at the inlet or outlet of the tunnel.

2.2 Anemometer locations

The positions of the instruments are shown in Figure 5. In the VECTIS co-ordinate system (where the origin is at the centre of the ship at sea level), the instrument positions are:

Cambell 1 3D prop (bow)	x = 31.43 m, y = 0.00 m, z=14.35 m
Campbell 1 cup (bow)	x = 31.94 m, y = -0.35 m, z=11.54 m
Starlogger 1 (bridge)	x = 12.91 m, y = 4.59 m, z=13.62 m
Starlogger 2 (bridge)	x = 9.26 m, y = -1.32 m, z=18.36 m
Starlogger 3 (bridge)	x = 9.62 m, y = -5.90 m, z=19.36 m
Starlogger 4 (bridge)	x = 9.71 m, y = -5.98 m, z=17.39 m
Starlogger 5 (bridge gantry)	x = -6.49 m, y = 2.70 m, z=15.64 m
Starlogger 6 (aft deck)	x = -20.03 m, y = 7.18 m, z= 8.74 m
Cambell 2 3D prop (aft gantry)	x = -28.30 m, y = 0.30 m, z=19.92 m
Cambell 2 cup (aft gantry)	x = -31.10 m, y = 1.38 m, z=19.56 m

2.3 The effect of flow distortion on wind speed for flows directly over the bow

The free stream velocities are extracted towards the edge of the tunnel at the anemometer height. The free stream flow has small, predictable gradients and can be estimated accurately at any given point on the vertical profile. In contrast, the flow at the instrument site can suffer from server distortion and large gradients in the velocity field. Additionally it is not always possible to define the mesh so that the instruments are at the exact centers of the computational cells (see Moat et al., 1996). Therefore the velocity at an instrument site is estimated from lines of data extracted in all three directions. Figures 6 to 15 show the lines of velocity data through the Campbell 1 3D prop, Campbell 1 cup, Starlogger cup anemometers 1 to 6, Campbell 2 3D prop and the Campbell 2 cup anemometers. The results of all anemometers are summarized in Table 1. The percentage wind speed error is given by:

$$\%Error = \left(\frac{Average\ velocity}{Free\ stream\ velocity} - 1 \right) \times 100 \qquad (1)$$

with a positive error indicating an acceleration of the flow.

Anemometer	Velocity from each direction (m/s)	Average velocity at anemometer site (m/s)	Free stream velocity (m/s)	% error
Campbell 1 3D prop	9.576 (x) 9.575 (y) 9.576 (z)	9.576	10.090	-5.10
Campbell 1 cup	9.424 (x) 9.430 (y) 9.430 (z)	9.438	10.080	-6.47
Starlogger 1	8.250 (x) 8.255 (y) 8.254 (z)	8.253	10.090	-18.21
Starlogger 2	11.040 (x) 11.045 (y) 11.050 (z)	11.045	10.100	9.36
Starlogger 3	10.673 (x) 10.672 (y) 10.674 (z)	10.673	10.100	5.67
Starlogger 4	10.872 (x) 10.874 (y) 10.879 (z)	10.875	10.100	7.67
Starlogger 5	3.126 (x) 3.069 (y) 3.100 (z)	3.098	10.107	-69.35
Starlogger 6	8.055 (x) 7.814 (y) 8.020 (z)	7.963	10.106	-21.21
Campbell 2 3D prop	8.480 (x) 8.448 (y) 8.590 (z)	8.506	10.111	-15.90
Campbell 2 cup	8.456 (x) 8.465 (y) 8.375 (z)	8.432	10.107	-16.57

Table 1 VECTIS velocity error estimates for the anemometers at 0° (head to wind).

An indication of the accuracy of the model and the severity of the flow distortion is also given by estimates of the gradient of the flow. Estimates of the gradient of the flow are made from Figures 6 to 15 and the rates of change for all the anemometers, per meter and per cell, are given in Table 2.

Anemometer	Velocity data line	Rate of change of velocity per meter (ms^{-1}/m)	Rate of change of velocity per cell ($ms^{-1}/cell$)
Campbell 1 3D prop	along (x) across (y) up (z)	0.030 0.001 0.040	-0.005 -0.005 0.023
Campbell 1 cup	along (x) across (y) up (z)	0.009 0.087 0.078	-0.039 0.014 0.049
Starlogger 1	along (x) across (y) up (z)	0.488 0.224 0.340	0.034 0.121 0.062
Starlogger 2	along (x) across (y) up (z)	-0.184 -0.009 -0.296	-0.062 -0.007 -0.044
Starlogger 3	along (x) across (y) up (z)	-0.178 0.036 -0.076	-0.029 0.007 -0.010
Starlogger 4	along (x) across (y) up (z)	-0.364 0.106 -0.140	-0.069 0.056 -0.015
Starlogger 5	along (x) across (y) up (z)	0.156 1.072 3.180	-0.122 -0.540 0.861
Starlogger 6	along (x) across (y) up (z)	0.018 1.576 1.494	-0.006 0.840 0.453
Campbell 2 3D prop	along (x) across (y) up (z)	-0.258 0.334 1.298	-0.172 0.3443 0.167
Campbell 2 cup	along (x) across (y) up (z)	0.043 0.960 -1.771	0.014 0.427 -0.307

Table 2 The rate of change of velocity for the anemometers at 0° (head to wind).

The rate of change of velocity per meter and per cell is low for the well-exposed Campbell 1 anemometers. The wind speeds at the Campbell 1 anemometer locations are decelerated by about 5 % of the free stream wind speed. The Starlogger 2, 3 and 4 anemometers are all located within a region of accelerated flow above the bridge top and experienced high flow distortion. The remaining Starlogger anemometers are located in regions of high flow distortion and are severely decelerated. For example, the wind speed is decelerated by 69 % of the free stream wind speed at the Starlogger 5 anemometer site. This is not unexpected as these instruments were intentionally located in regions of high velocity gradients and the results have been used for validation of the GERRIS code (Popinet et al, 2004). The Campbell 2 anemometers are located in the down wind wake of the bridge superstructure and have high rates of change in velocity at this wind direction.

2.4 Conclusions

The Campbell 1 anemometers are located in a region of low rates of change in velocity and the wind speed error range from 1 % for the Campbell 1 3D prop to -6 % for the Campbell 1 cup. The Campbell 2 anemometers located on the aft frame are positioned within the wake of the upstream superstructure and have high rates of change in velocity. The wind speed errors range from -16 % for the Campbell 2 3D prop and -17 % for the Campbell 2 cup anemometer.

The Starlogger 2, 3 and 4 anemometers are located above the front edge of the bridge and are situated in a region of low rates of change of velocity. The wind speed errors range from 9 % for the Starlogger 2, 6 % for Starlogger 3 and 8 % for the Starlogger 4 anemometers. The Starlogger 1 anemometer was located in front of the bridge and is situated in a region of high flow distortion. The wind speed error for this instrument was 1 %. The remaining Starlogger anemometers are located in the wake region of the upstream superstructure and are severely decelerated with high rates of change in velocity.

3. THE WIND SPEED ERROR FOR FLOWS AT ±15° OFF THE BOW

3.1 Introduction

This section examines the error in the wind speed measurements made from a number of anemometers mounted on the RV *Tangaroa*. The VECTIS simulation was performed using a uniform inlet wind speed profile of 10 ms^{-1} at a relative wind direction of 15° off the port bow. Data are extracted from VECTIS run 3.7/9. Effective anemometer positions have been calculated to simulate the flow over the starboard bow. The ship geometry was enclosed in the centre of a computational domain 600 m in length ($-300\ m < x < 300\ m$), 600 m wide ($-300\ m < y < 300\ m$) and 150 m high ($0\ m < z < 150\ m$). The domain width has been increased to account for the increased blockage created by the ship. The flow in the tunnel was examined to confirm that free stream conditions existed at the sides and ends of the tunnel, i.e. that the presence of the ship did not cause a significant blockage of the flow to these regions. Whilst the computational solver was running the velocities at 8 locations were monitored, 7 abeam of the ship in free stream flow and one at the Campbell 1 3D prop anemometer location. The data from these points show the solution had converged after approximately 17500 time steps with the velocities at the monitoring points constant to the 4th significant figure. Figure 16 shows the velocity data for the last 250 time steps. Once the model had converged a post-processing file was written for the extraction of the data throughout the computational volume. Illustrations of the output can be found in the Appendix and a detailed description of the data extraction procedure can be found in Moat et al. (1996).

The flow in the tunnel was examined to confirm that free stream conditions existed at the sides and ends of the tunnel, i.e. that the presence of the ship did not cause a significant blockage of the flow. Figure 17a shows the variation in the velocity along the tunnel at x=±300 m, at heights of 10, 20, 30 and 50 m on a plane at y=275 m, i.e. towards one side of the tunnel. The central section is shown in greater detail in Figure 17b, with the velocity data shown directly abeam of the ship on a plane at y=275 m and x=±50 m. The coarse mesh directly abeam of the ship has created a variation of less than 0.01 ms^{-1} in the free stream velocity. This creates an insignificant change in the calculation of the wind speed error and shows that the blockage in the tunnel is minimal. However, since the changes are not zero, the free stream velocity for a particular instrument site is estimated using the vertical profile of velocity at 275 m directly abeam of the instrument site, rather than the profiles at the inlet or outlet of the tunnel.

3.2 Anemometer locations

The anemometer sites for an airflow 15° over the port bow, in the VECTIS co-ordinate system (where the origin is at the centre of the ship at sea level), are:

Cambell 1 3D prop (bow)	x= 30.36 m, y= -8.13 m, z=14.35 m
Campbell 1 cup (bow)	x= 30.76 m, y= -8.60 m, z=11.54 m
Starlogger 1 (bridge)	x= 13.66 m, y= 1.09 m, z=13.62 m
Starlogger 2 (bridge)	x= 8.60 m, y= -3.67 m, z=18.36 m
Starlogger 3 (bridge)	x= 7.76 m, y= -8.19 m, z=19.36 m
Starlogger 4 (bridge)	x= 7.83 m, y= -8.29 m, z=17.39 m
Starlogger 5 (bridge gantry)	x= -5.57 m, y= 4.28 m, z=15.64 m
Starlogger 6 (aft deck)	x= -17.49 m, y= 12.13 m, z= 8.74 m
Cambell 2 3D prop (aft gantry)	x= -27.26 m, y= 7.61 m, z=19.92 m
Cambell 2 cup (aft gantry)	x = -29.68 m, y= 9.38 m, z=19.56 m

Effective anemometer positions were created to enable the velocity errors for winds at 15° off the starboard bow to be calculated from the VECTIS simulations of the airflow over the port bow (Moat and Yelland, 1997). The flow conditions at the effective Starlogger 6 anemometer location are unrealistic of a flow over the starboard bow because of obstacles upwind of the anemometer (Figure A5). Therefore, no wind speed error at this anemometer site will be calculated. The remaining anemometer positions for an effective flow over the starboard bow are:

Cambell 1 3D prop (bow)	x= 30.36 m, y= -8.13 m, z=14.35 m
Campbell 1 cup (bow)	x= 30.94 m, y= -7.93 m, z=11.54 m
Starlogger 1 (bridge)	x= 11.28 m, y= -7.76 m, z=13.62 m
Starlogger 2 (bridge)	x= 9.29 m, y= -1.12 m, z=18.36 m
Starlogger 3 (bridge)	x= 10.82 m, y= 3.21 m, z=19.36 m
Starlogger 4 (bridge)	x= 10.927 m, y= 3.26 m, z=17.39 m
Starlogger 5 (bridge gantry)	x= -6.97 m, y= -0.93 m, z=15.64 m
Starlogger 6 (aft deck)	x= n/a , y= n/a , z= n/a
Cambell 2 3D prop (aft gantry)	x= -27.41 m, y= 7.03 m, z=19.92 m
Cambell 2 cup (aft gantry)	x= -30.40 m, y= 6.72 m, z=19.56 m

The anemometer positions have not changed in relation to the ship, therefore the positions of the anemometers are as indicated in Figure 1.

3.3 The effect of flow distortion for an airflow 15° off the port bow

The free stream velocities are extracted towards the edge of the tunnel at the anemometer height. The free stream flow has small, predictable gradients and can be estimated accurately at any given point on the vertical profile. In contrast, the flow at the instrument site can suffer from server distortion and large gradients in the velocity field. Additionally it is not always possible to define the mesh so that the instruments are at the exact centers of the computational cells (see Moat et al., 1996). Therefore the velocity at an instrument site is estimated from lines of data extracted in all three directions. Figures 18 to 27 show the lines of velocity data through the Campbell 1 3D prop, Campbell 1 cup, Starlogger cup anemometers 1 to 6, Campbell 2 3D prop and the Campbell 2 cup anemometers. The results of all anemometers are summarized in Table 3. The percentage wind speed error is given by Equation 1 with a positive error indicating an acceleration of the flow.

Anemometer	Velocity from each direction (m/s)	Average velocity at anemometer site (m/s)	Free stream velocity (m/s)	% error
Campbell 1 3D prop	9.580 (x) 9.379 (y) 9.578 (z)	9.579	10.076	-4.96
Campbell 1 cup	9.383 (x) 9.377 (y) 9.382 (z)	9.381	10.073	-6.87
Starlogger 1	7.580 (x) 7.587 (y) 7.585 (z)	7.584	10.077	-24.74
Starlogger 2	11.222 (x) 11.231 (y) 11.228 (z)	11.227	10.077	11.41
Starlogger 3	10.833 (x) 10.854 (y) 10.854 (z)	10.847	10.077	7.64
Starlogger 4	11.042(x) 11.000 (y) 11.042 (z)	11.028	10.077	9.44
Starlogger 5	10.972 (x) 10.951 (y) 10.953 (z)	10.959	10.078	8.74
Starlogger 6	10.360 (x) 10.357 (y) 10.363 (z)	10.360	10.079	2.79
Campbell 2 3D prop	10.238 (x) 10.223 (y) 10.227 (z)	10.229	10.079	1.48
Campbell 2 cup	11.119 (x) 11.112 (y) 11.120 (z)	11.117	10.079	10.29

Table 3 VECTIS velocity error estimates for the anemometers at 15° off the port bow.

An indication of the accuracy of the model and the severity of the flow distortion is also given by estimates of the gradient of the flow. Estimates of the gradient of the flow are made from Figures 18 to 27 and the rates of change for all the anemometers, per meter and per cell, are given in Table 4.

Anemometer	Velocity data line	Rate of change of velocity per meter (ms^{-1}/m)	Rate of change of velocity per cell ($ms^{-1}/cell$)
Campbell 1 3D prop	along (x)	0.052	-0.012
	across (y)	0.037	-0.007
	up (z)	0.052	0.009
Campbell 1 cup	along (x)	-0.077	-0.019
	across (y)	-0.066	-0.054
	up (z)	0.105	0.040
Starlogger 1	along (x)	0.799	0.129
	across (y)	0.234	0.053
	up (z)	0.652	0.124
Starlogger 2	along (x)	-0.241	-0.078
	across (y)	0.041	0.015
	up (z)	-0.302	-0.057
Starlogger 3	along (x)	-0.117	-0.110
	across (y)	0.084	0.051
	up (z)	-0.190	-0.025
Starlogger 4	along (x)	-0.187	-0.184
	across (y)	0.158	0.122
	up (z)	-0.172	-0.042
Starlogger 5	along (x)	0.040	0.021
	across (y)	-0.412	-0.077
	up (z)	1.578	0.140
Starlogger 6	along (x)	0.066	0.029
	across (y)	-0.036	-0.015
	up (z)	-0.046	-0.010
Campbell 2 3D prop	along (x)	-0.183	-0.176
	across (y)	0.050	0.053
	up (z)	0.105	0.026
Campbell 2 cup	along (x)	0.008	-0.013
	across (y)	-0.052	-0.030
	up (z)	0.464	-0.078

Table 4 The rate of change of velocity for the anemometers at 15° off the port bow.

The rate of change of velocity per meter and per cell is low for the Campbell 1 instruments suggesting the bow location is a reliable site for locating anemometers. The well-exposed Starlogger anemometers (Starloggers 2, 3, 4) above the bridge top are in a region of high rates of change of velocity with accelerations in wind speed of between 7 % and 11 %. The Starlogger 6 anemometer is moderately well-exposed at this wind direction, has low rates of change in velocity and experiences a 2 % increase in wind speed. The remaining Starlogger anemometers are badly exposed and experience high rates of change in velocity with the Starlogger 1 anemometer decelerated by about 24 % of the free stream wind speed. At this relative wind direction the frame on which the Campbell 2 anemometers are attached distorts the wind speed to the anemometer location (Figure A4). The Campbell 2 3D prop is higher and further forwards than the Campbell 2 cup anemometer and experiences an acceleration of 1.5 %, whilst the wind speed at the Campbell 2 cup is accelerated by 10 %.

3.4 The effect of flow distortion for an airflow 15° off the starboard bow

The free stream velocities are extracted towards the edge of the tunnel at the anemometer height. The free stream flow has small, predictable gradients and can be estimated accurately at any given point on the vertical profile. In contrast, the flow at the instrument site can suffer from server distortion and large gradients in the velocity field. Additionally it is not always possible to define the mesh so that the instruments are at the exact centers of the computational cells (see Moat et al., 1996). Therefore the velocity at an instrument site is estimated from lines of data extracted in all three directions. Figures 28 to 36 show the lines of velocity data through the Campbell 1 3D prop, Campbell 1 cup, Starlogger cup anemometers 1 to 6, Campbell 2 3D prop and the Campbell 2 cup anemometers. The results of all anemometers are summarized in Table 5. The percentage wind speed error is given by Equation 1 with a positive error indicating an acceleration of the flow.

Anemometer	Velocity from each direction (m/s)	Average velocity at anemometer site (m/s)	Free stream velocity (m/s)	% error
Campbell 1 3D prop	9.580 (x) 9.379 (y) 9.578 (z)	9.579	10.076	-4.96
Campbell 1 cup	9.326 (x) 9.325 (y) 9.326 (z)	9.326	10.073	-7.42
Starlogger 1	8.898 (x) 8.898 (y) 8.991 (z)	8.929	10.077	-11.39
Starlogger 2	11.102 (x) 11.104 (y) 11.107 (z)	11.104	10.077	10.19
Starlogger 3	10.511 (x) 10.515 (y) 10.514 (z)	10.513	10.077	4.33
Starlogger 4	10.636 (x) 10.633 (y) 10.634 (z)	10.634	10.077	5.53
Starlogger 5	6.122 (x) 6.316 (y) 6.088 (z)	6.175	10.078	-38.72
Starlogger 6	n/a (x) n/a (y) n/a (z)	n/a	n/a	n/a
Campbell 2 3D prop	10.217 (x) 10.232 (y) 10.207 (z)	10.219	10.079	1.39
Campbell 2 cup	11.192 (x) 11.195 (y) 11.209 (z)	11.199	10.079	11.11

Table 5 VECTIS velocity error estimates for the anemometers at 15° off the starboard bow.

An indication of the accuracy of the model and the severity of the flow distortion is also given by estimates of the gradient of the flow. Estimates of the gradient of the flow are made from Figures 28 to 36 and the rates of change for all the anemometers, per meter and per cell, are given in Table 6.

Anemometer	Velocity data line	Rate of change of velocity per meter (ms^{-1}/m)	Rate of change of velocity per cell ($ms^{-1}/cell$)
Campbell 1 3D prop	along (x) across (y) up (z)	0.052 0.037 0.052	-0.012 -0.007 0.009
Campbell 1 cup	along (x) across (y) up (z)	-0.070 -0.068 0.120	-0.022 -0.062 0.047
Starlogger 1	along (x) across (y) up (z)	0.028 -0.440 0.399	-0.019 -0.282 0.166
Starlogger 2	along (x) across (y) up (z)	-0.206 0.017 -0.348	-0.076 0.011 -0.099
Starlogger 3	along (x) across (y) up (z)	-0.198 -0.036 -0.070	-0.080 -0.017 -0.020
Starlogger 4	along (x) across (y) up (z)	-0.470 -0.086 -0.078	-0.172 -0.038 -0.024
Starlogger 5	along (x) across (y) up (z)	-0.304 1.004 3.953	-0.226 1.093 0.487
Starlogger 6	along (x) across (y) up (z)	n/a n/a n/a	n/a n/a n/a
Campbell 2 3D prop	along (x) across (y) up (z)	-0.176 0.062 0.140	-0.142 0.056 0.045
Campbell 2 cup	along (x) across (y) up (z)	-0.092 0.034 -0.361	-0.014 0.029 -0.149

Table 6 Rate of change of velocity for the anemometers at 15° off the starboard bow.

The rate of change of velocity per meter and per cell is low for the Campbell 1 instruments suggesting the bow location is a reliable site for locating an anemometer. As the Campbell 1 3D prop anemometer is located on the centerline of the ship the airflow distortion is the same for port and starboard flows. The well-exposed Starlogger anemometers above the bridge top are in a region of high rates of change of velocity with accelerations in wind speed of between 6 % and 10 %. The Starlogger 6 anemometer is within the down wind wake of the bridge superstructure and is decelerated by 97 % of the free stream wind speed. The remaining Starlogger anemometers are badly exposed and experience high rates of change in velocity with the Starlogger 5 anemometer decelerated by about 39 % of the free stream wind speed. The Campbell 2 anemometers are well-exposed at this wind direction and experience a similar airflow distortion as the flow 15 degrees off the port bow. The Campbell 2 3D anemometer experiences an acceleration of 1 %, whilst the wind speed at the Campbell 2 cup is accelerated by 11 %. The main source of flow distortion is the airflow around the frame on which the anemometers are located.

3.5 Conclusions

The well-exposed Campbell 1 anemometers located above the bow are in a region of low rates of change in velocity, which suggest that the results are reliable. Percentage errors for these anemometers varied from -5 % to -7 % of the free stream wind speed. The Starlogger 2, 3, 4 anemometers located above the bridge top are well-exposed, but are located in a region of high rates of change in velocity. The wind speed errors for these instruments typically range from increases of 5 % to 11 % of the free stream wind speed.

The Starlogger 6 anemometer, located on the aft deck, is moderately well-exposed for flows over the port side and experiences a flow distortion of about 3 %. The remaining Starlogger anemometers (Starlogger 1 and 5) are located in badly exposed locations with high rates of change in velocity. The airflow distortion ranges from accelerations of 9 % to decelerations of up to 38 % of the free stream wind speed.

The Campbell 2 anemometers located above the aft frame are well-exposed to the airflow. However, the instruments are affected by the airflow over the frame on which they are located. The wind speed errors range from overestimates of 1 % for the Campbell 2 3D prop to overestimates of 10 % for the Campbell 2 cup anemometer.

4. THE WIND SPEED ERROR FOR FLOWS AT ±30° OFF THE BOW

4.1 Introduction

This section examines the error in the wind speed measurements made from a number of anemometers mounted on the RV *Tangaroa*. The run is a uniform profile at 30° off the port bow and data are extracted from VECTIS run 3.8/4. Effective anemometer positions have been calculated to simulate the flow over the starboard bow. The ship geometry was enclosed in the centre of a computational domain 600 m in length (-300 m < x < 300 m), 1000 m wide (-500 m < y < 500 m) and 150 m high (0 m < z < 150 m). The domain width has been increased to account for the increased blockage created by the ship. The flow in the tunnel was examined to confirm that free stream conditions existed at the sides and ends of the tunnel, i.e. that the presence of the ship did not cause a significant blockage of the flow to these regions. Whilst the computational solver was running the velocities at 8 locations were monitored, 7 abeam of the ship in free stream flow and one at the Campbell 1 3D prop anemometer location. The data from these points show the solution had converged after approximately 37800 time steps with the velocities at the monitoring points constant to the 4th significant figure. Figure 37 shows the velocity data for the last 250 time steps. Once the model had converged a post-processing file was written for the extraction of the data throughout the computational volume. Illustrations of the output can be found in the Appendix and a detailed description of the data extraction procedure can be found in Moat et al. (1996).

The flow in the tunnel was examined to confirm that free stream conditions existed at the sides and ends of the tunnel, i.e. that the presence of the ship did not cause a significant blockage of the flow. Figure 38a shows the variation in the velocity along the tunnel at x=±300 m, at heights of 10, 20, 30 and 50 m on a plane at y=450 m, i.e. towards one side of the tunnel. The central section is shown in greater detail in Figure 38b, with the velocity data shown directly abeam of the ship on a plane at y=450 m and x=±50 m. The changes in velocity with height on this plane along the length of the ship are less than 0.01 ms^{-1}. These results show that the blockage in the tunnel is minimal. However, since the changes are not zero, the free stream velocity for a particular instrument site is estimated using the vertical profile of velocity at 450 m directly abeam of the instrument site, rather than the profiles at the inlet or outlet of the tunnel.

4.2 Anemometer locations

The anemometer sites for an airflow 30° over the port bow, in the VECTIS co-ordinate system (where the origin is at the centre of the ship at sea level), are:

Cambell 1 3D prop (bow)	x= 27.22 m, y= -15.72 m, z= 14.35 m
Campbell 1 cup (bow)	x= 27.49 m, y= -16.27 m, z= 11.54 m
Starlogger 1 (bridge)	x= 13.48 m, y= -2.48 m, z= 13.62 m
Starlogger 2 (bridge)	x= 7.36 m, y= -5.77 m, z= 18.36 m
Starlogger 3 (bridge)	x= 5.38 m, y= -9.92 m, z= 19.36 m
Starlogger 4 (bridge)	x= 5.42 m, y= -10.03 m, z= 17.39 m
Starlogger 5 (bridge gantry)	x= -4.27 m, y= 5.58 m, z= 15.64 m
Starlogger 6 (aft deck)	x= -13.75 m, y= 16.24 m, z= 8.74 m
Cambell 2 3D prop (aft gantry)	x= -24.36 m, y= 14.41 m, z= 19.92 m
Cambell 2 cup (aft gantry)	x= -26.24 m, y= 16.75 m, z= 19.56 m

Effective anemometer positions were created to enable the velocity errors for winds at 30° off the starboard bow to be calculated from the VECTIS simulations of the airflow over the port bow (Moat and Yelland, 1997). The flow conditions at the effective Starlogger 6 anemometer location are unrealistic of a flow over the starboard bow because of obstacles upwind of the anemometer (Figure A6). Therefore, no wind speed error at this anemometer site will be calculated. The remaining anemometer positions for an effective flow over the starboard bow are:

Cambell 1 3D prop (bow)	x= 27.22 m, y = -15.72 m, z=14.35 m
Campbell 1 cup (bow)	x= 27.84 m, y= -15.67 m, z=11.54 m
Starlogger 1 (bridge)	x= 8.89 m, y= -10.43 m, z=13.62 m
Starlogger 2 (bridge)	x= 8.49 m, y= -3.49 m, z=18.36 m
Starlogger 3 (bridge)	x= 10.28 m, y= 0.30 m, z=19.36 m

Starlogger 4 (bridge)	x= 11.40 m, y= 0.32 m, z=17.39 m
Starlogger 5 (bridge gantry)	x= -6.97 m, y= 0.91 m, z=15.64 m
Starlogger 6 (aft deck)	x= n/a, y= n/a , z= n/a
Cambell 2 3D prop (aft gantry)	x= -24.66 m, y= 13.89 m, z=19.92 m
Cambell 2 cup (aft gantry)	x= -27.62 m, y= 14.36 m, z=19.56 m

The anemometer positions have not changed in relation to the ship, therefore the positions of the anemometers are as indicated in Figure 1.

4.3 The effect of flow distortion for an airflow 30° off the port bow

The free stream velocities are extracted towards the edge of the tunnel at the anemometer height. The free stream flow has small, predictable gradients and can be estimated accurately at any given point on the vertical profile. In contrast, the flow at the instrument site can suffer from server distortion and large gradients in the velocity field. Additionally it is not always possible to define the mesh so that the instruments are at the exact centers of the computational cells (see Moat et al., 1996). Therefore the velocity at an instrument site is estimated from lines of data extracted in all three directions. Figures 39 to 48 show the lines of velocity data through the Campbell 1 3D prop, Campbell 1 cup, Starlogger cup anemometers 1 to 6, Campbell 2 3D prop and the Campbell 2 cup anemometers. The results of all anemometers are summarized in Table 7. The percentage wind speed error is given by Equation 1 with a positive error indicating an acceleration of the flow.

Anemometer	Velocity from each direction (m/s)	Average velocity at anemometer site (m/s)	Free stream velocity (m/s)	% error
Campbell 1 3D prop	9.905 (x) 9.901 (y) 9.903 (z)	9.903	9.982	-0.8
Campbell 1 cup	9.866 (x) 9.856 (y) 9.866 (z)	9.863	9.980	-1.2
Starlogger 1	8.403 (x) 8.415 (y) 8.416 (z)	8.411	9.987	-15.8
Starlogger 2	11.522 (x) 11.522 (y) 11.514 (z)	11.519	9.990	15.3
Starlogger 3	11.306 (x) 11.312 (y) 11.314 (z)	11.311	9.991	13.2
Starlogger 4	11.605 (x) 11.610 (y) 11.609 (z)	11.608	9.990	16.2
Starlogger 5	7.564 (x) 7.493 (y) 7.662 (z)	7.573	9.995	-24.2
Starlogger 6	10.322 (x) 10.340 (y) 10.378 (z)	10.347	10.000	3.5
Campbell 2 3D prop	11.008 (x) 11.019 (y) 11.131 (z)	11.053	10.005	10.5
Campbell 2 cup	10.704 (x) 10.806 (y) 10.706 (z)	10.705	10.005	7.0

Table 7 VECTIS velocity error estimates for the anemometers at 30° off the port bow.

An indication of the accuracy of the model and the severity of the flow distortion is also given by estimates of the gradient of the flow. Estimates of the gradient of the flow are made from Figures 39 to 48 and the rates of change for all the anemometers, per meter and per cell, are given in Table 8.

Anemometer	Velocity data line	Rate of change of velocity per meter (ms^{-1}/m)	Rate of change of velocity per cell (ms^{-1}/cell)
Campbell 1 3D prop	along (x)	-0.095	-0.012
	across (y)	-0.054	-0.042
	up (z)	0.011	0.060
Campbell 1 cup	along (x)	-0.204	-0.025
	across (y)	0.036	-0.017
	up (z)	-0.105	-0.004
Starlogger 1	along (x)	-0.554	0.290
	across (y)	-0.282	-0.144
	up (z)	-0.306	0.147
Starlogger 2	along (x)	0.156	-0.116
	across (y)	-0.042	0.016
	up (z)	0.314	-0.091
Starlogger 3	along (x)	0.137	-0.183
	across (y)	0.091	0.056
	up (z)	-0.546	-0.041
Starlogger 4	along (x)	-0.206	-0.209
	across (y)	0.153	0.074
	up (z)	-0.182	-0.053
Starlogger 5	along (x)	-0.536	0.182
	across (y)	4.931	1.619
	up (z)	-2.060	-0.272
Starlogger 6	along (x)	0.028	0.025
	across (y)	-0.210	-0.440
	up (z)	-0.052	-0.021
Campbell 2 3D prop	along (x)	-0.114	-0.329
	across (y)	0.180	0.573
	up (z)	-0.126	0.005
Campbell 2 cup	along (x)	0.146	-0.387
	across (y)	-0.068	-0.014
	up (z)	0.109	0.026

Table 8 The rate of change of velocity for the anemometers at 30° off the port bow.

The rate of change of velocity per meter and per cell is low for the Campbell 1 instruments suggesting the bow location is a reliable site for locating anemometers. The wind speed is decelerated by about 1 % of the free stream wind speed. The well-exposed Starlogger anemometers above the bridge top (Starlogger 2, 3, 4) are in a region of high rates of change of velocity with accelerations in wind speed of between 13 % and 16 % of the free stream wind speed. The Starlogger 6 anemometer was moderately well-exposed at this wind direction, has high rates of change in velocity and experiences a 4 % increase in wind speed. The remaining Starlogger anemometers are badly exposed and experience high rates of change in velocity with the Starlogger 1 anemometer decelerated by about 16 % of the free stream wind speed. The previously well-exposed Campbell 2 anemometers are now located in a region of high rates of change in velocity and experience an increase in wind speed of up to 11 %.

4.4 The effect of flow distortion for an airflow 30° off the starboard bow

The free stream velocities are extracted towards the edge of the tunnel at the anemometer height. The free stream flow has small, predictable gradients and can be estimated accurately at any given point on the vertical profile. In contrast, the flow at the instrument site can suffer from server distortion and large gradients in the velocity field. Additionally it is not always possible to define the mesh so that the instruments are at the exact centers of the computational cells (see Moat et al., 1996). Therefore the velocity at an instrument site is estimated from lines of data extracted in all three directions. Figures 49 to 57 show the lines of velocity data through the Campbell 1 3D prop, Campbell 1 cup, Starlogger cup anemometers 1 to 6, Campbell 2 3D prop and the Campbell 2 cup anemometers. The results of all anemometers are summarized in Table 9. The percentage wind speed error is given by Equation 1 with a positive error indicating an acceleration of the flow.

Anemometer	Velocity from each direction (m/s)	Average velocity at anemometer site (m/s)	Free stream velocity (m/s)	% error
Campbell 1 3D prop	9.905 (x) 9.901 (y) 9.903 (z)	9.903	9.982	-0.8
Campbell 1 cup	9.744 (x) 9.741 (y) 9.745 (z)	9.743	9.980	-2.37
Starlogger 1	10.785 (x) 10.785 (y) 10.782 (z)	10.784	9.989	7.96
Starlogger 2	11.368 (x) 11.379 (y) 11.385 (z)	11.377	9.990	13.89
Starlogger 3	10.482 (x) 10.479 (y) 10.482 (z)	10.481	9.989	4.93
Starlogger 4	10.676 (x) 10.674 (y) 10.680 (z)	10.677	9.987	6.91
Starlogger 5	6.130 (x) 6.320 (y) 6.068 (z)	6.173	9.996	-38.25
Starlogger 6	n/a (x) n/a (y) n/a (z)	n/a	n/a	n/a
Campbell 2 3D prop	10.992 (x) 11.030 (y) 11.008 (z)	11.01	10.005	10.05
Campbell 2 cup	11.354 (x) 11.310 (y) 11.354 (z)	11.339	10.006	13.33

Table 9 VECTIS velocity error estimates for the anemometers at 30° off the starboard bow.

An indication of the accuracy of the model and the severity of the flow distortion is also given by estimates of the gradient of the flow. Estimates of the gradient of the flow are made from Figures 49 to 57 and the rates of change for all the anemometers, per meter and per cell, are given in Table 10.

Anemometer	Velocity data line	Rate of change of velocity per meter (ms^{-1}/m)	Rate of change of velocity per cell (ms^{-1}/cell)
Campbell 1 3D prop	along (x) across (y) up (z)	-0.095 -0.053 0.010	-0.012 -0.042 0.060
Campbell 1 cup	along (x) across (y) up (z)	-1.170 -0.090 0.046	-0.026 -0.068 0.004
Starlogger 1	along (x) across (y) up (z)	-1.309 -0.076 -0.014	-0.191 0.031 -0.011
Starlogger 2	along (x) across (y) up (z)	-0.111 0.003 -0.393	-0.068 -0.004 -0.115
Starlogger 3	along (x) across (y) up (z)	-0.229 -0.043 -0.081	-0.128 -0.027 -0.029
Starlogger 4	along (x) across (y) up (z)	-0.559 -0.090 -0.168	-0.281 -0.047 -0.049
Starlogger 5	along (x) across (y) up (z)	0.906 0.706 4.523	1.180 -4.471 2.249
Starlogger 6	along (x) across (y) up (z)	n/a n/a n/a	n/a n/a n/a
Campbell 2 3D prop	along (x) across (y) up (z)	0.101 0.178 -0.014	0.210 0.517 0.021
Campbell 2 cup	along (x) across (y) up (z)	0.000 -0.090 -0.410	0.093 -0.081 -0.048

Table 10 The rate of change of velocity for the anemometers at 30° off the starboard bow.

The rate of change of velocity per meter and per cell is low for the Campbell 1 instruments suggesting the bow location is a reliable site for locating anemometers. The well-exposed Starlogger anemometers (Starloggers 2, 3, 4) above the bridge top are in a region of high rates of change of velocity with accelerations in wind speed of between 7 % and 14 % of the free stream wind speed. The remaining Starlogger anemometers are badly exposed and experience high rates of change in velocity with the Starlogger 5 anemometer decelerated by about 38 % of the free stream wind speed. The previously well-exposed Campbell 2 anemometers are now located in a region of high rates of change in velocity and experience an increase in wind speed of up to 11 %.

4.5 Conclusions

For an airflow ±30° off the bow, the Campbell 1 anemometers located above the bow are in a region of low rates of change in velocity, which suggest that the results are reliable. The wind speed errors for these anemometers were decreased by up to 2 % of the free stream wind speed. The Starlogger 2, 3, 4 anemometers located above the bridge top are well-exposed, but are located in a region of high rates of change in velocity. The wind speed errors for these instruments typically range from increases of 7 % to 14 % of the free stream wind speed.

For flows over the port side the Starlogger 6 anemometer, located on the aft deck, is moderately well-exposed and experiences a flow distortion of about 4 %. The remaining Starlogger anemometers (Starlogger 1 and 5) are located in badly exposed locations with high rates of change in velocity. The airflow distortion ranges from accelerations of 8 % to decelerations of up to 38 % of the free stream wind speed.

The Campbell 2 anemometers located above the aft frame are well-exposed to the airflow. However, the instruments are affected by the airflow over the frame on which they are located. The wind speed errors range from overestimates of 1 % for the Campbell 2 3D prop to overestimates of 10 % for the Campbell 2 cup anemometer.

5. SUMMARY

The distortion of the airflow to ten anemometer locations on the RV *Tangaroa* has been quantified for a wind speed of 10 ms^{-1} blowing at five relative wind directions. These ranged from ±30°, ±15° and a flow directly over the bow (0°). The distortion of the flow is only that created by the ship's hull and superstructure, since small-scale obstructions (the railings and thin masts) cannot be modelled. The wind speed errors for all the instruments are summarized in Table 11.

The effect of flow distortion on the measured wind speed is sensitive to the position of the anemometer. The wind speed at the well-exposed Campbell 1 anemometers, located above the bow of the ship, was decelerated by 1 % to 7 % of the free stream wind speed. In contrast the wind speed at the well-exposed Starlogger anemometers (Starloggers 2, 3 and 4) located above the bridge top were all in a region of accelerated flow (maximum of 16 % of the free stream wind speed). Therefore the wind speed error can still be large for seemingly well-exposed instruments.

The remaining Starlogger anemometers were deliberately located in badly exposed locations. The wind speed error at these anemometer locations varied from increases of about 10 % to decreases of about 69 % of the free stream wind speed. The Campbell 2 anemometers located on the frame above the aft deck were in the wake region of the bridge superstructure for flows directly over the bow. At this relative wind direction the wind speed was decelerated by about 15 %. For all other wind directions modeled, the wind speed was accelerated by about 10 %. The main source of wind speed error for these anemometers was the distortion of the airflow over the frame the anemometers were located on.

	30° port	15° port	0° (head to wind)	15° starboard	30° starboard
	Δu	Δu	Δu	Δu	Δu
Camp 1 3D prop	-1	-5	-5	-5	-1
Camp 1 cup	-1	-7	-7	-7	-2
Star 1	-16	-25	-18	-11	8
Star 2	15	11	9	10	14
Star 3	13	8	6	4	5
Star 4	16	9	8	6	7
Star 5	-24	9	-69	-39	-38
Star 6	4	3	-21	n/a	n/a
Camp 2 3D prop	11	1	-16	1	11
Camp 2 cup	7	10	-17	11	13

Table 11 The percentage wind speed errors, Δu, at the anemometer locations.

Popinet et al (2004) compared the in situ wind speed measurements from all the anemometers to numerical flow simulations over the RV *Tangaroa*. The simulations were performed at a number of relative wind directions using the CFD code GERRIS (Popinet, 2002). All VECTIS CFD modeled wind speeds will be compared to these results in a separate study.

ACKNOWLEDGEMENTS

The authors wish to thank Dr. Stephane Popinet (NIWA, New Zealand) for providing the RV *Tangaroa* geometry used in the VECTIS airflow studies. This work was partially funded by the National Oceanography Centre, Southampton technology innovation fund (TIF).

REFERENCES

Moat, B. I., Yelland, M. J. and Hutchings, J. 1996: Airflow over the RRS Discovery using the Computational Fluid Dynamics package VECTIS, *SOC Internal Document No. 2*, Southampton Oceanography Centre, Southampton. UK. 41 pp**.**

Moat, B. I. and M. J. Yelland, 1997: Airflow 15 and 30 degrees off the bow of the R.R.S. Discovery: the disturbance of the flow at the anemometer sites for cruises D199-D201 and D213-D214, *SOC Internal Document No. 25*, Southampton Oceanography Centre, Southampton. UK. 44 pp.

Popinet , S. M. 2002: The GERRIS flow solver. Release 0.6.0. [available online at http://gfs.sourceforge.net/]

Popinet, S. M., M. Smith and C. Stevens, 2004: Experimental and numerical characteristics of airflow around a research vessel, *Journal of Atmospheric and Oceanic Technology*, 21(10), 1575 – 1589.

Ricardo, 2003: VECTIS computational fluid dynamics (Release 3.7) users guide. Ricardo Consulting Engineers Ltd, UK. 264 pp. [available from Ricardo Consulting Engineers Ltd, Bridge Works, Shoreham-by-Sea, West Sussex, UK. BN43 5FG].

Yakhot, V., S. A. Orszag, S. Thangam, T. B. Gatski, and G. Speziale, 1992: Development of turbulence models for shear flows by a double expansion technique, *Physics of Fluids*, **A4**(7), 1510-1520.

FIGURES

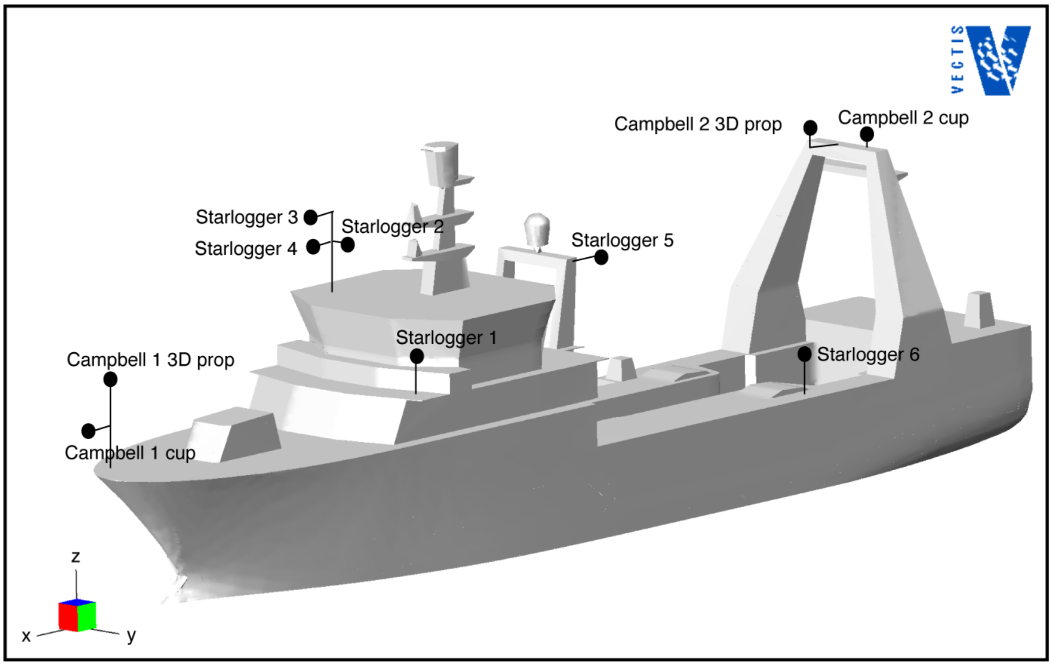

Figure 1 The anemometer positions on the R/V *Tangaroa* (adapted from Popinet et al., 2004).

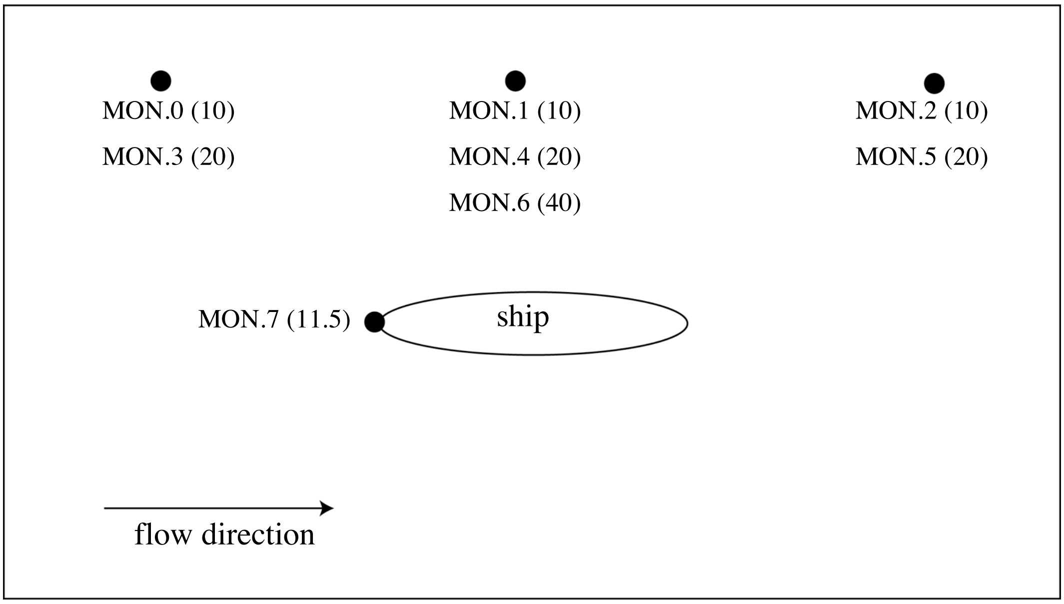

Figure 2 Schematic plan view of the computational domain. The solid circles show the locations of the monitoring points and their heights in meters are indicated in brackets.

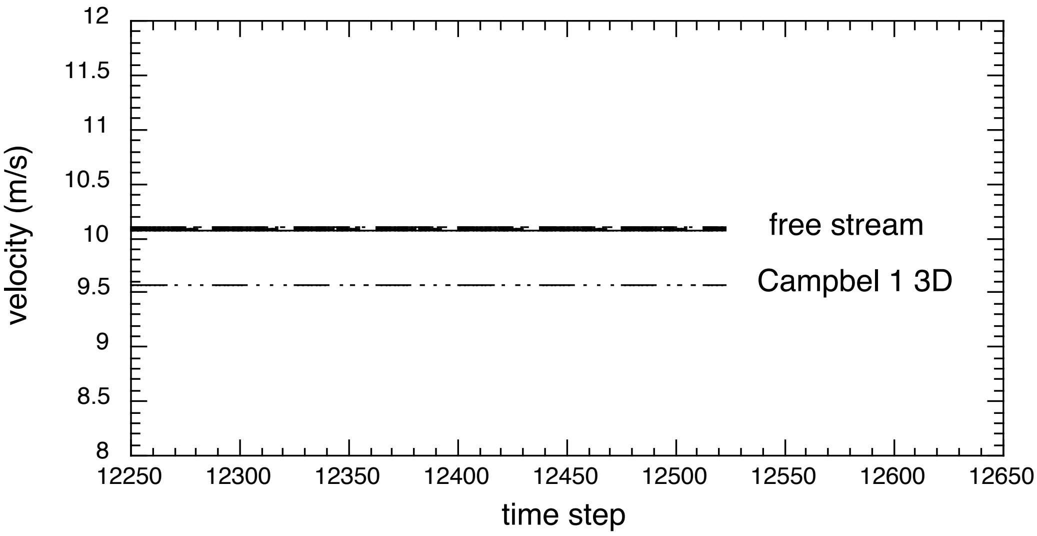

Figure 3 The velocity at each monitoring location in the 0 degree flow (head to wind) simulation. The last 250 time steps are shown.

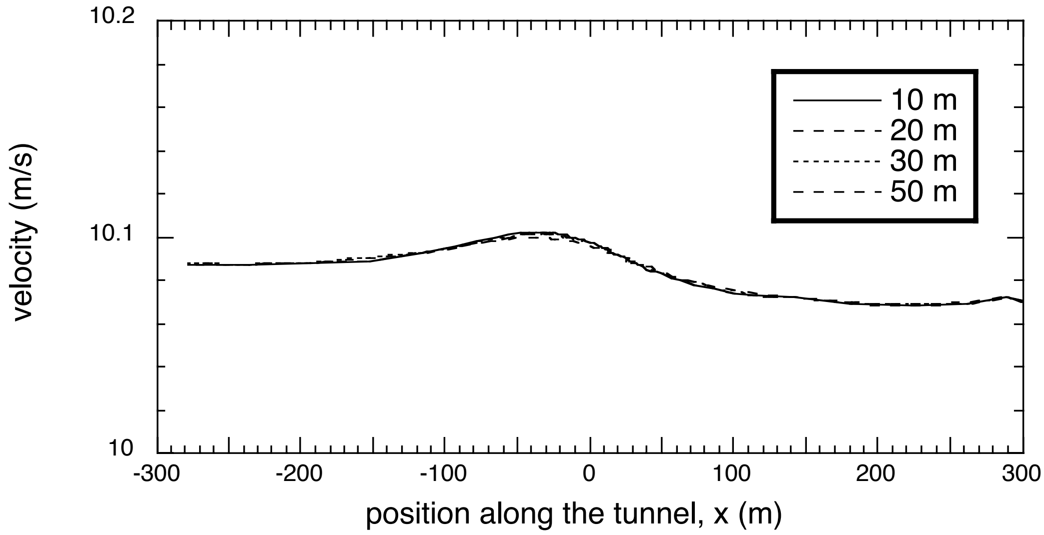

Figure 4a Lines of velocity data along the length of the computational domain at the heights shown. The data were obtained from the free stream region on the port side of the tunnel at y= 125 m.

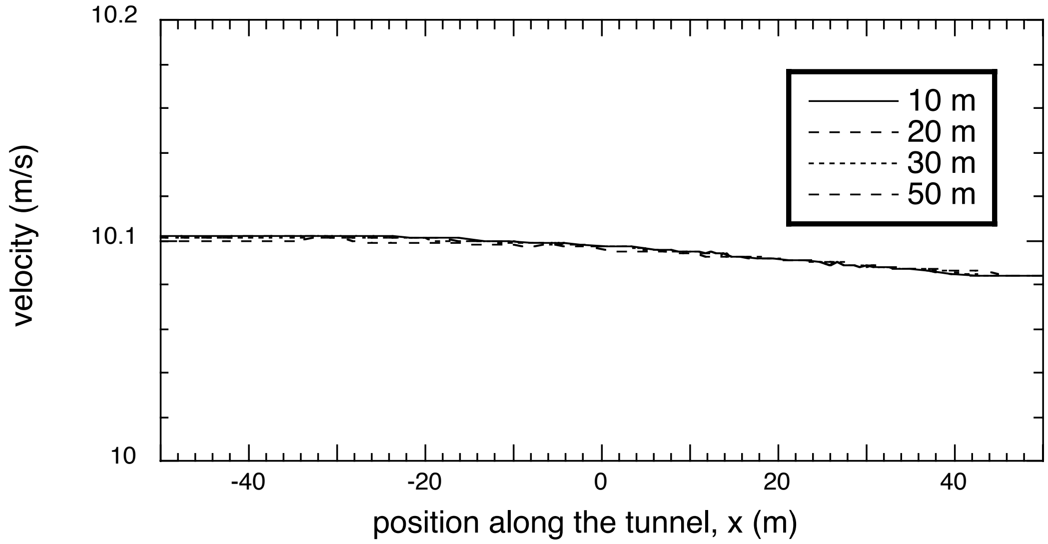

Figure 4b As Figure 4a, showing the central portion of the computational domain only.

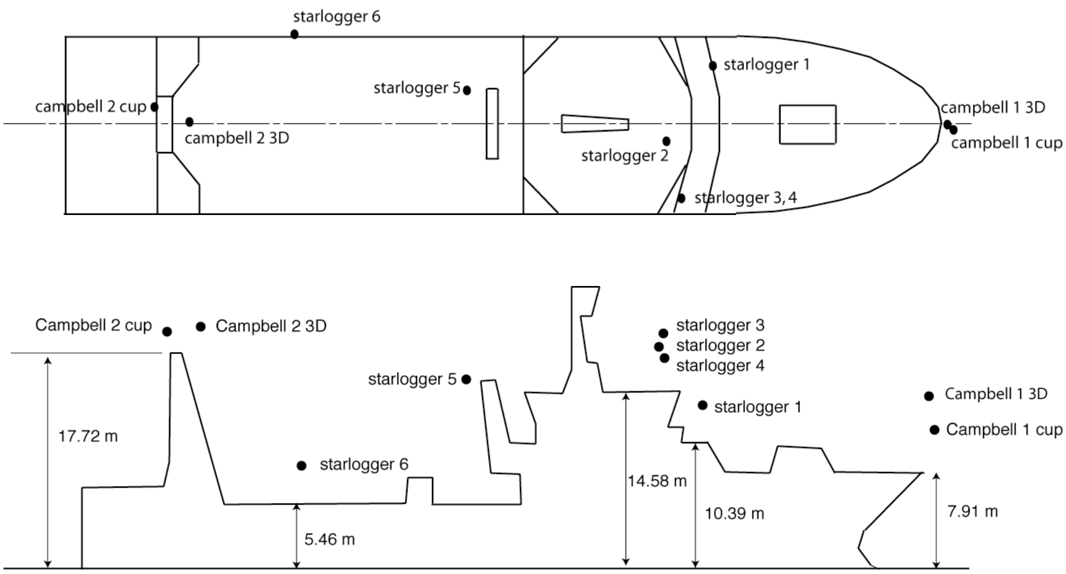

Figure 5 Schematic showing the instrument position and corresponding deck height. Note: the heights of the instruments above the sea surface and the distances from the centreline are shown in Section 2.2.

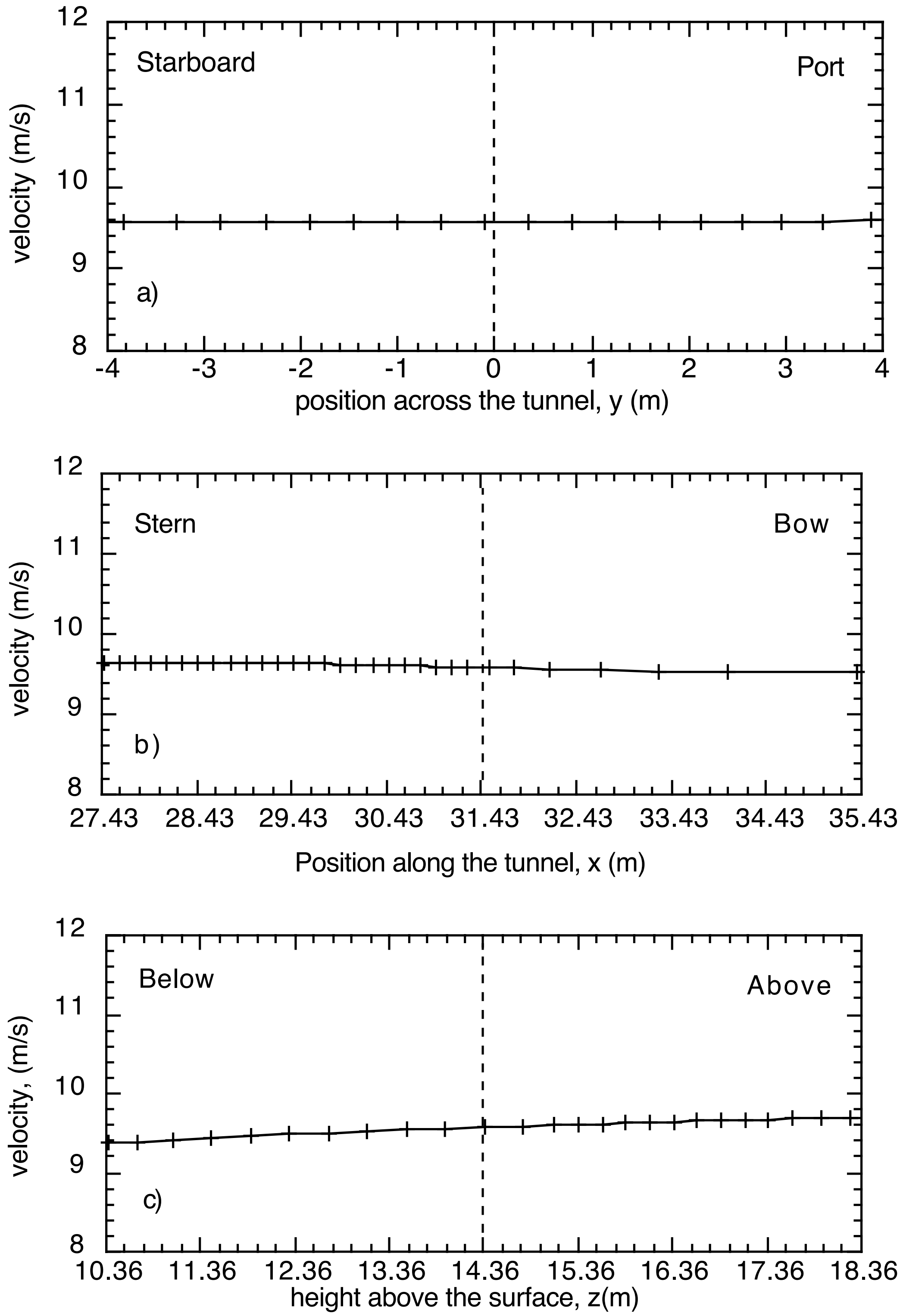

Figure 6 Lines of velocity data through the Campbell 1 3D anemometer position (indicated by the dashed line) in all three directions; a) across the tunnel (y). b) along the tunnel (x) and c) vertically (z). Results are from a bow-on flow (head to wind).

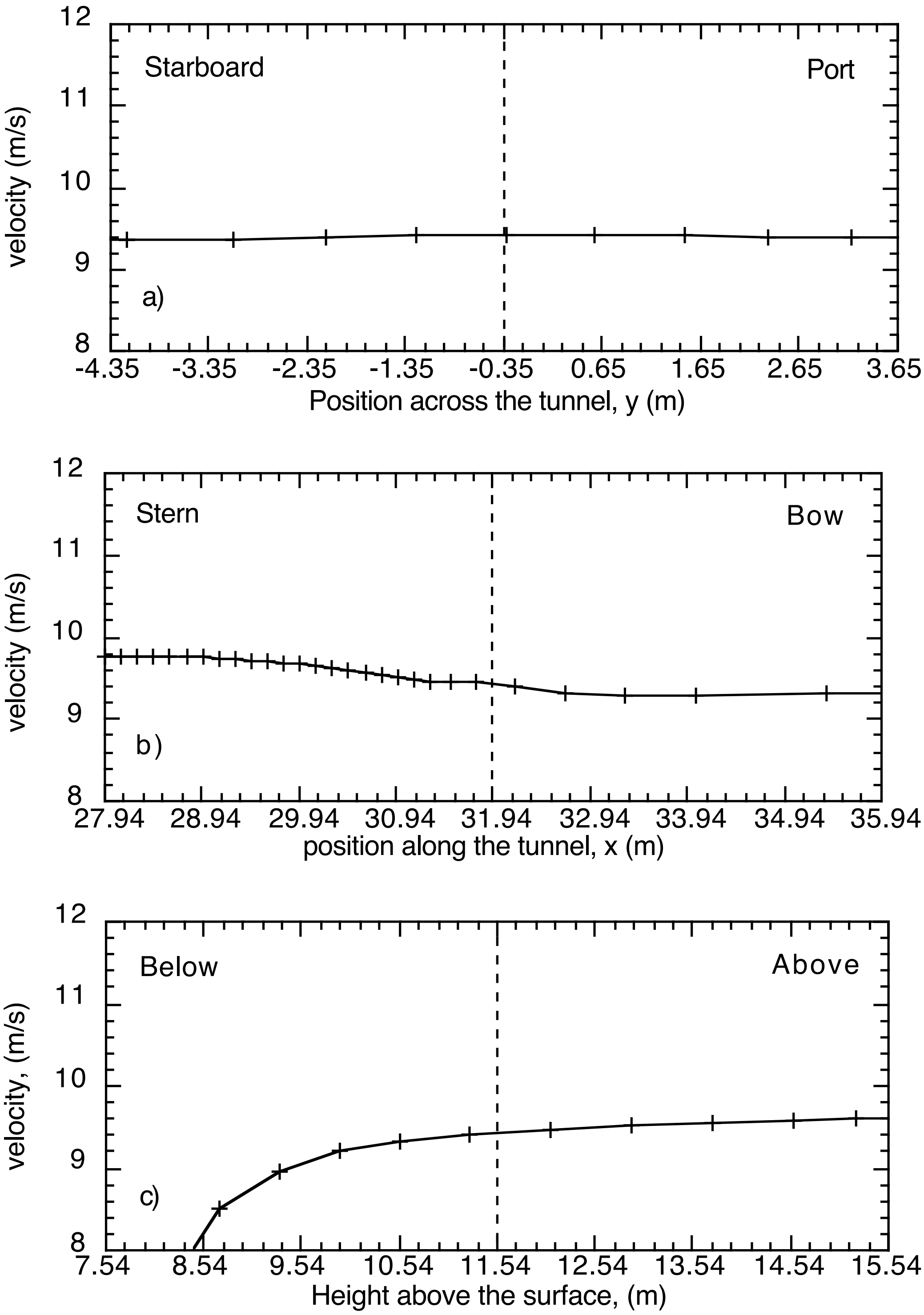

Figure 7 As for Figure 6, but for the Campbell 1 cup anemometer. Results are from a bow-on flow (head to wind).

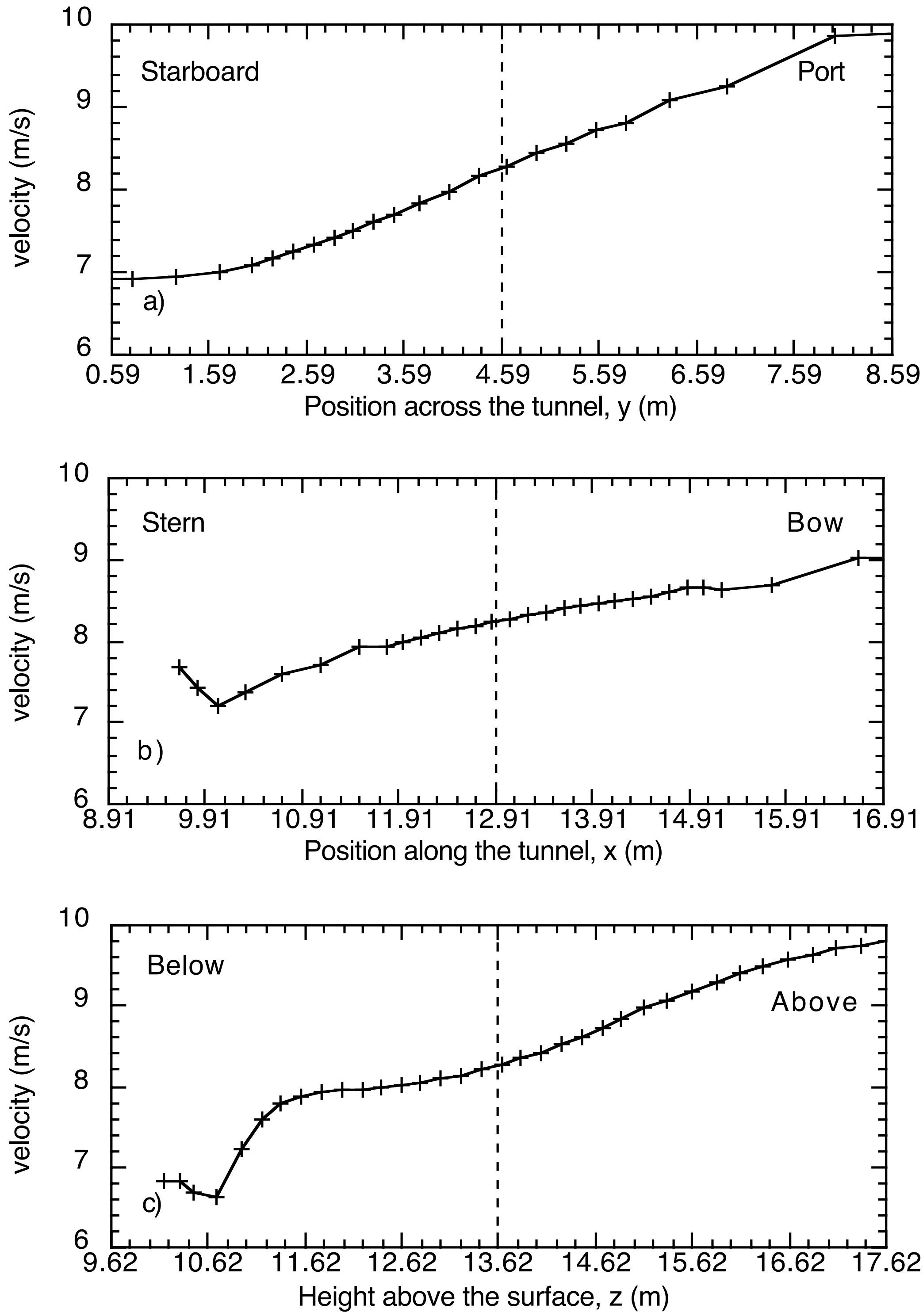

Figure 8 As for Figure 6, but for the Starlogger 1 cup anemometer. Results are from a bow-on flow (head to wind).

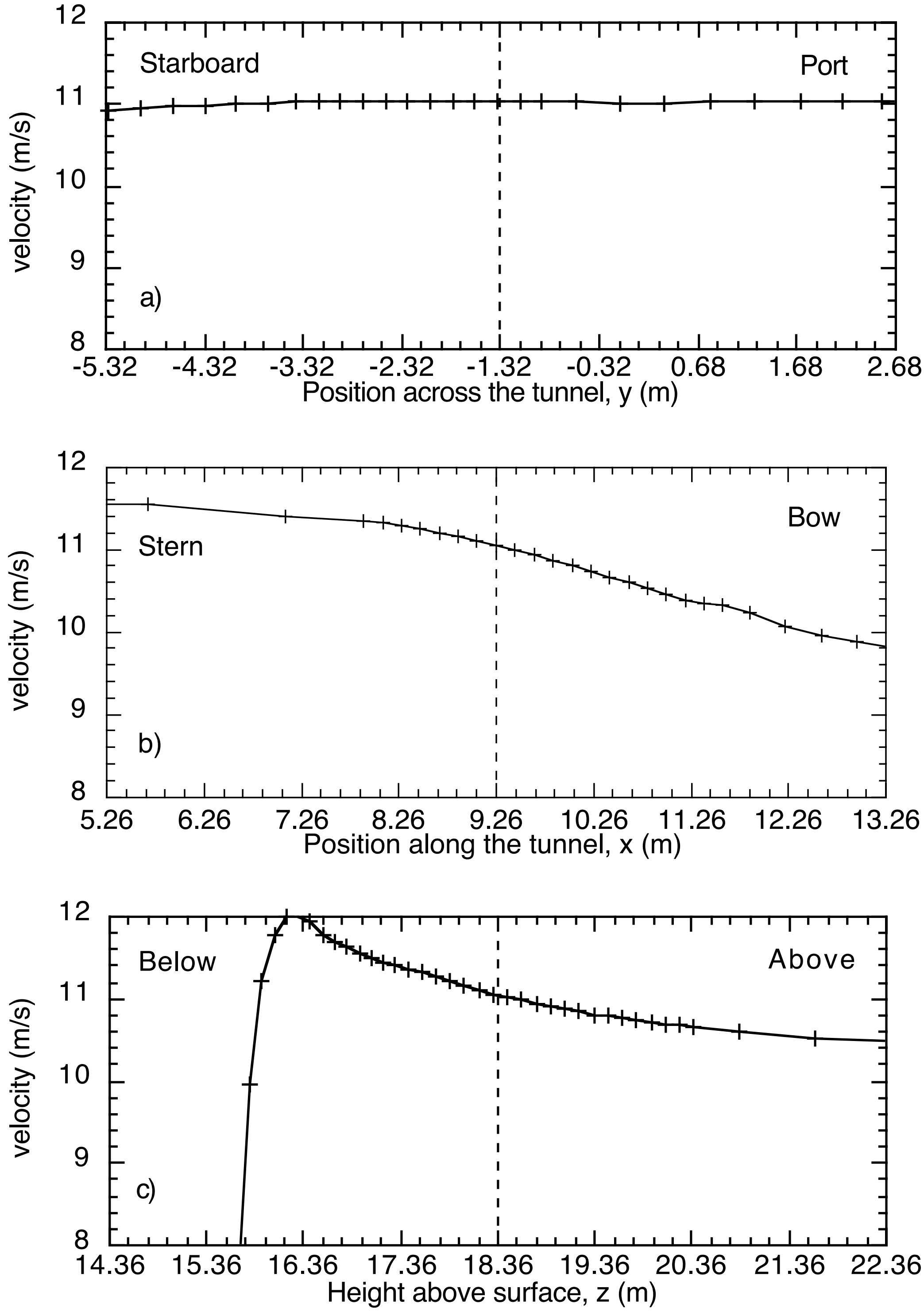

Figure 9 As for Figure 6, but for the Starlogger 2 cup anemometer. Results are from a bow-on flow (head to wind).

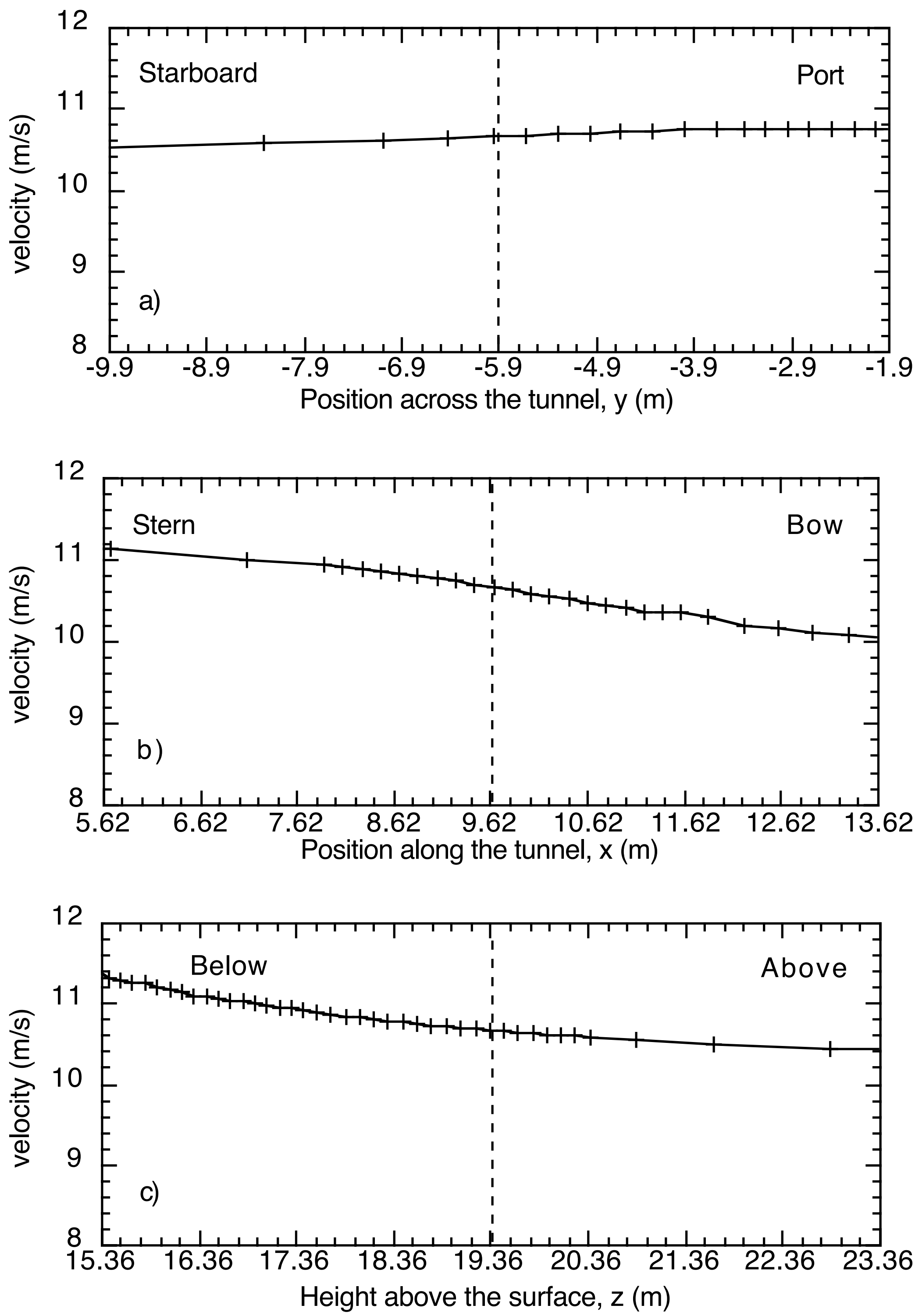

Figure 10 As for Figure 6, but for the Starlogger 3 cup anemometer. Results are from a bow-on flow (head to wind).

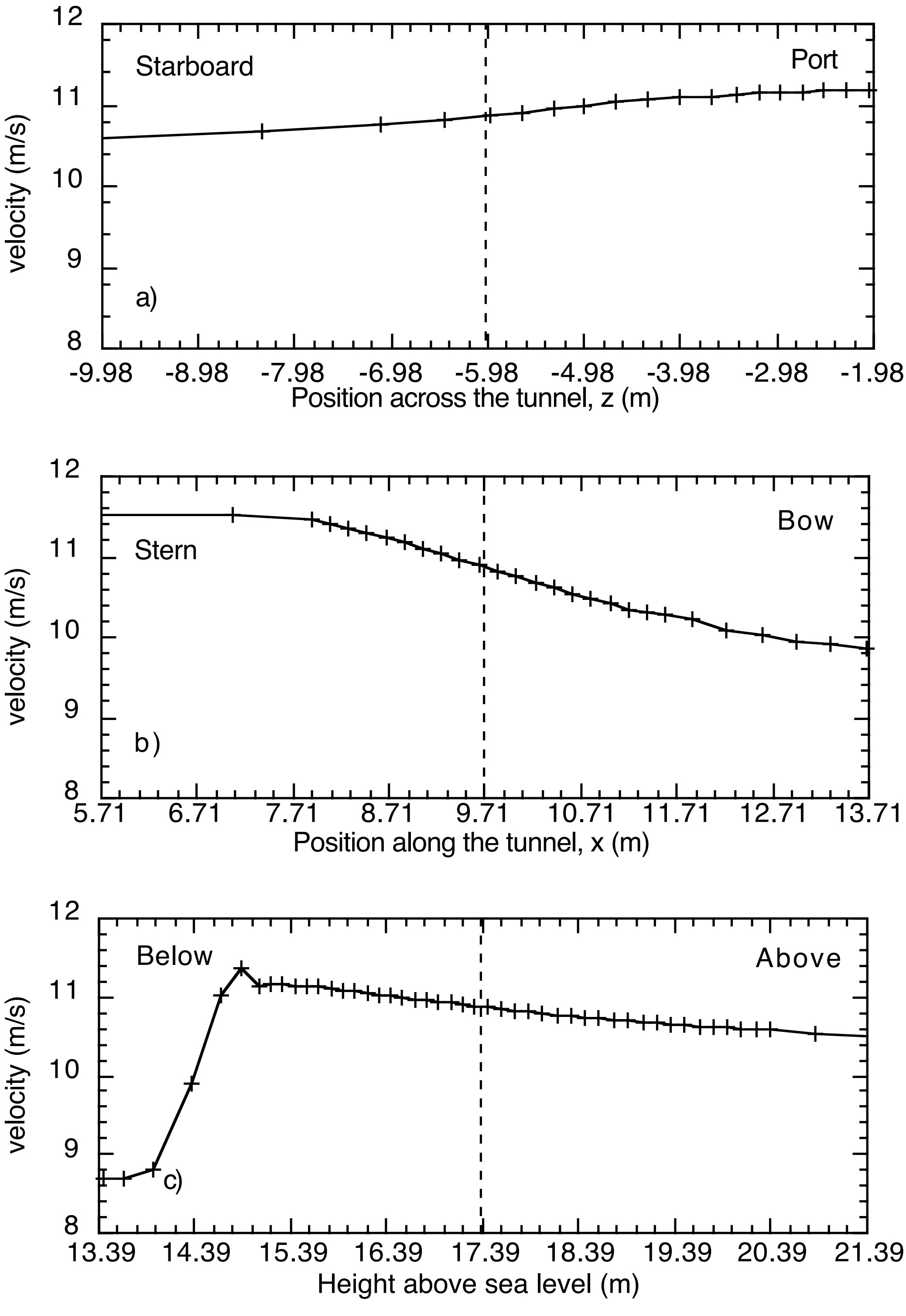

Figure 11 As for Figure 6, but for the Starlogger 4 cup anemometer. Results are from a bow-on flow (head to wind).

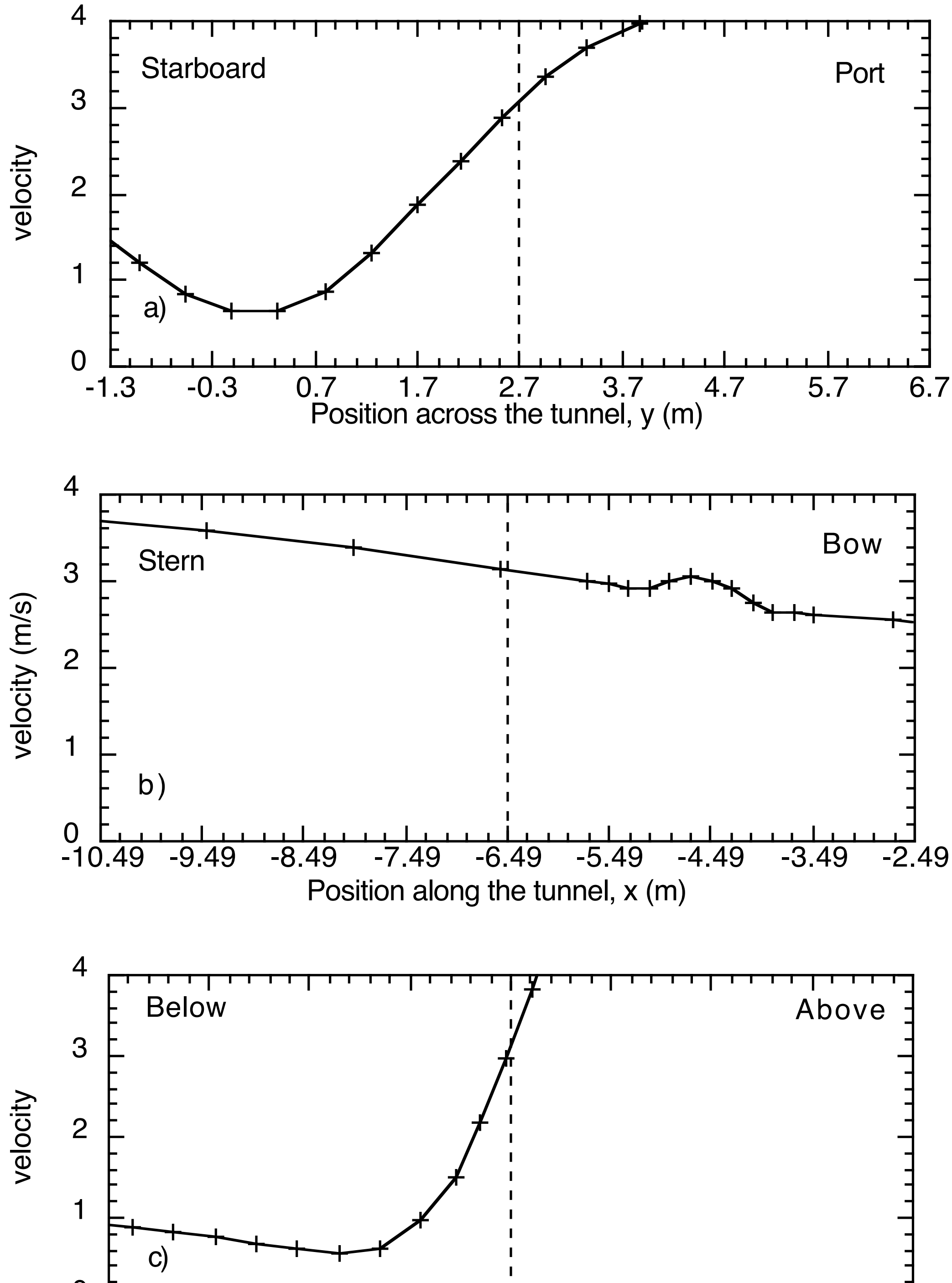

Figure 12 As for Figure 6, but for the Starlogger 5 cup anemometer. Results are from a bow-on flow (head to wind).

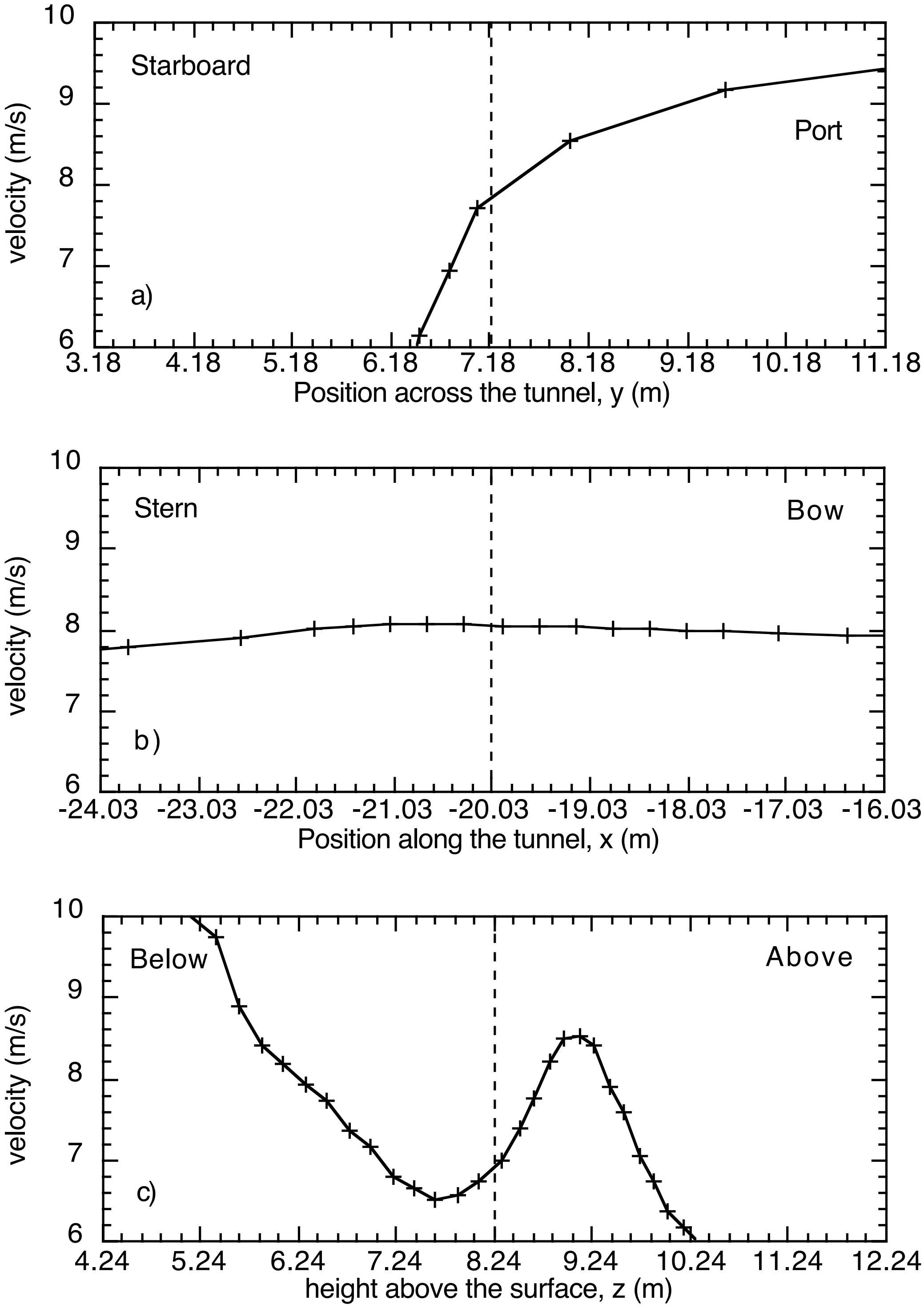

Figure 13 As for Figure 6, but for the Starlogger 6 cup anemometer. Results are from a bow-on flow (head to wind).

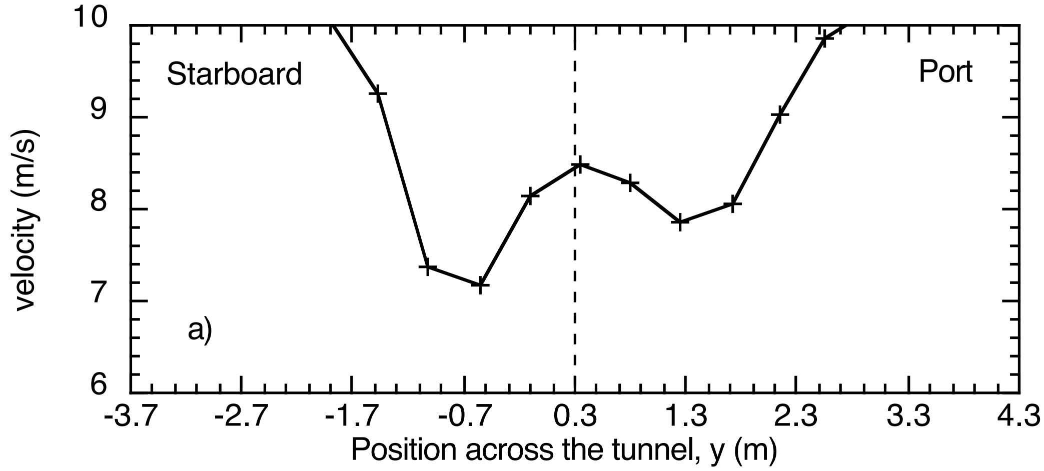

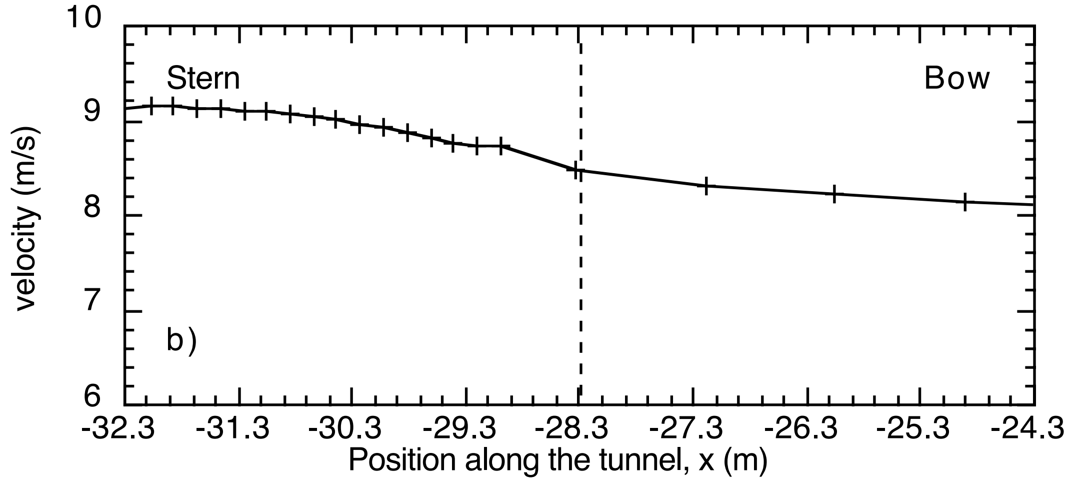

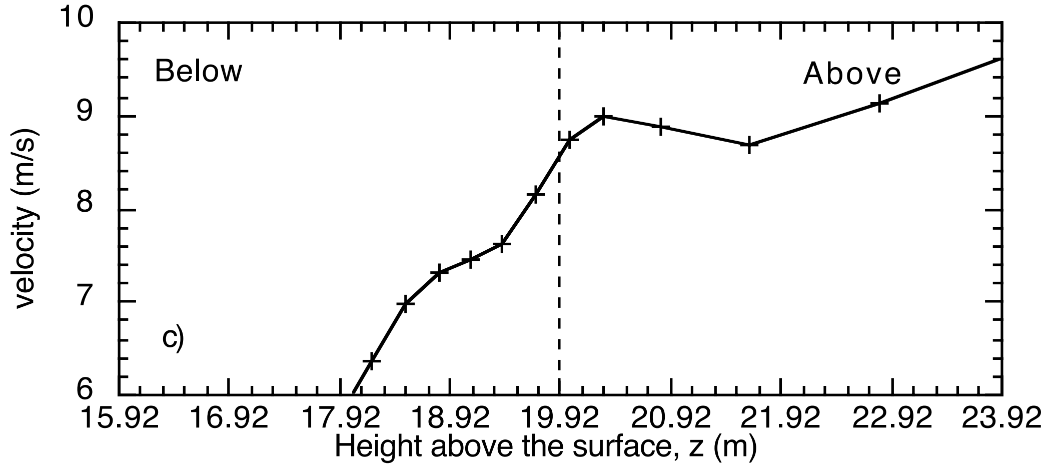

Figure 14 As for Figure 6, but for the Campbell 2 3D prop anemometer. Results are from a bow-on flow (head to wind).

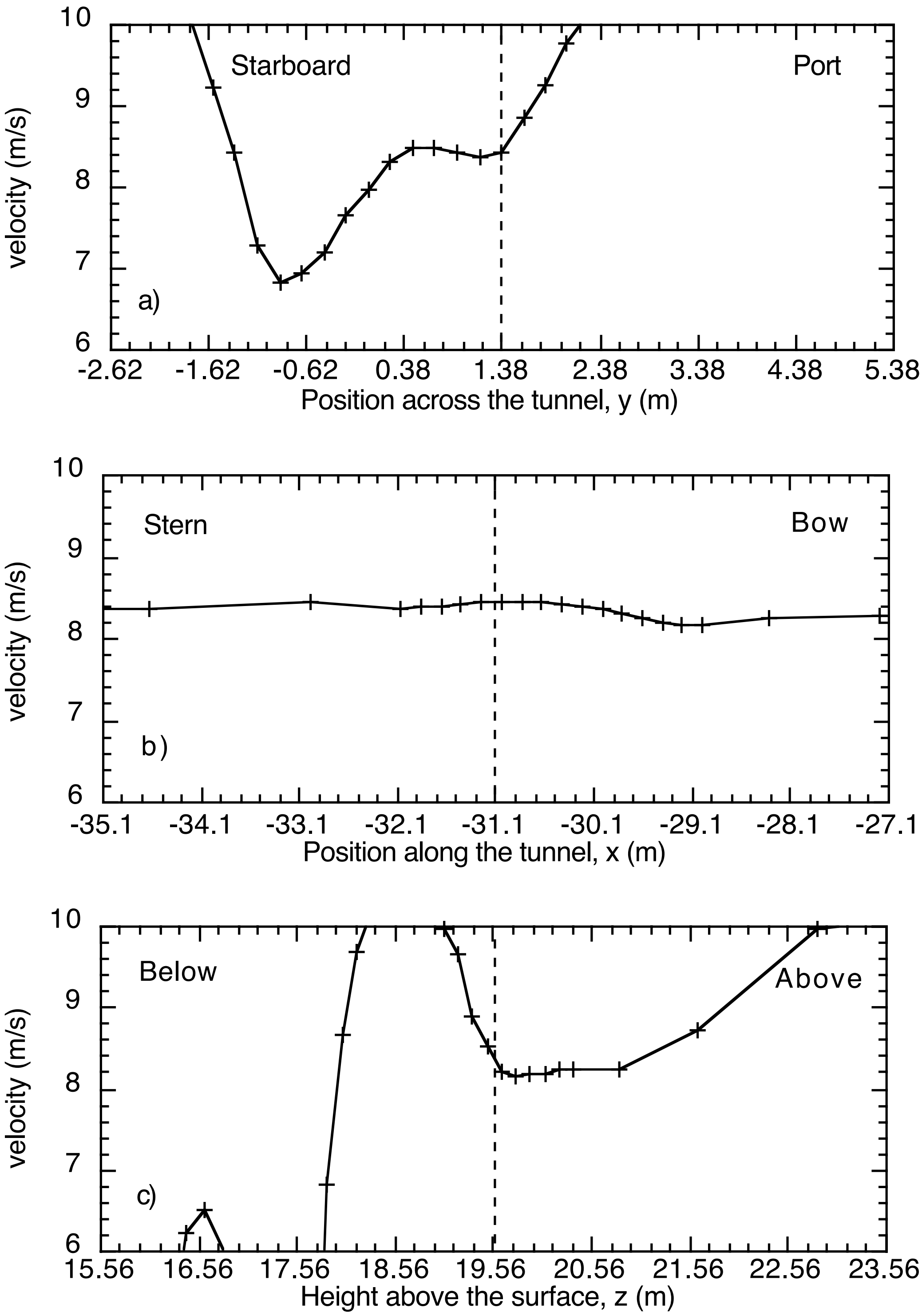

Figure 15 As for Figure 6, but for the Campbell 2 cup anemometer. Results are from a bow-on flow (head to wind).

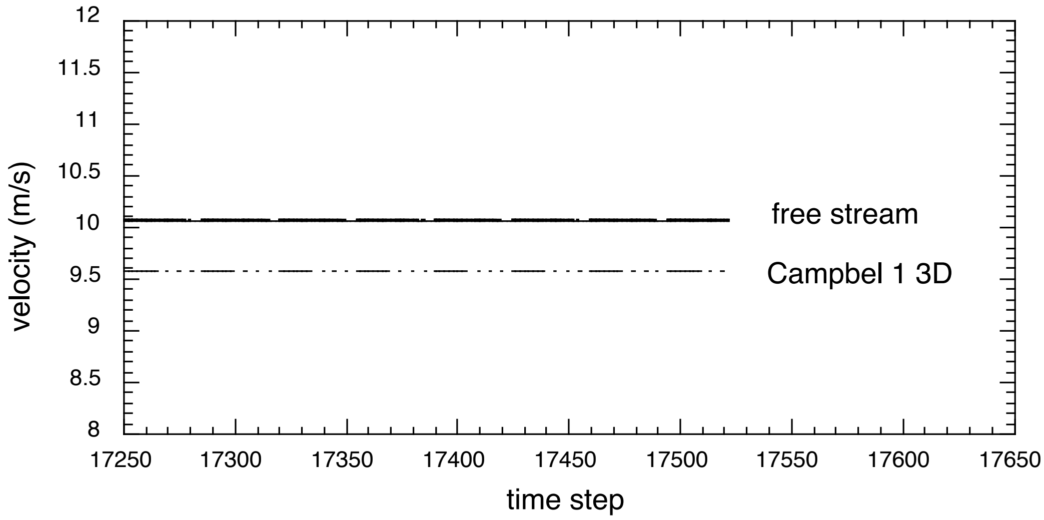

Figure 16 The velocity at each monitoring location in the 15 degree flow simulation. The last 250 time steps are shown.

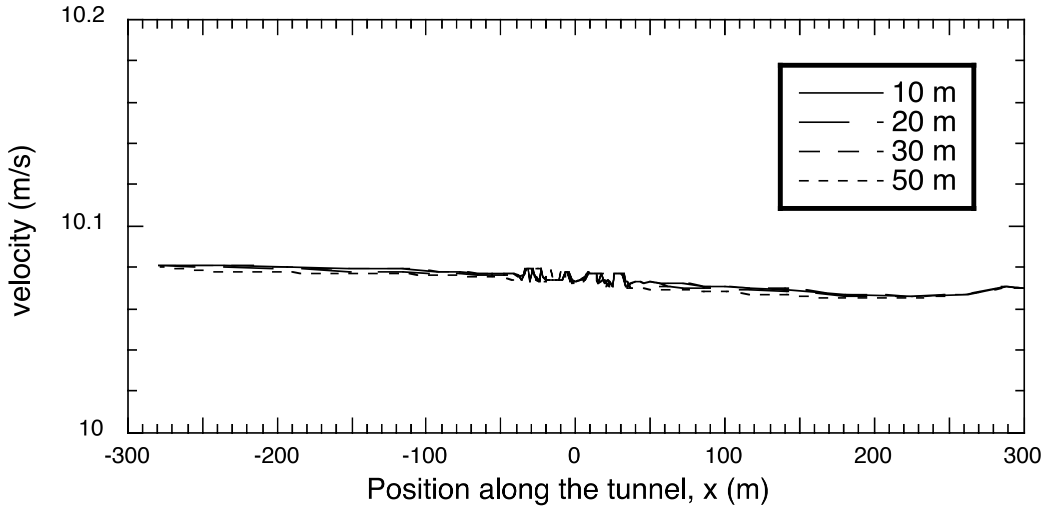

Figure 17a Lines of velocity data along the length of the tunnel at the heights shown. The data were obtained from the free stream region on the port side of the tunnel at y= 275 m.

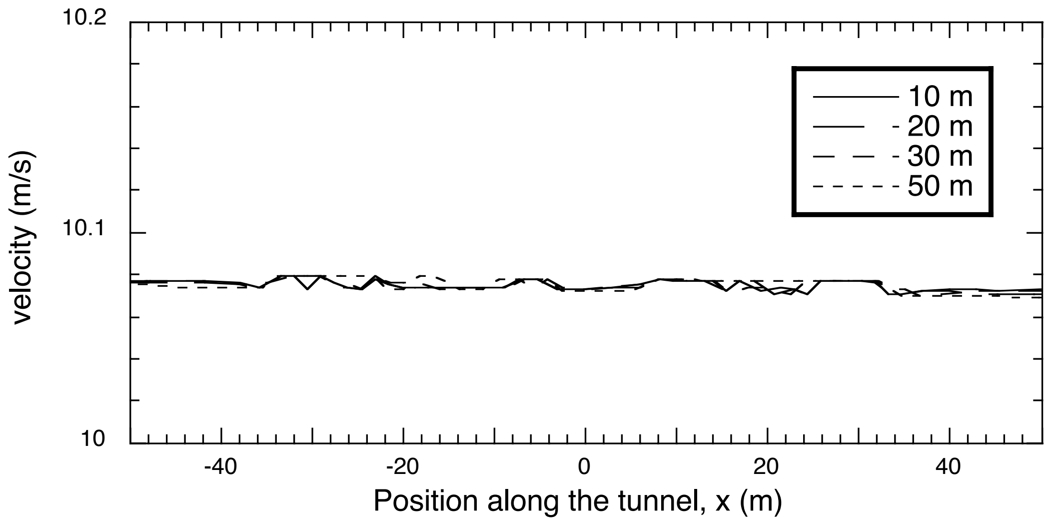

Figure 17b As Figure 17a, showing the central portion of the tunnel only.

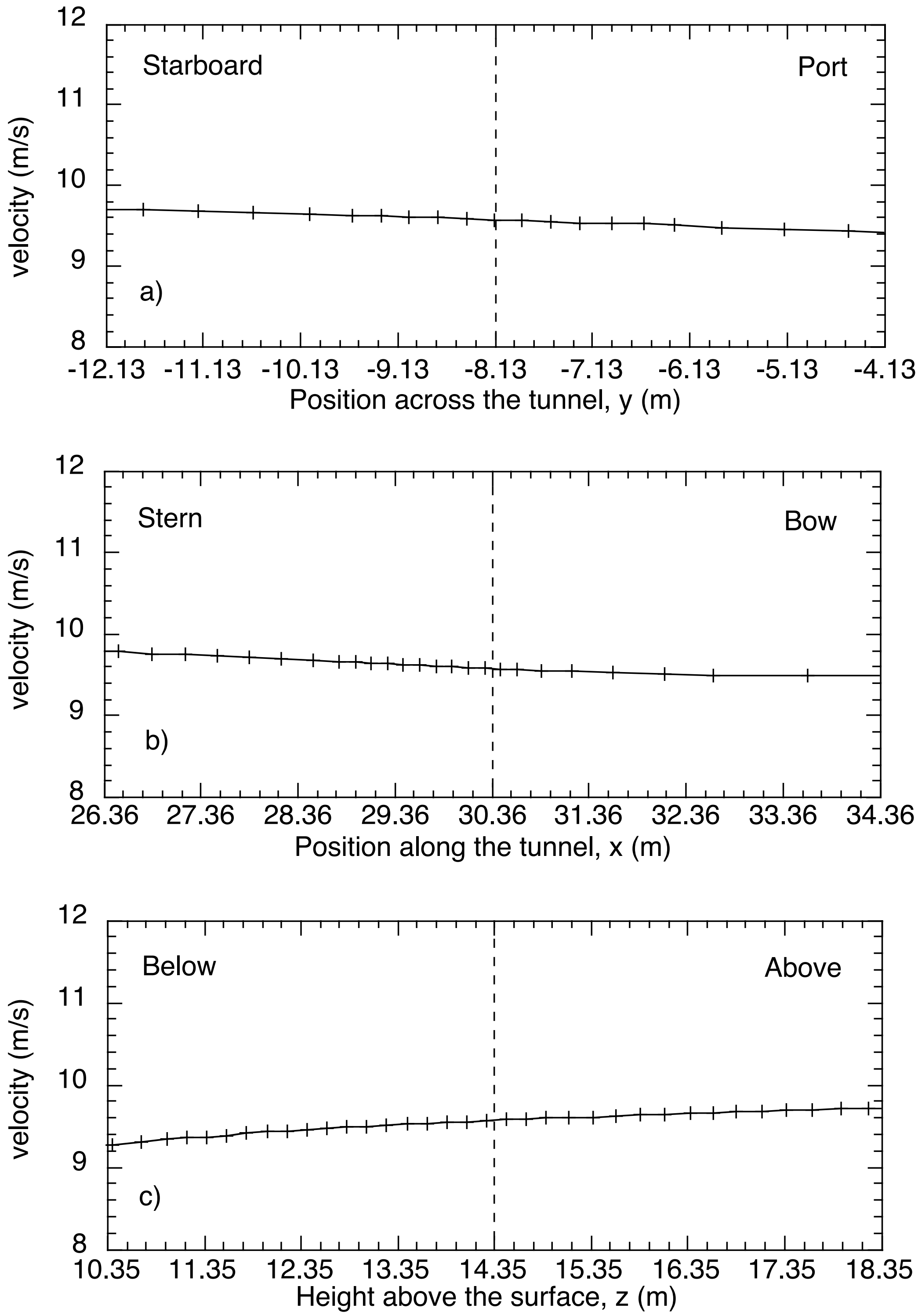

Figure 18 Lines of velocity data through the Campbell 1 3D anemometer position (indicated by the dashed line) in all three directions; a) across the tunnel (y). b) along the tunnel (x) and c) vertically (z). Results are from a flow 15° off the port bow.

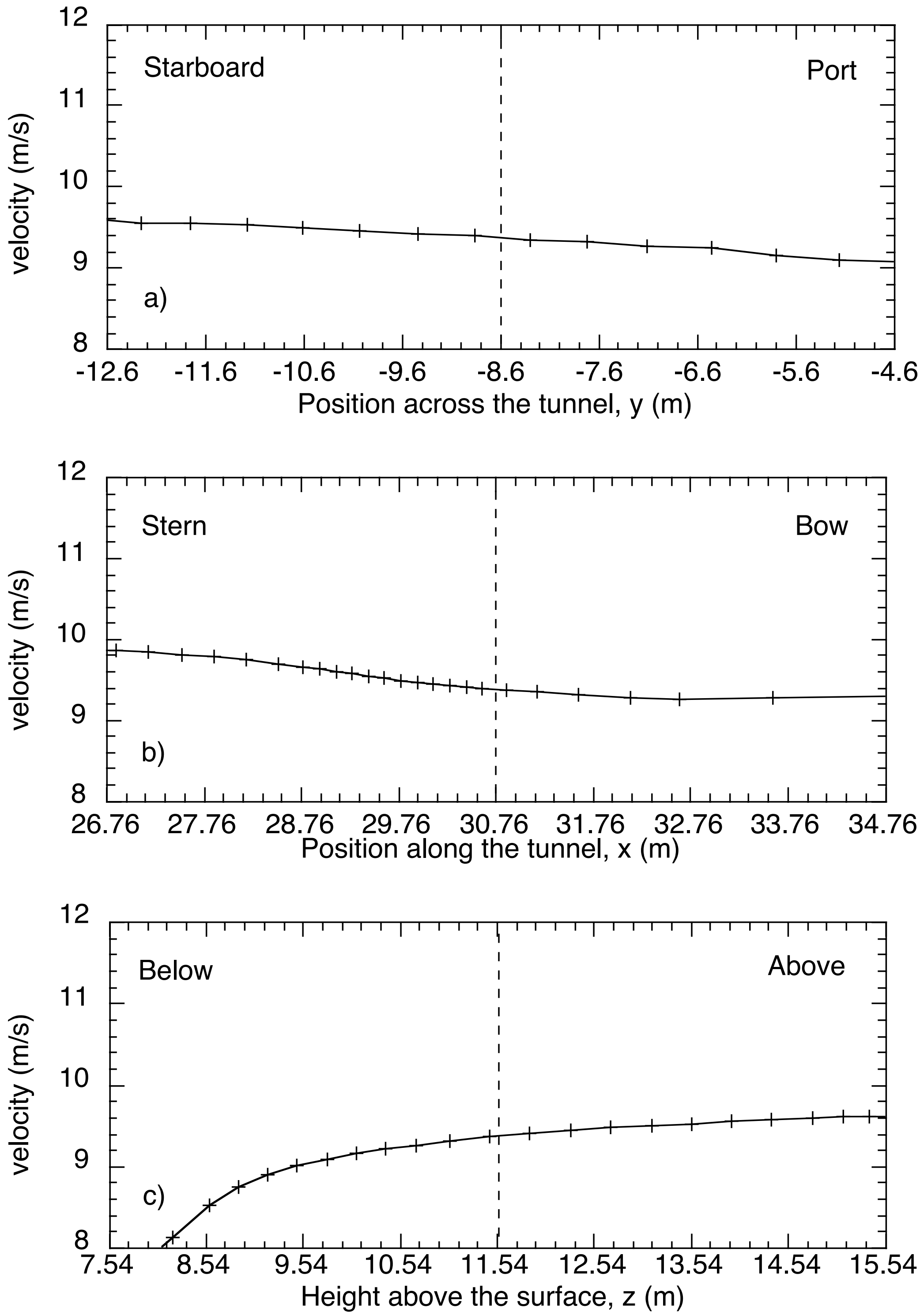

Figure 19 As for Figure 18, but for the Campbell 1 cup anemometer. Results are from a flow 15° off the port bow.

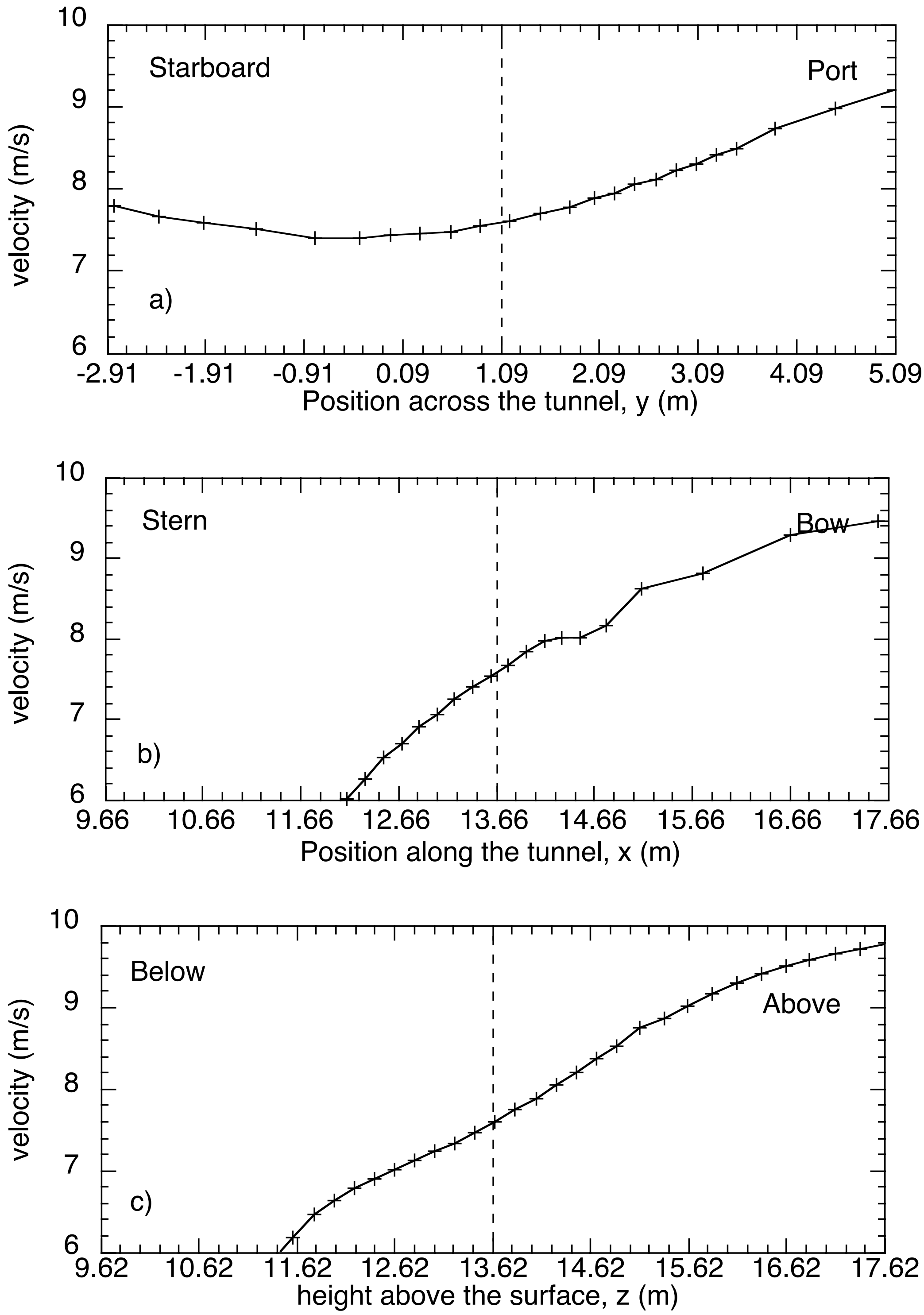

Figure 20 As for Figure 18, but for the Starlogger 1 cup anemometer. Results are from a flow 15° off the port bow.

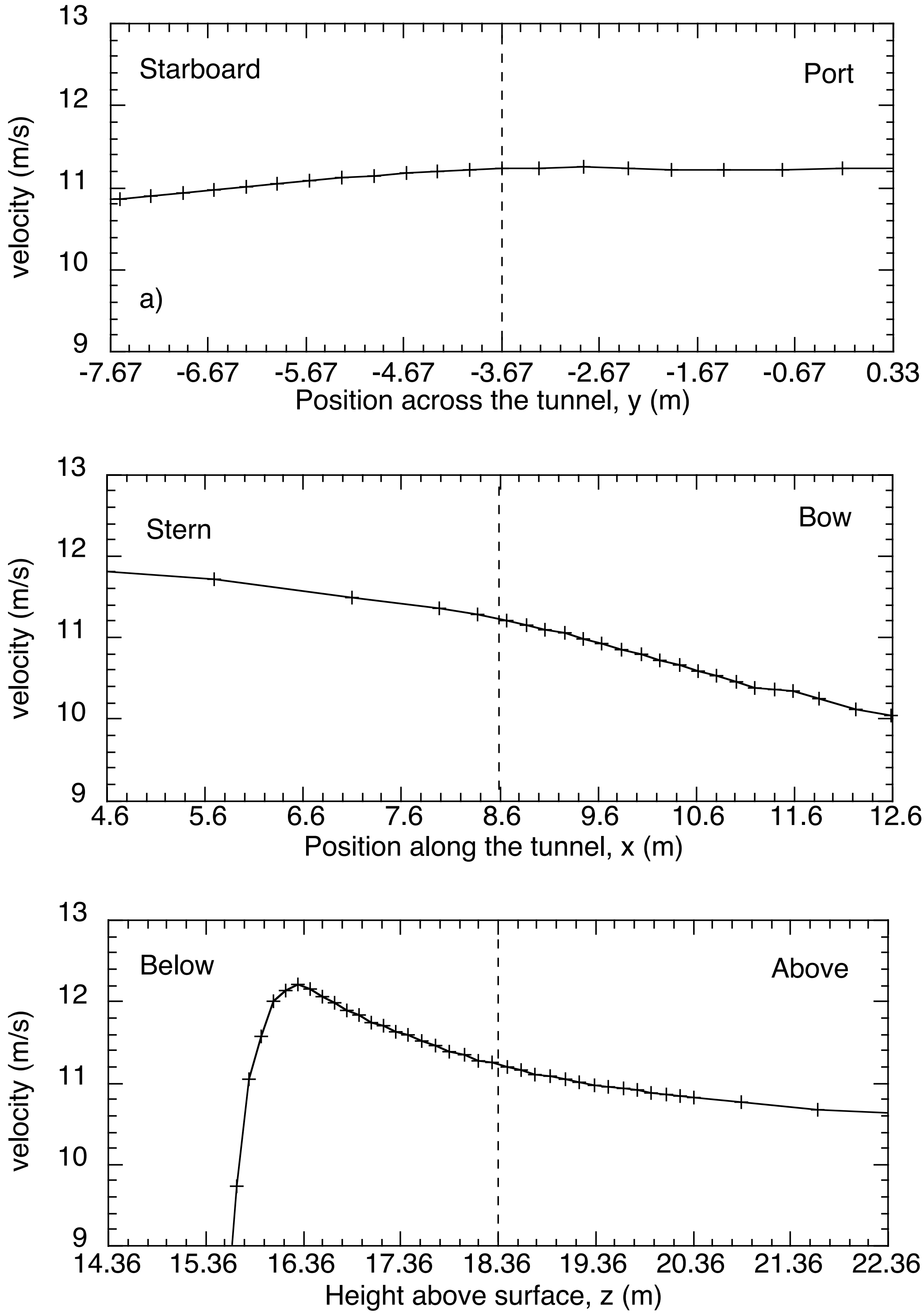

Figure 21 As for Figure 18, but for the Starlogger 2 cup anemometer. Results are from a flow 15° off the port bow.

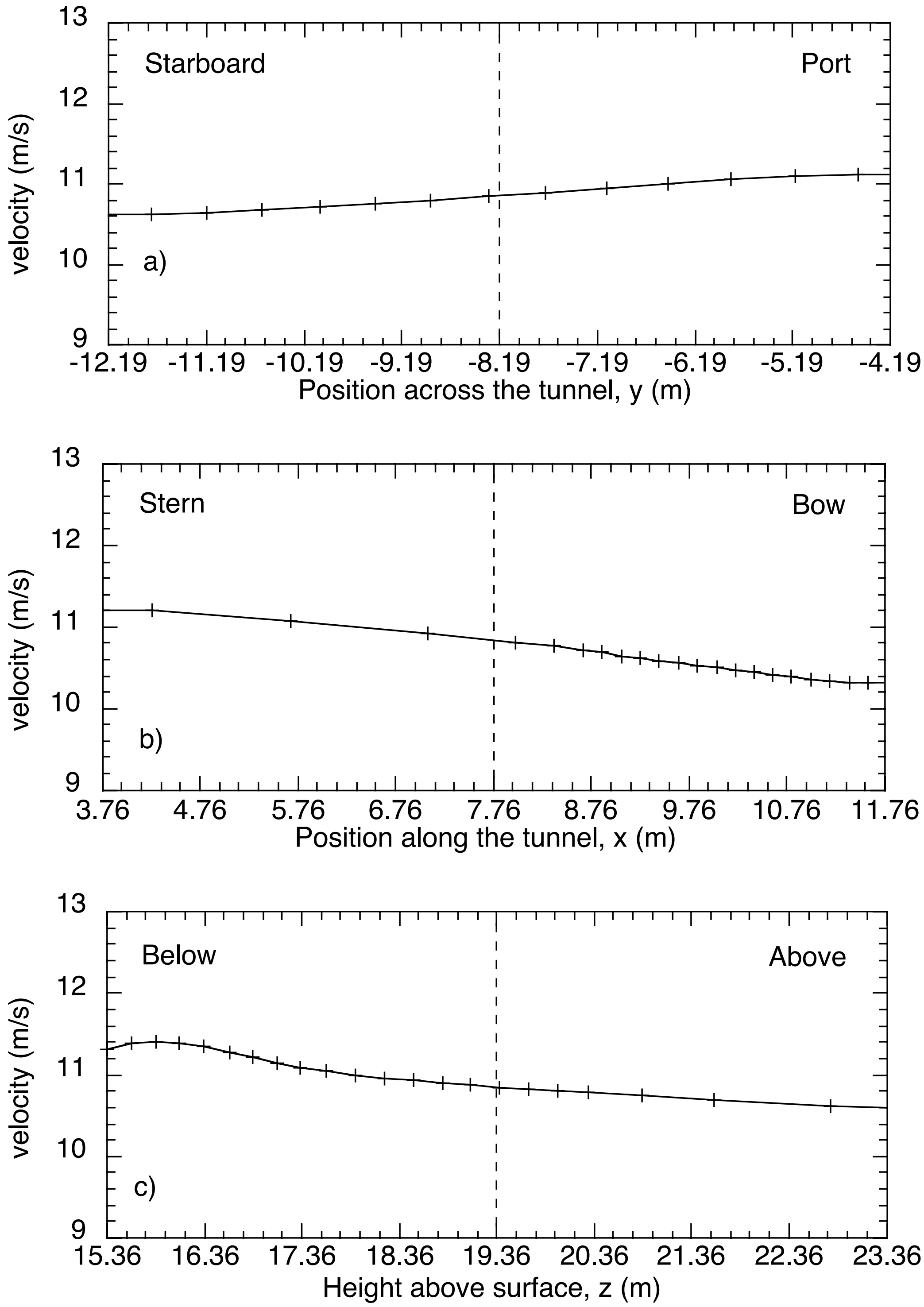

Figure 22 As for Figure 18, but for the Starlogger 3 cup anemometer. Results are from a flow 15° off the port bow.

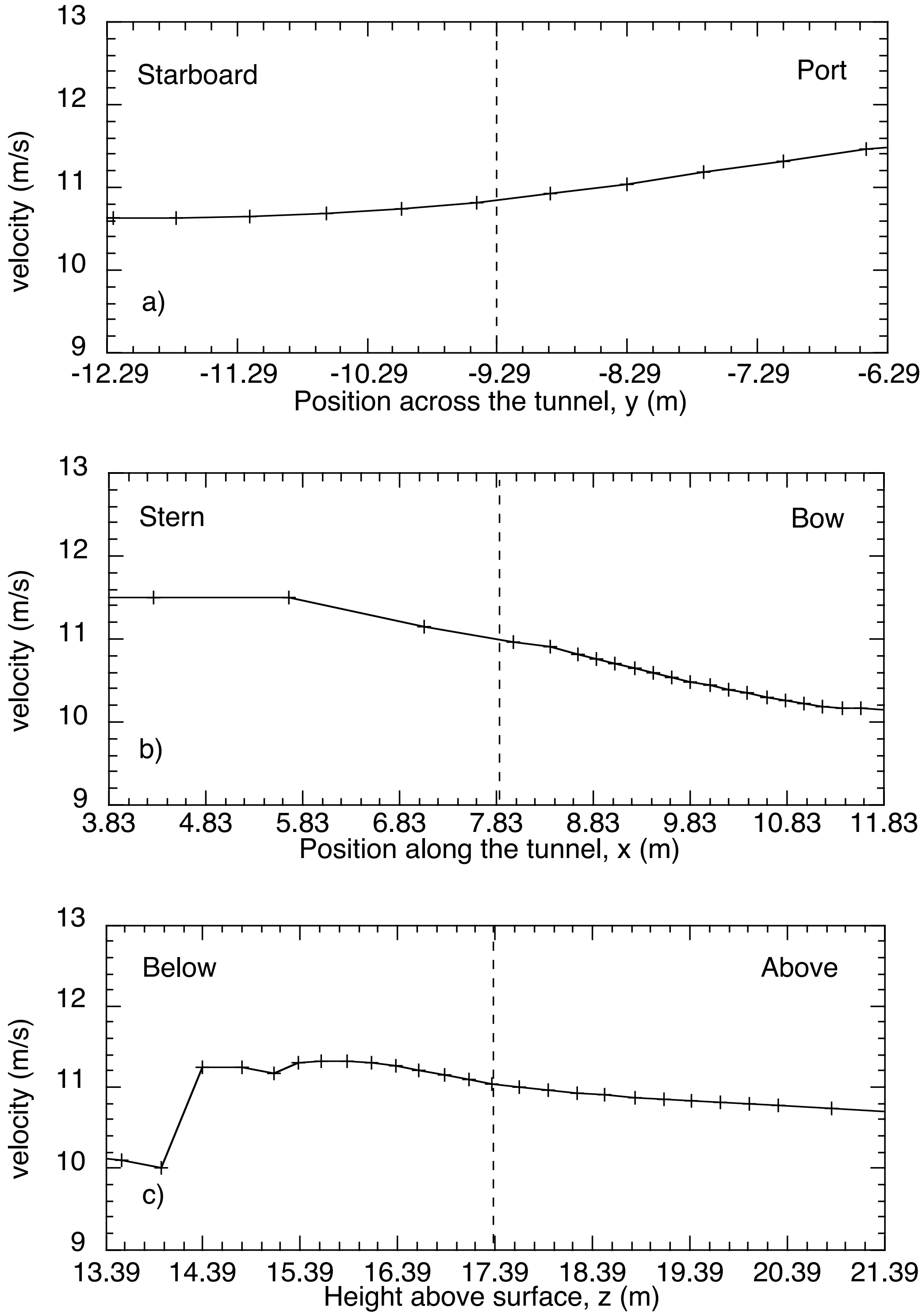

Figure 23 As for Figure 18, but for the Starlogger 4 cup anemometer. Results are from a flow 15° off the port bow.

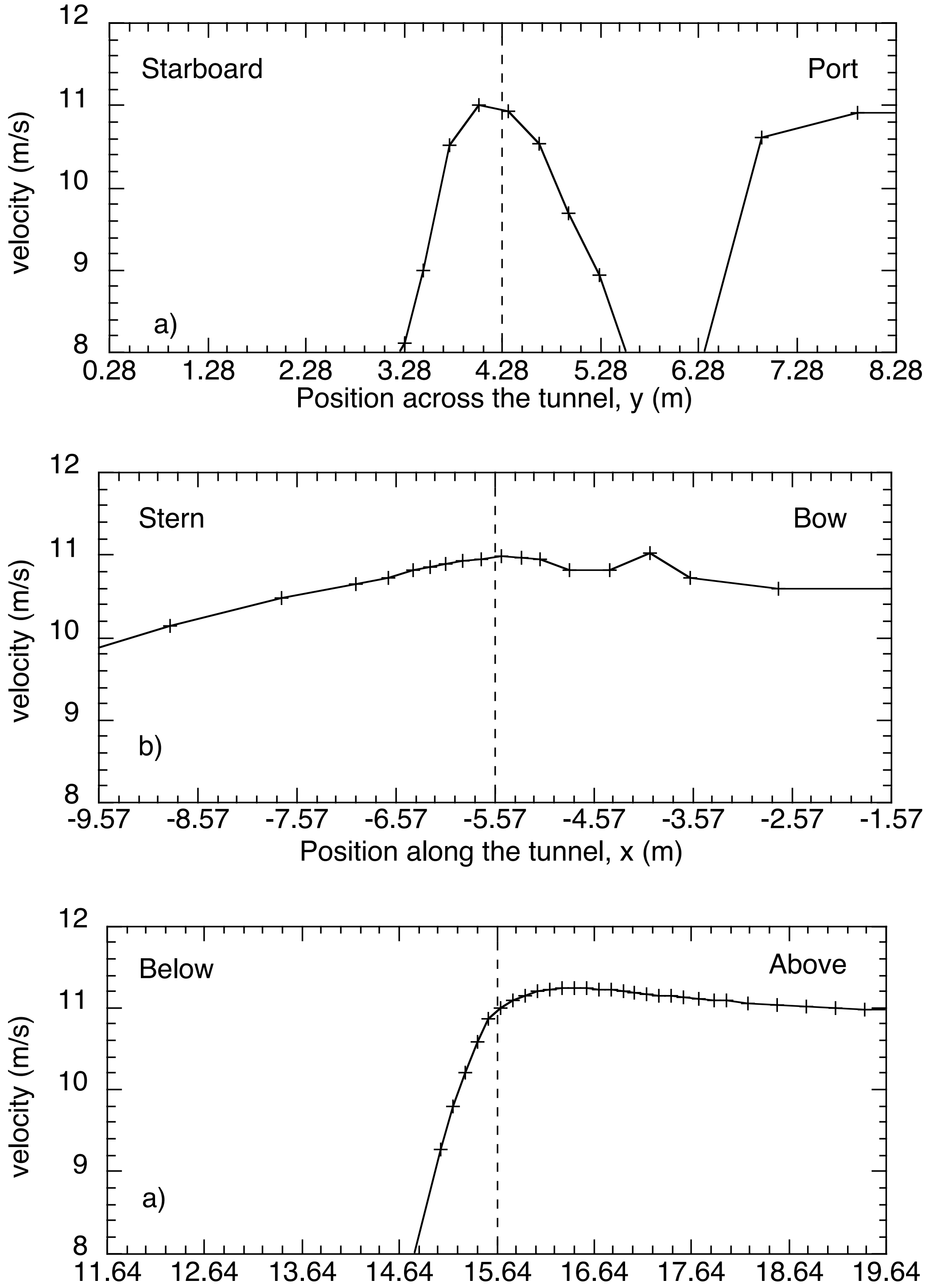

Figure 24 As for Figure 18, but for the Starlogger 5 cup anemometer. Results are from a flow 15° off the port bow.

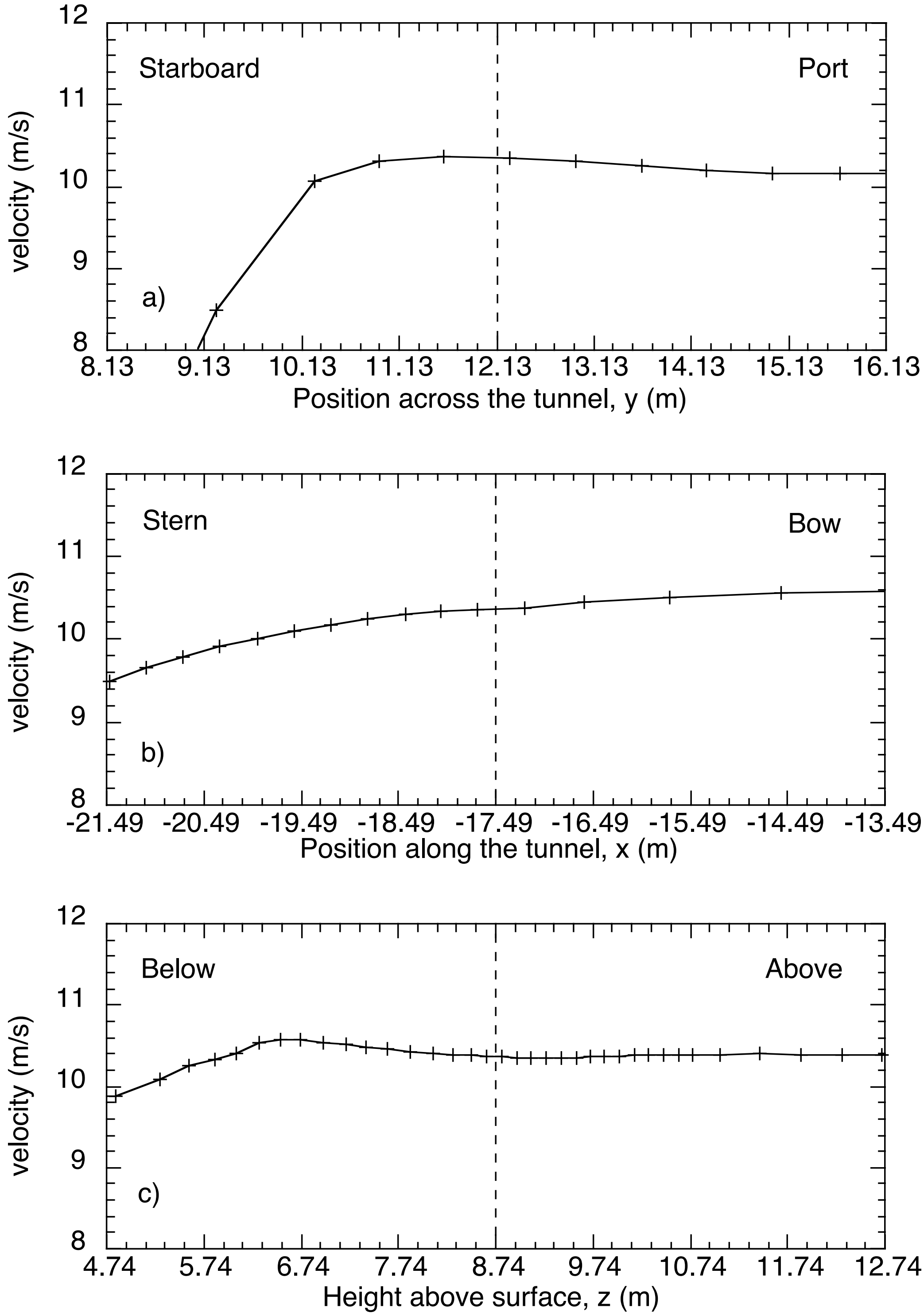

Figure 25 As for Figure 18, but for the Starlogger 6 cup anemometer. Results are from a flow 15° off the port bow.

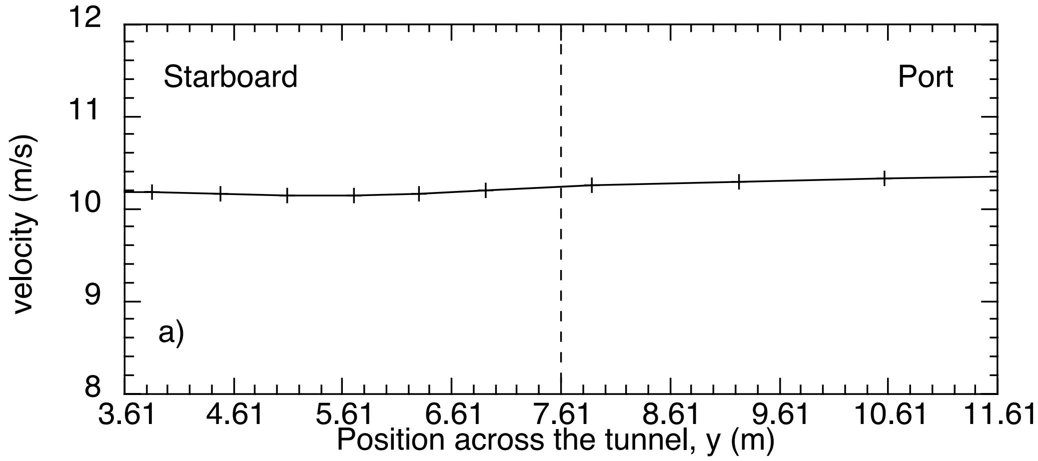

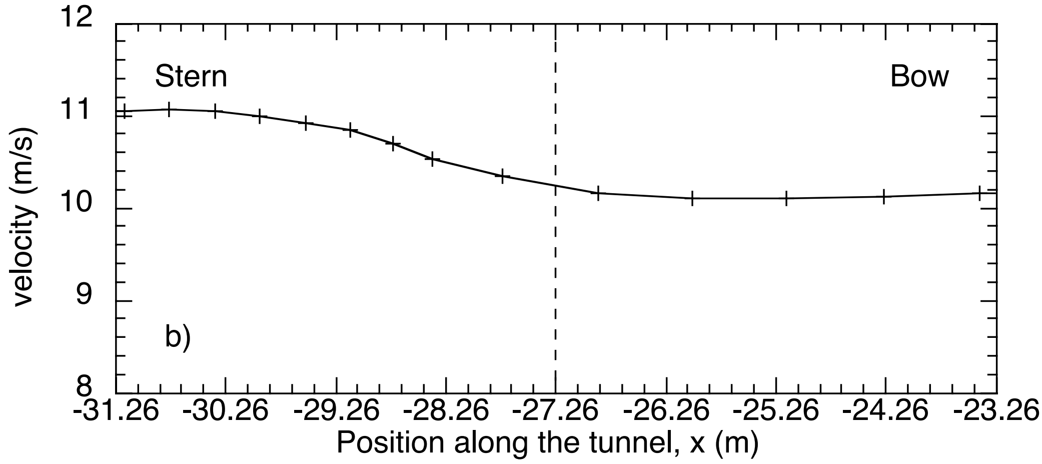

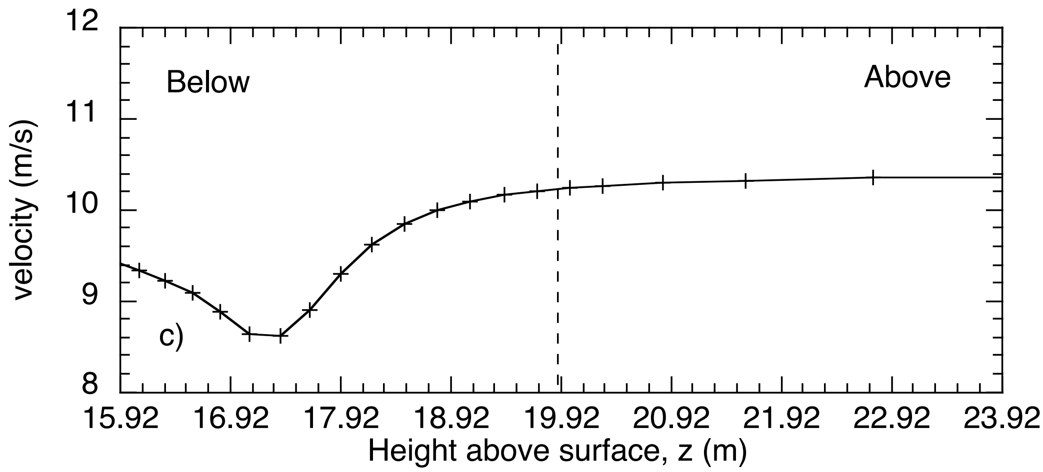

Figure 26 As for Figure 18, but for the Campbell 2 3D prop anemometer. Results are from a flow 15° off the port bow.

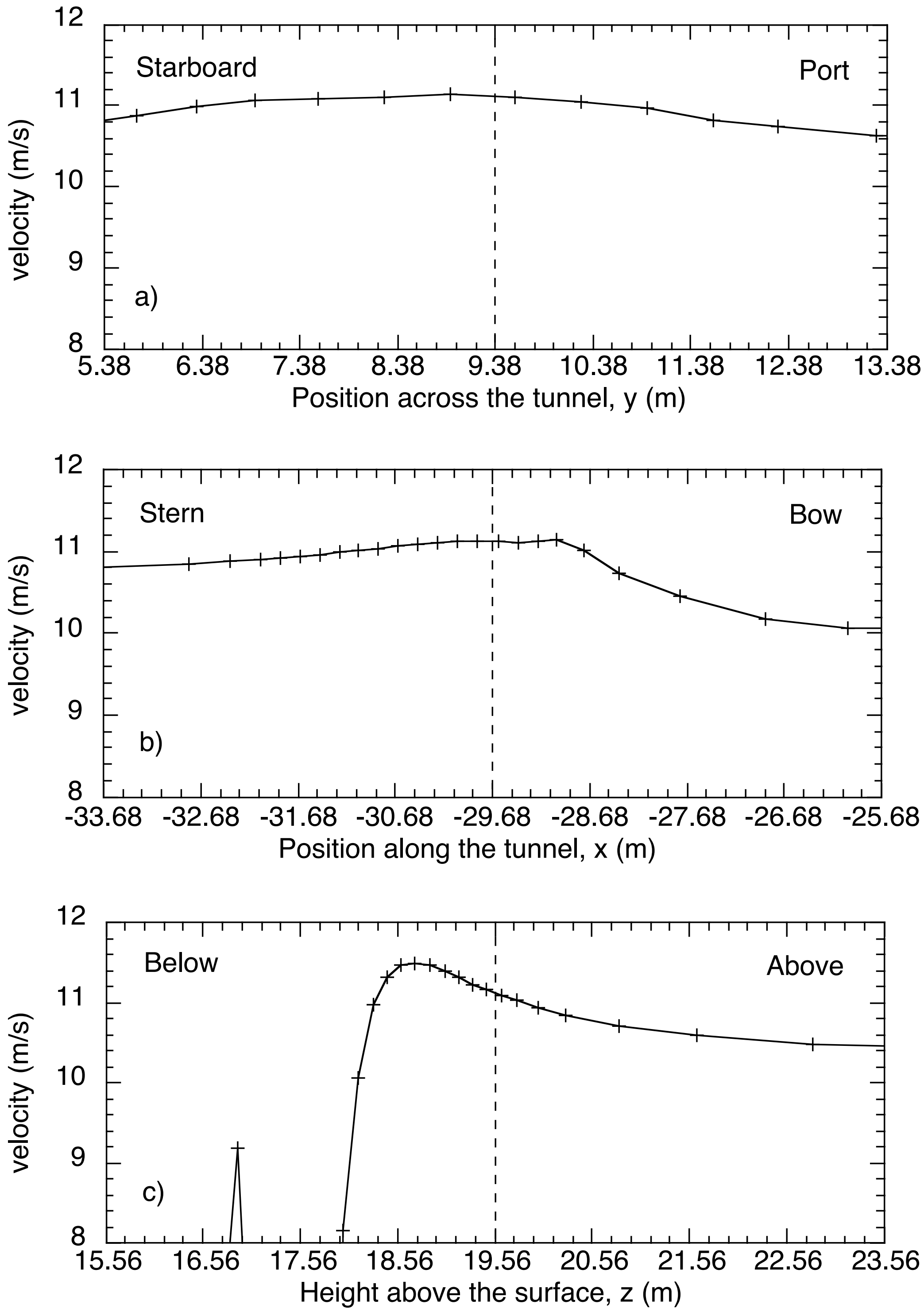

Figure 27 As for Figure 18, but for the Campbell 2 cup anemometer. Results are from a flow 15° off the port bow.

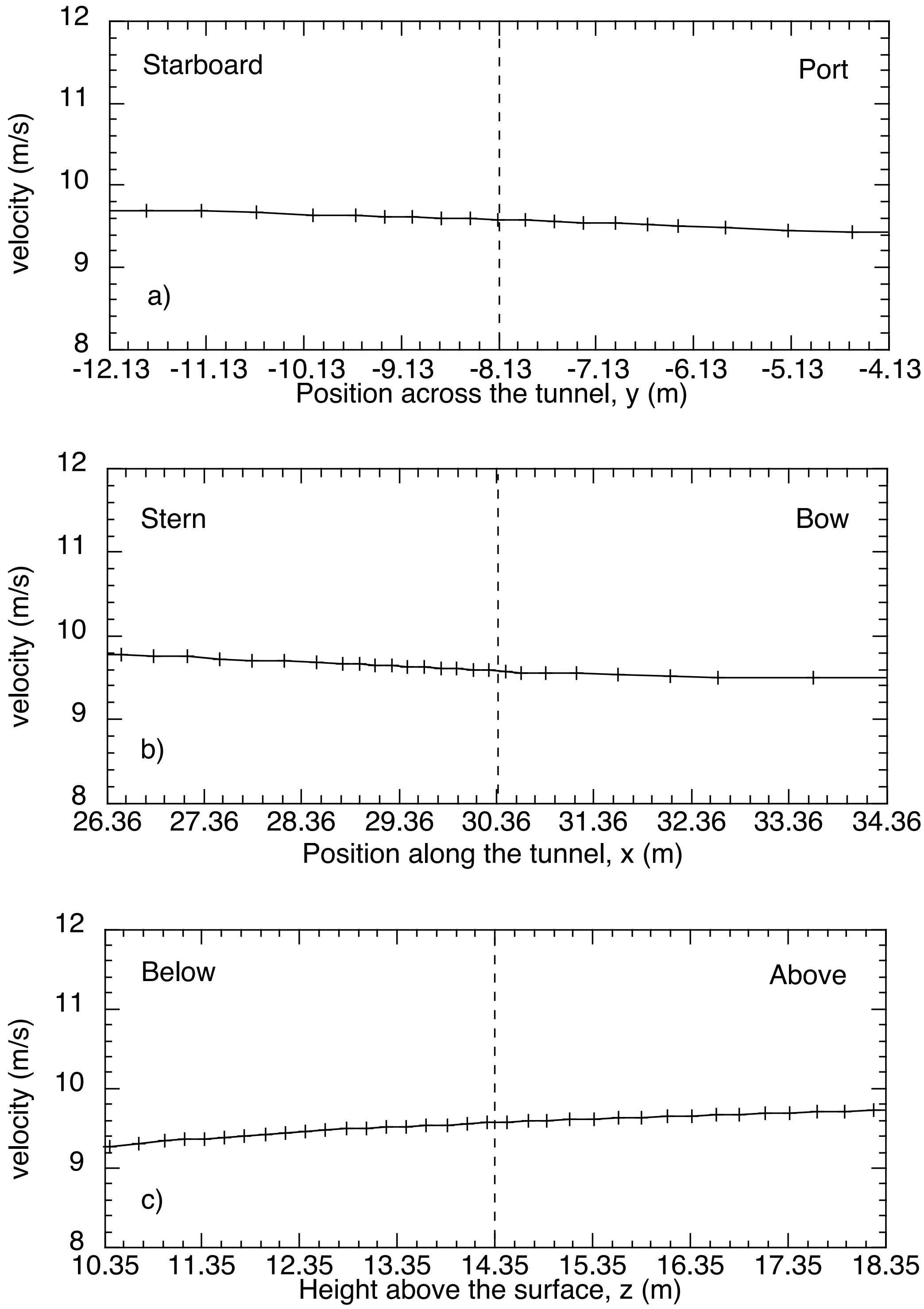

Figure 28 Lines of velocity data through the Campbell 1 3D anemometer position (indicated by the dashed line) in all three directions; a) across the tunnel (y). b) along the tunnel (x) and c) vertically (z). Results are from a flow 15° off the starboard bow.

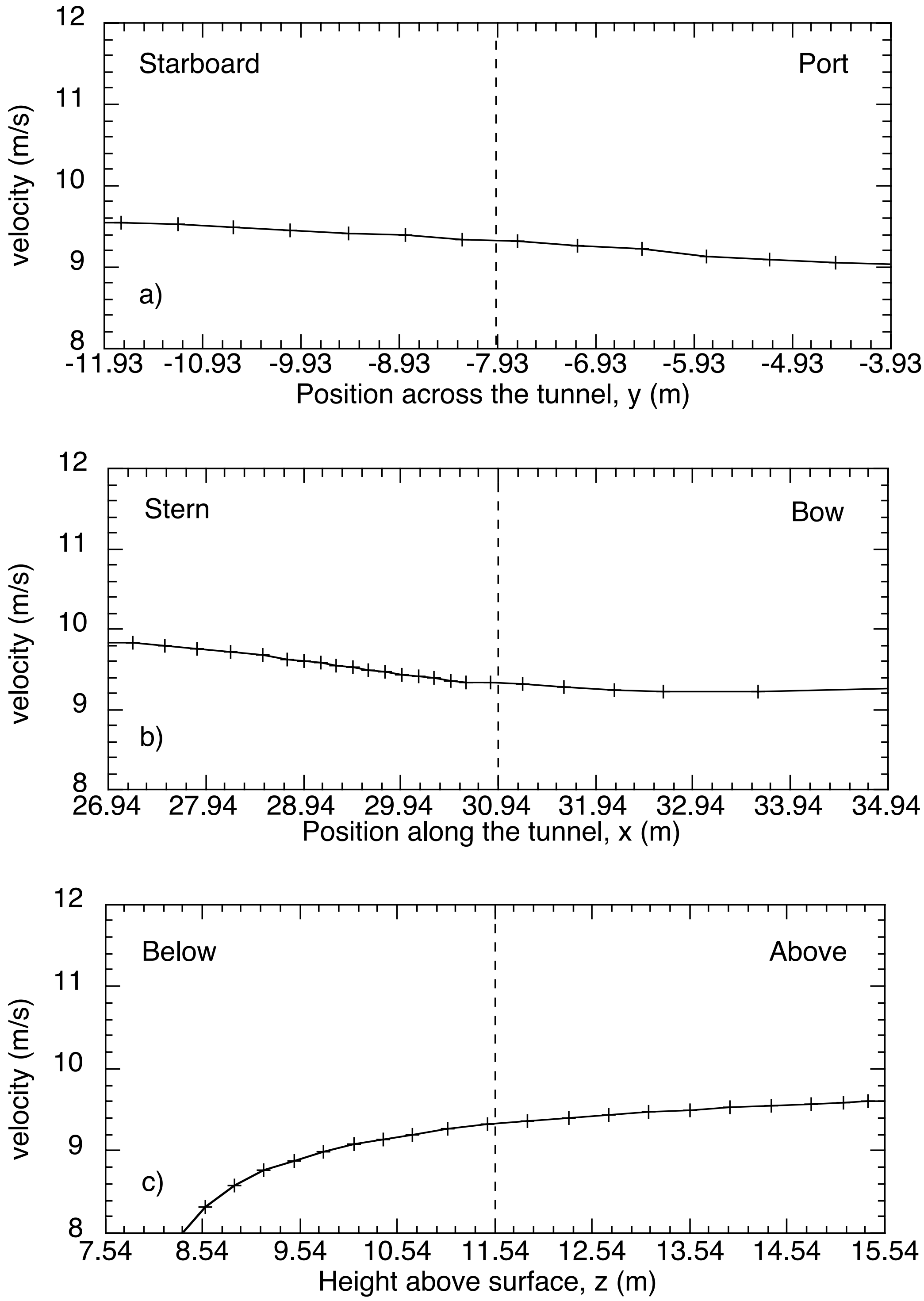

Figure 29 As for Figure 28, but for the Campbell 1 cup anemometer. Results are from a flow 15° off the starboard bow.

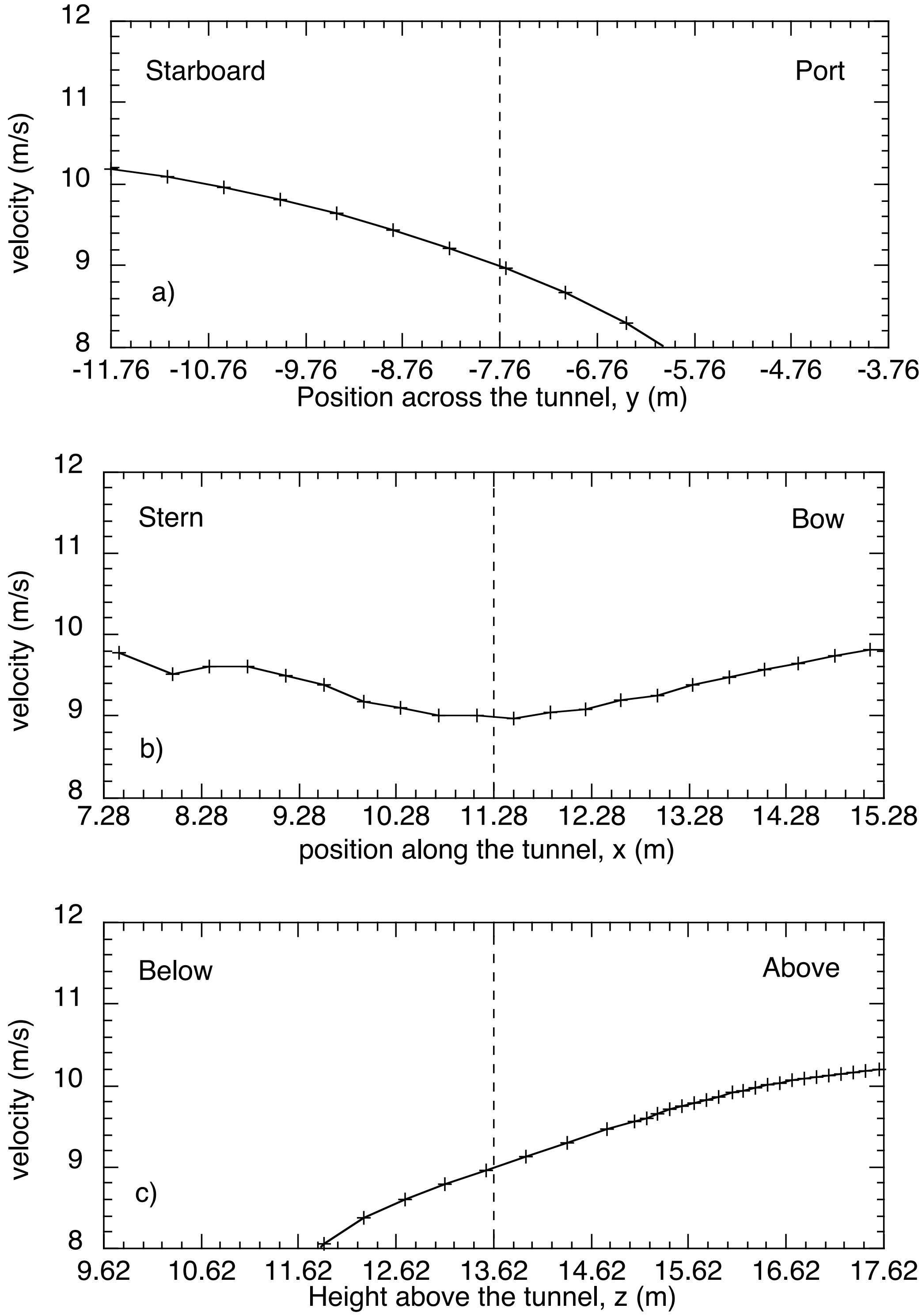

Figure 30 As for Figure 28, but for the Starlogger 1 cup anemometer. Results are from a flow 15° off the starboard bow.

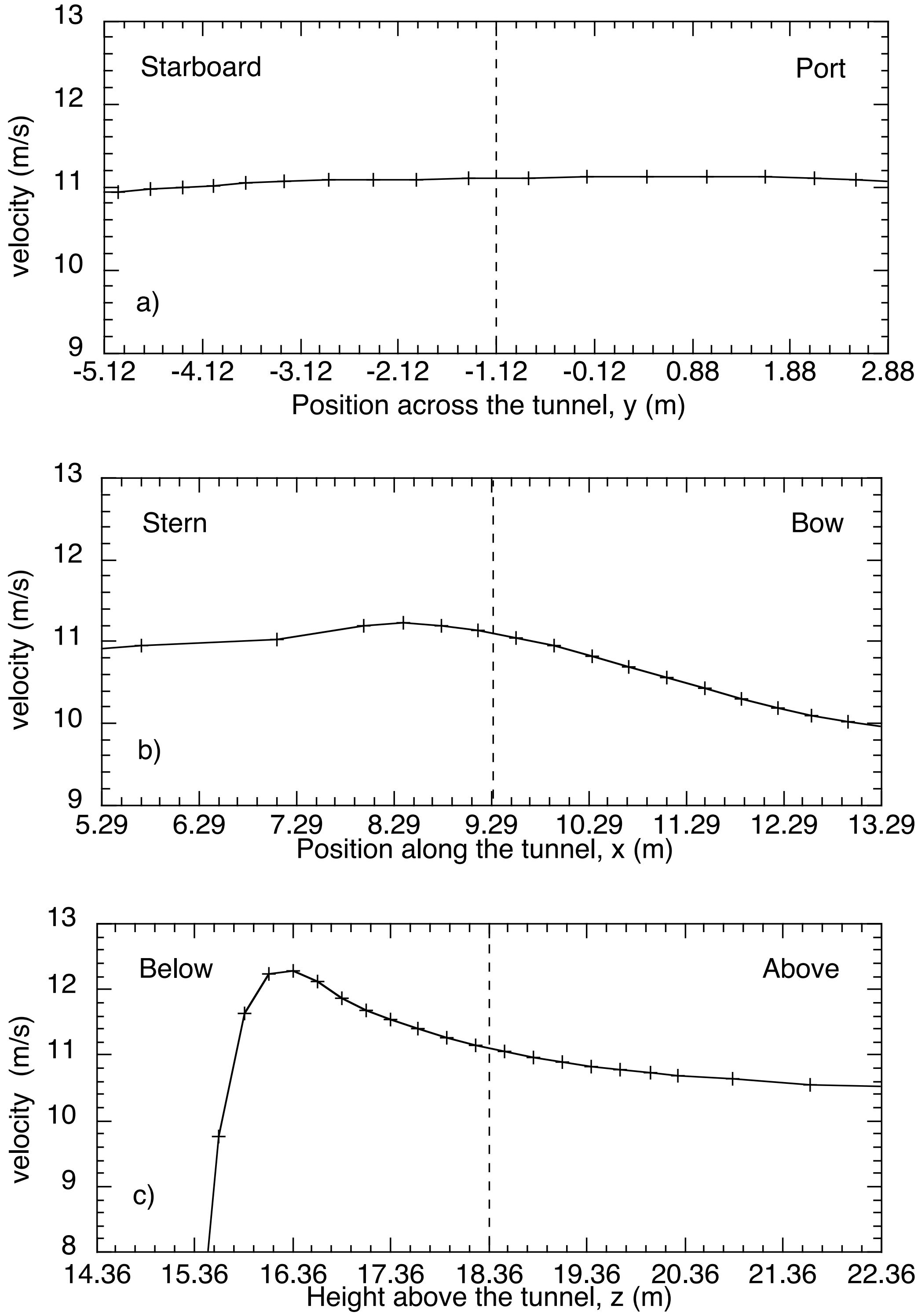

Figure 31 As for Figure 28, but for the Starlogger 2 cup anemometer. Results are from a flow 15° off the starboard bow.

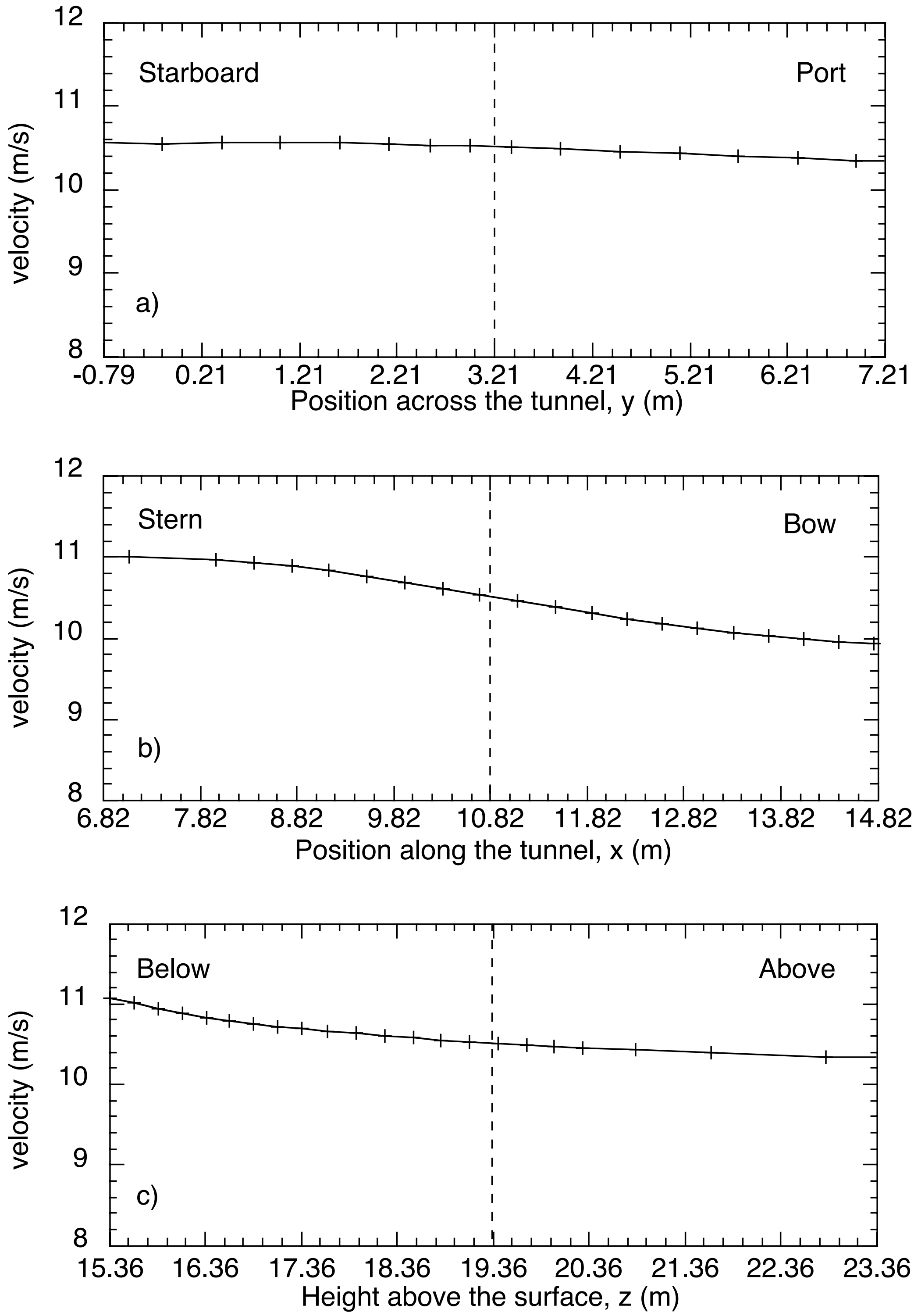

Figure 32 As for Figure 28, but for the Starlogger 3 cup anemometer. Results are from a flow 15° off the starboard bow.

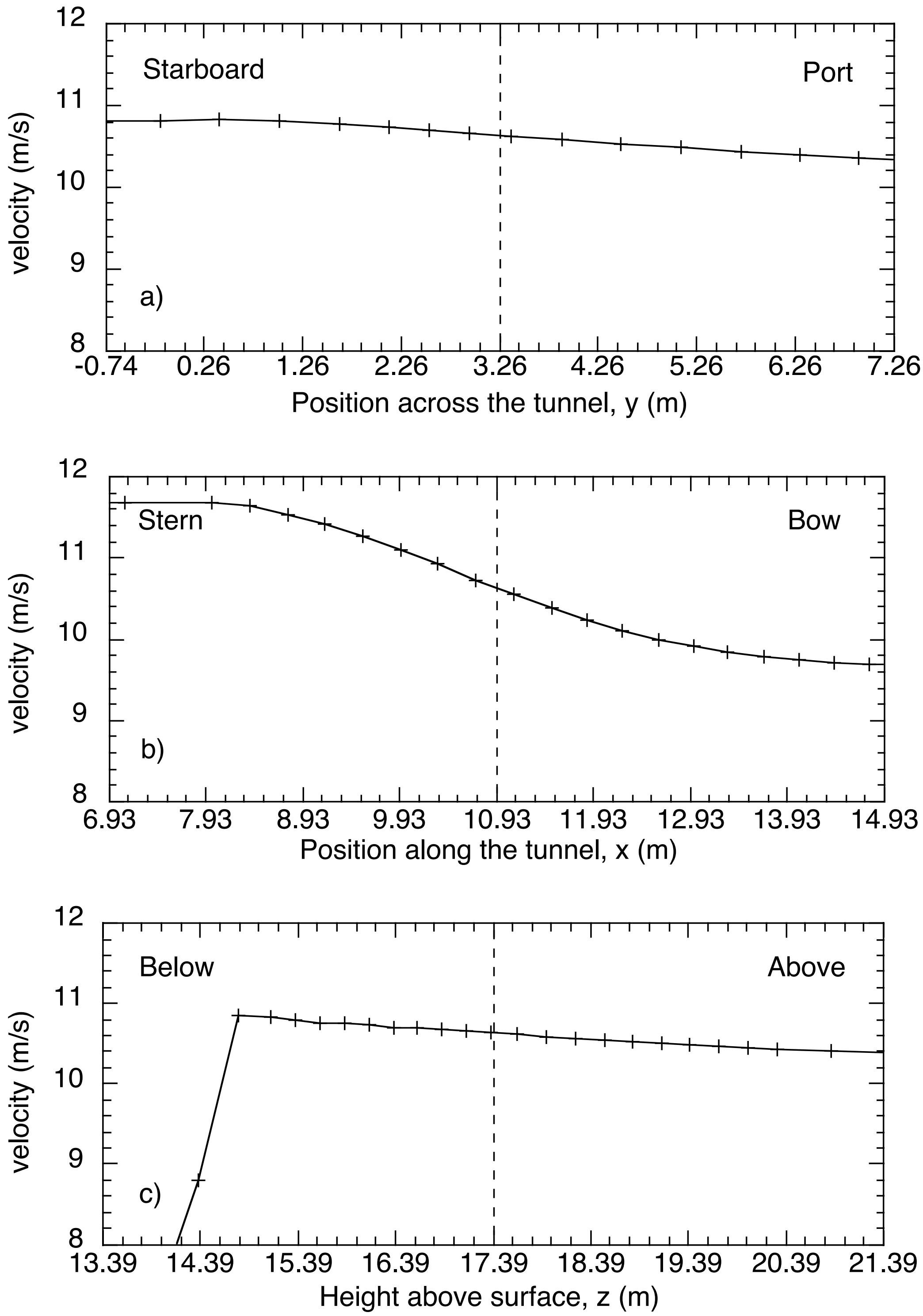

Figure 33 As for Figure 28, but for the Starlogger 4 cup anemometer. Results are from a flow 15° off the starboard bow.

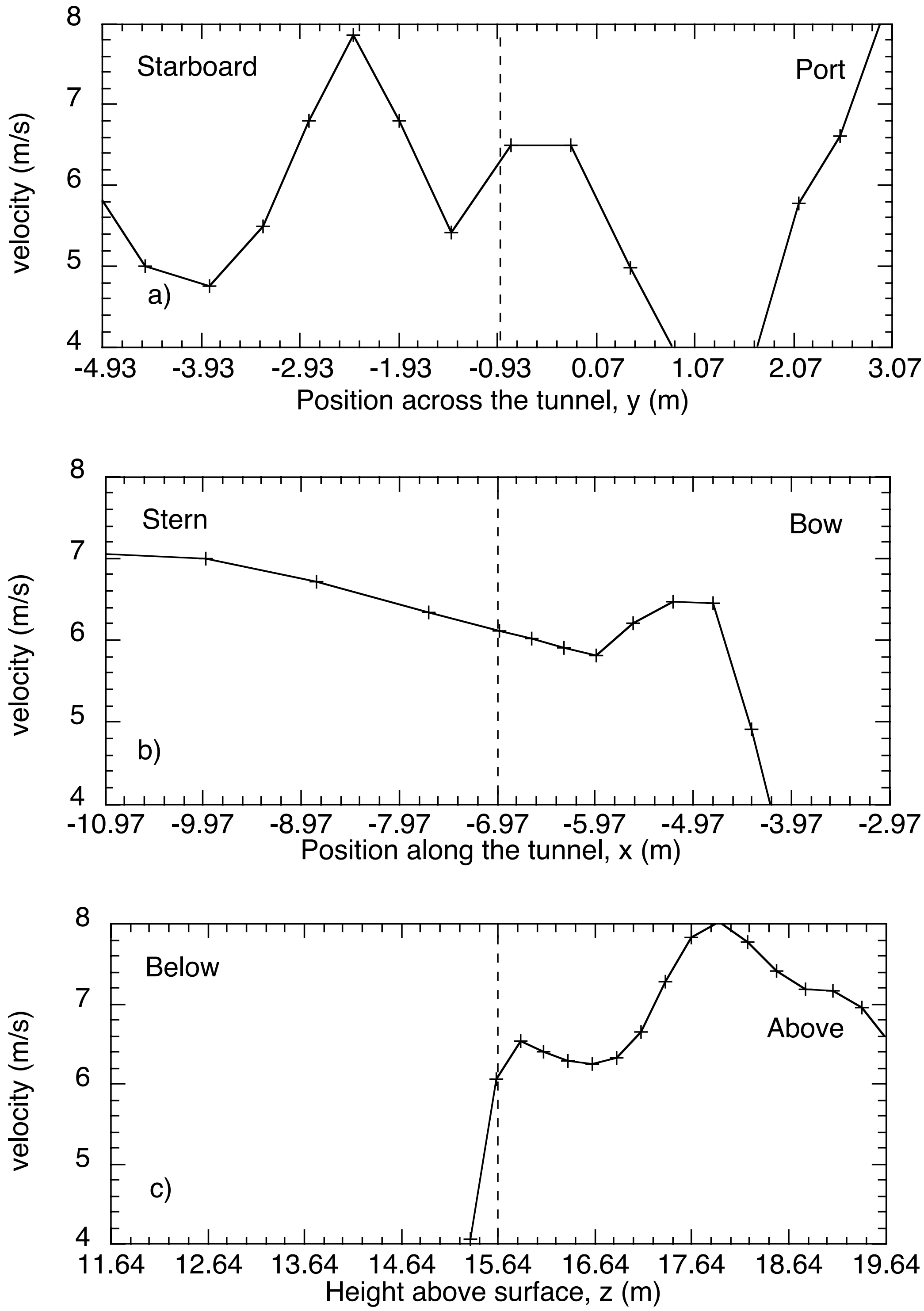

Figure 34 As for Figure 28, but for the Starlogger 5 cup anemometer. Results are from a flow 15° off the starboard bow.

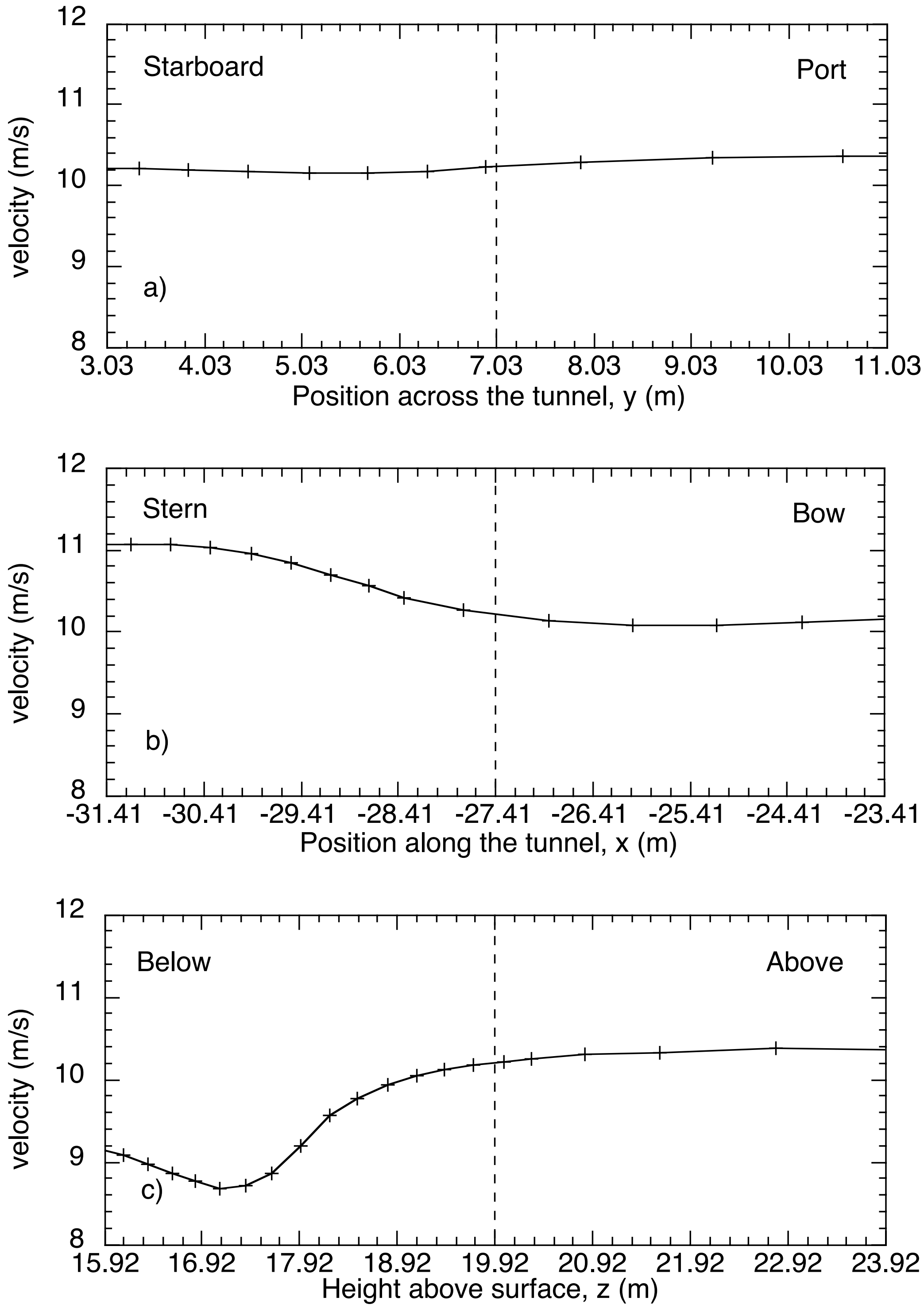

Figure 35 As for Figure 28, but for the Campbell 2 3D prop anemometer. Results are from a flow 15° off the starboard bow.

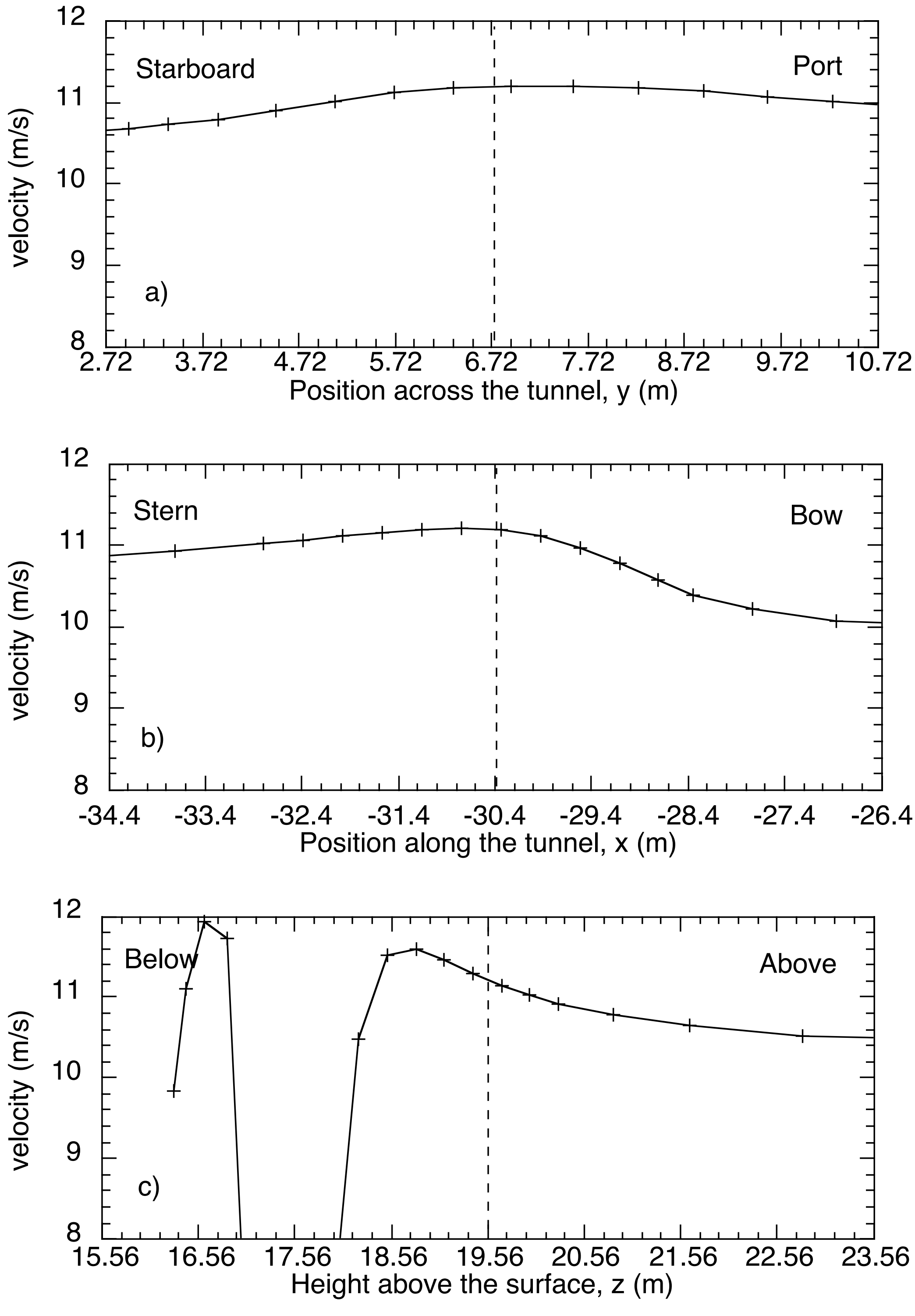

Figure 36 As for Figure 28, but for the Campbell 2 cup anemometer. Results are from a flow 15° off the starboard bow.

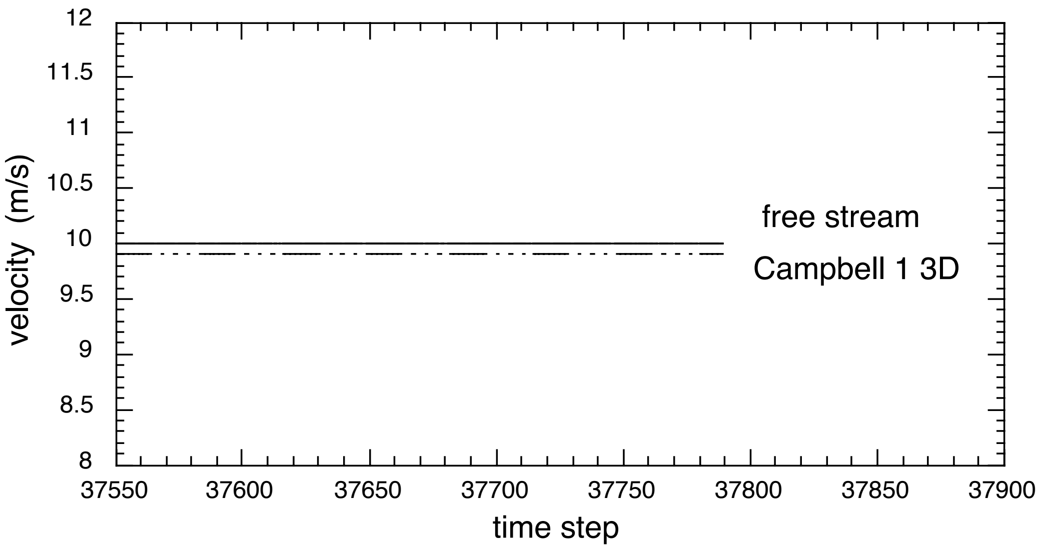

Figure 37 The velocity at each monitoring location in the 30 degree flow simulation. The last 250 time steps are shown.

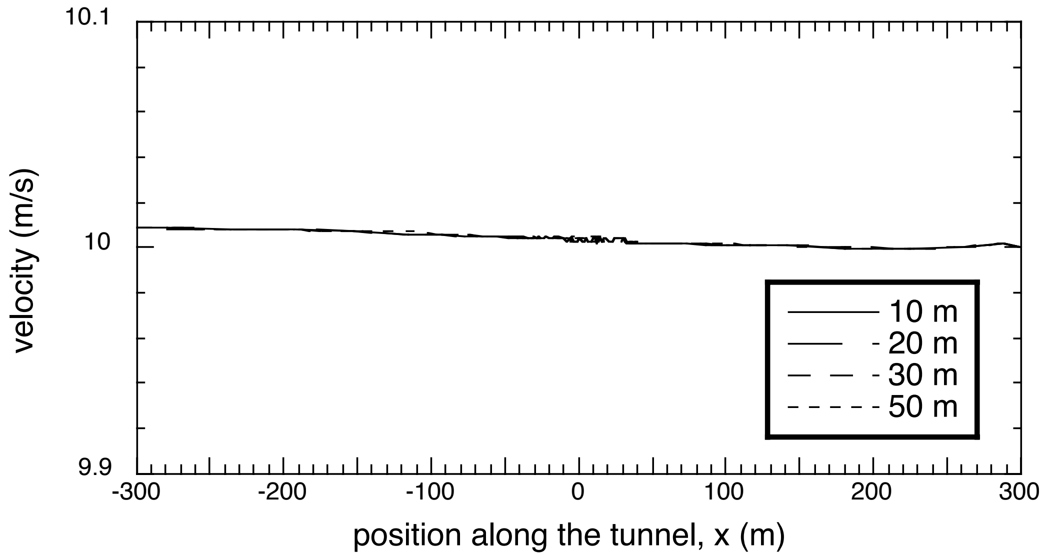

Figure 38a Lines of velocity data along the length of the computational domain at the heights shown. The data were obtained from the free stream region on the port side of the tunnel at y= 450 m.

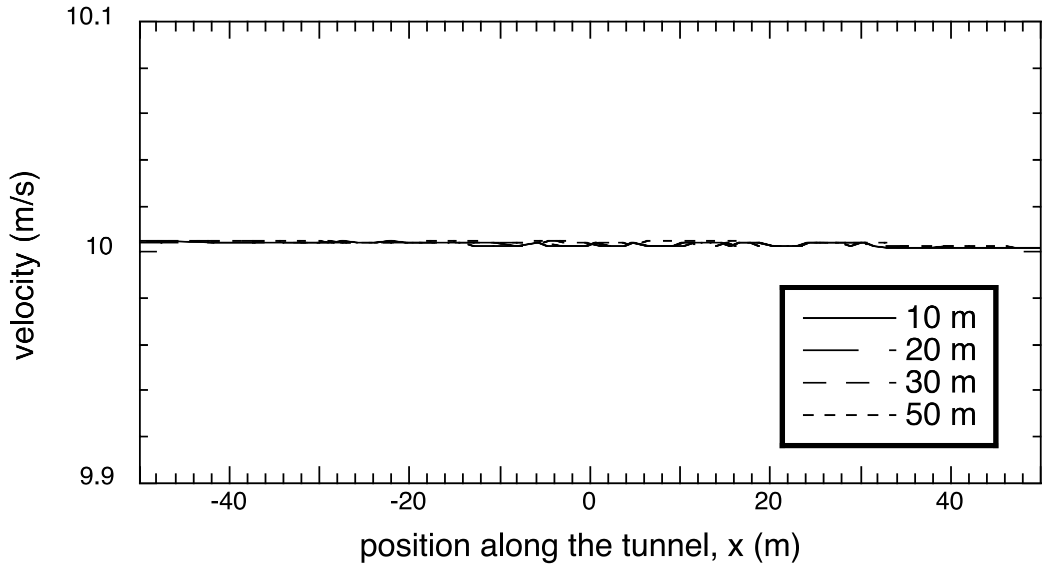

Figure 38b As Figure 38a, showing the central portion of the computational domain only.

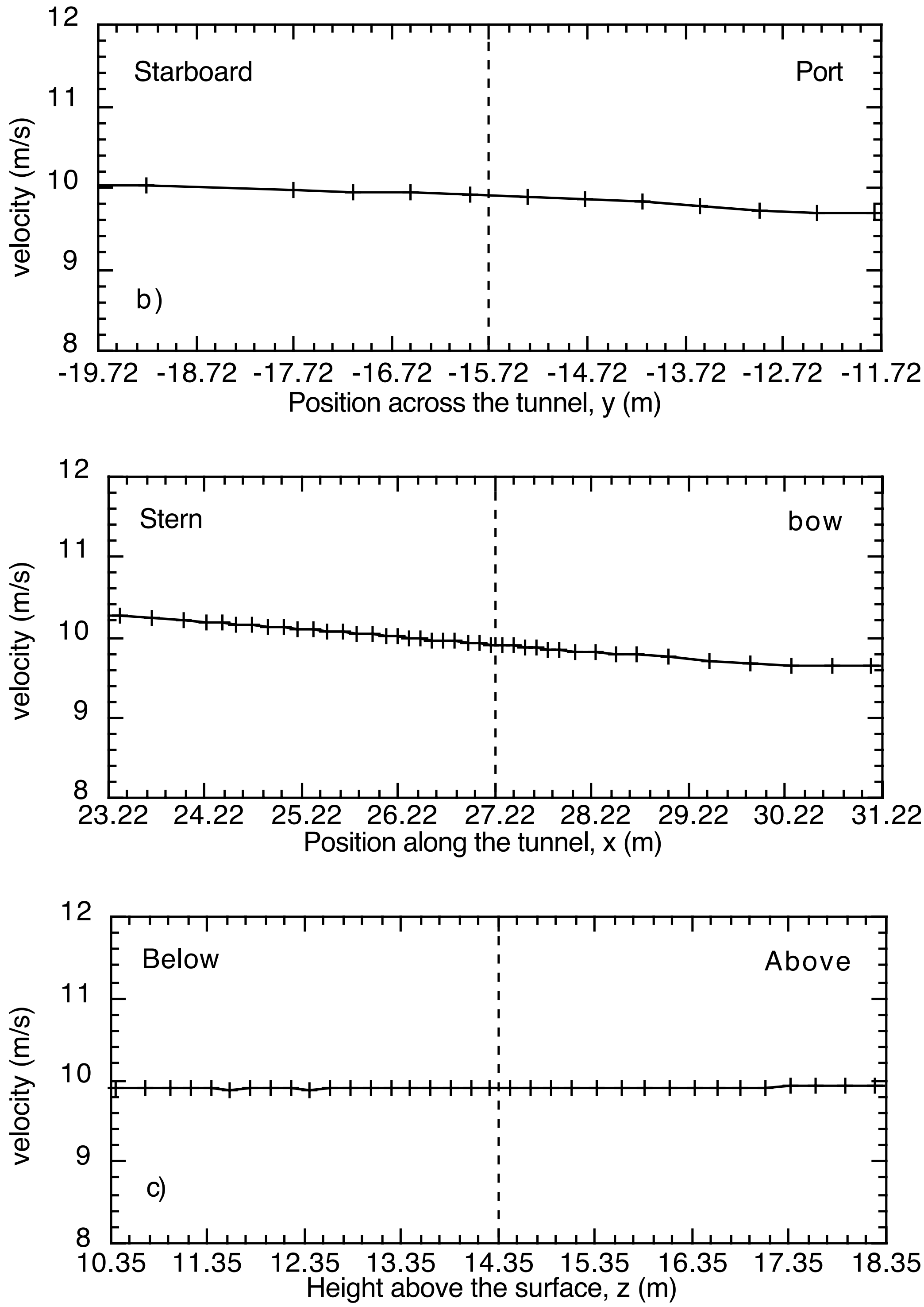

Figure 39 Lines of velocity data through the Campbell 1 3D anemometer position (indicated by the dashed line) in all three directions; a) across the tunnel (y). b) along the tunnel (x) and c) vertically (z). Results are from a flow 30° off the port bow.

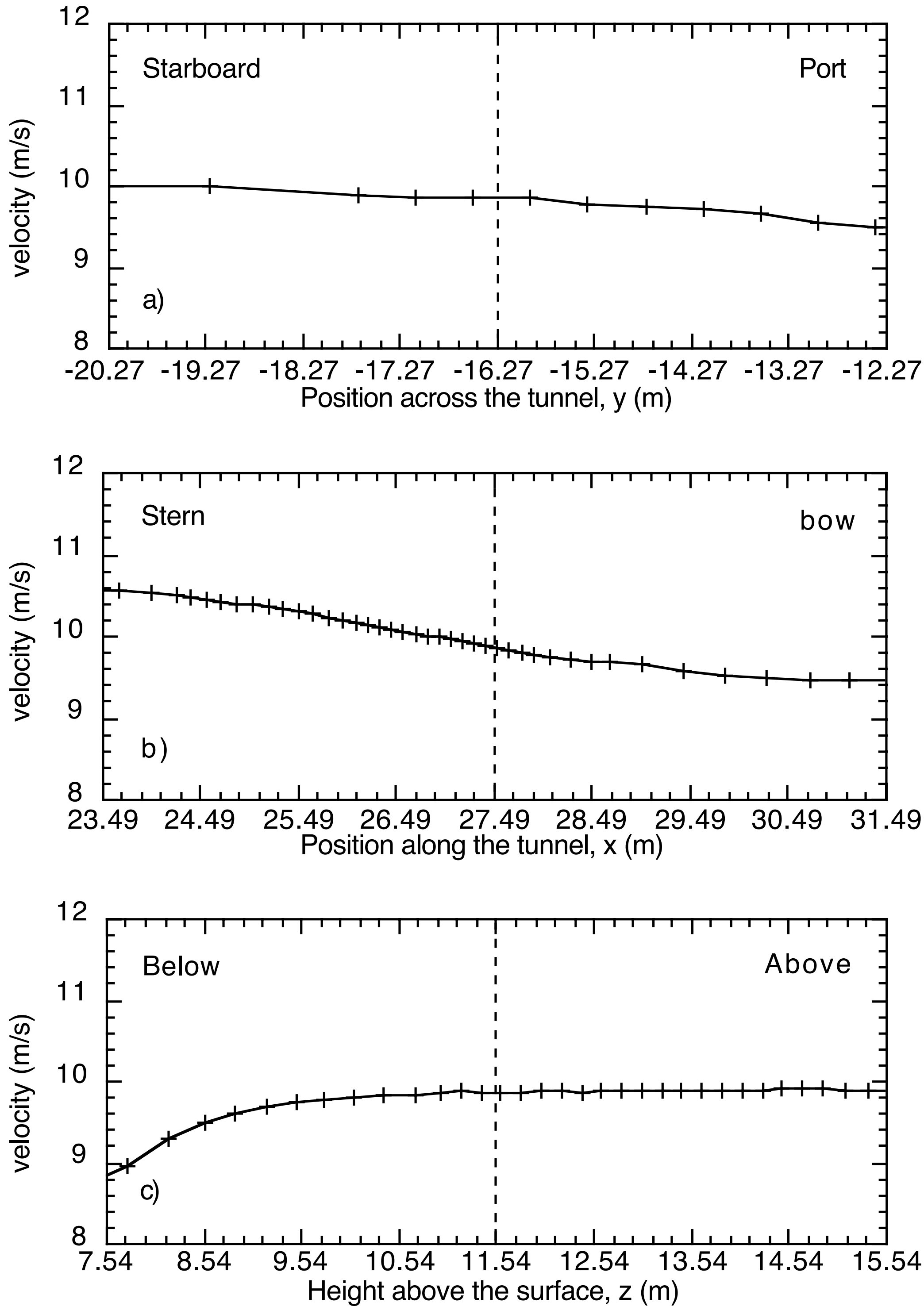

Figure 40 As for Figure 39, but for the Campbell 1 cup anemometer. Results are from a flow 30° off the port bow.

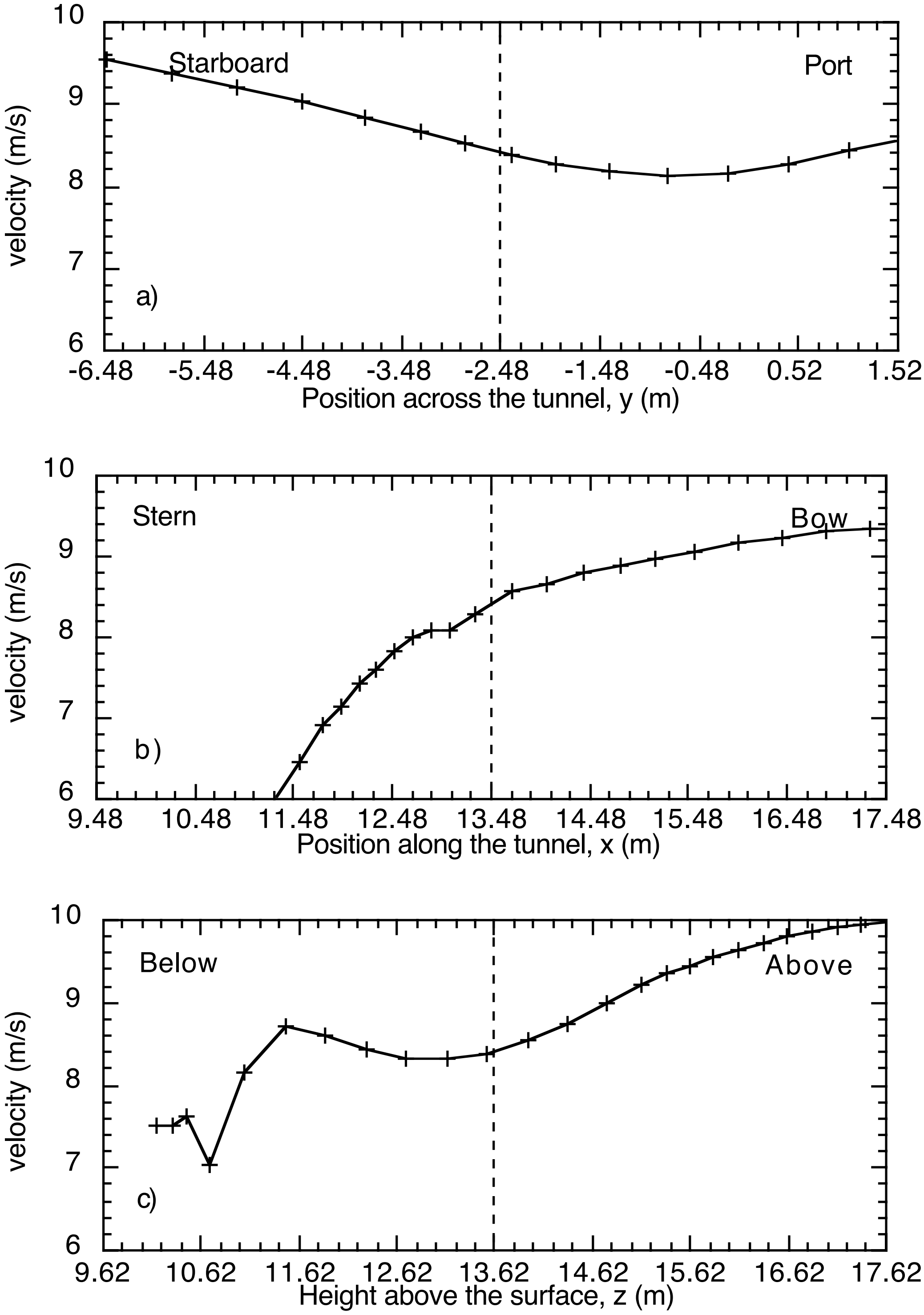

Figure 41 As for Figure 39, but for the Starlogger 1 cup anemometer. Results are from a flow 30° off the port bow.

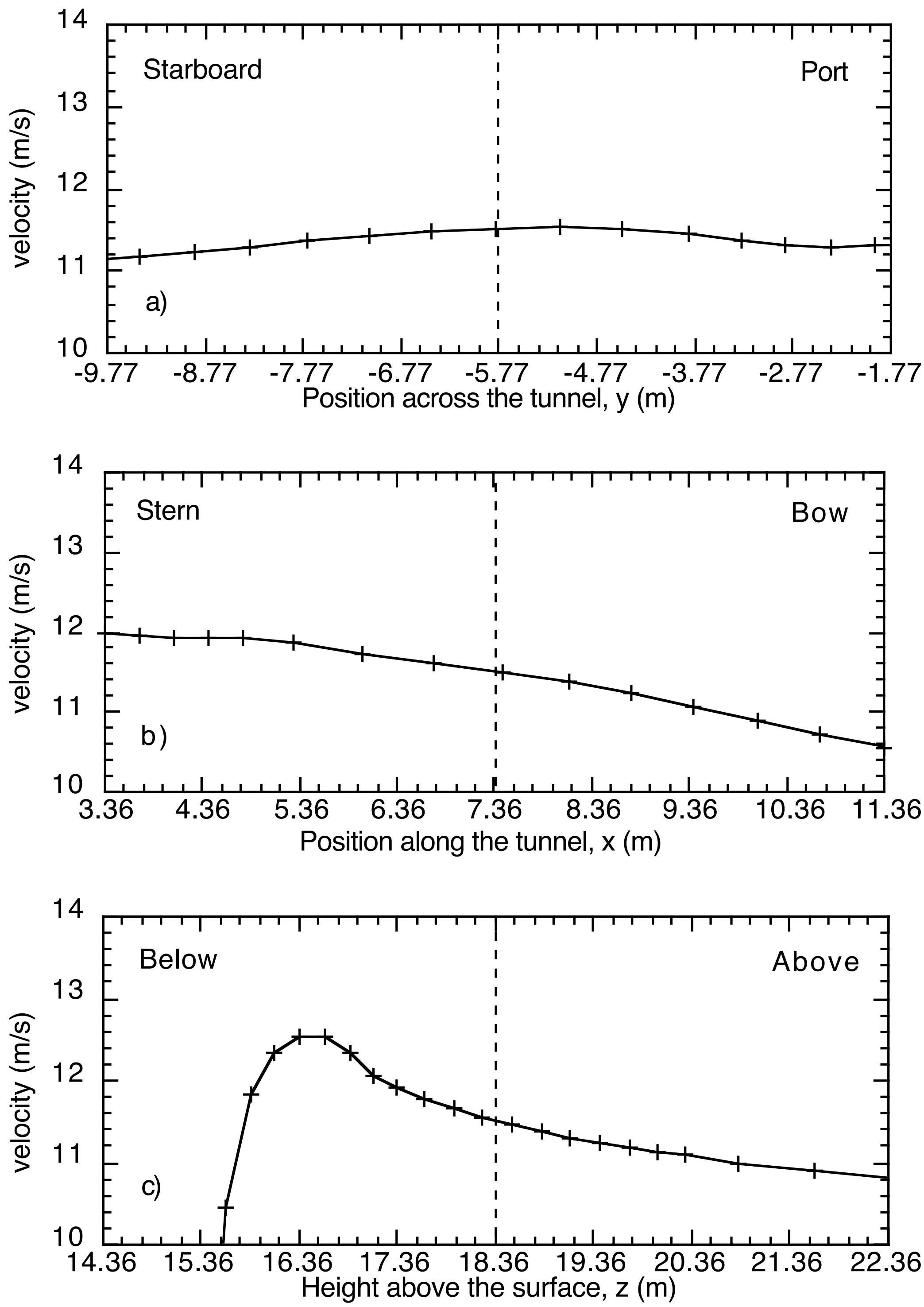

Figure 42 As for Figure 39, but for the Starlogger 2 cup anemometer. Results are from a flow 30° off the port bow.

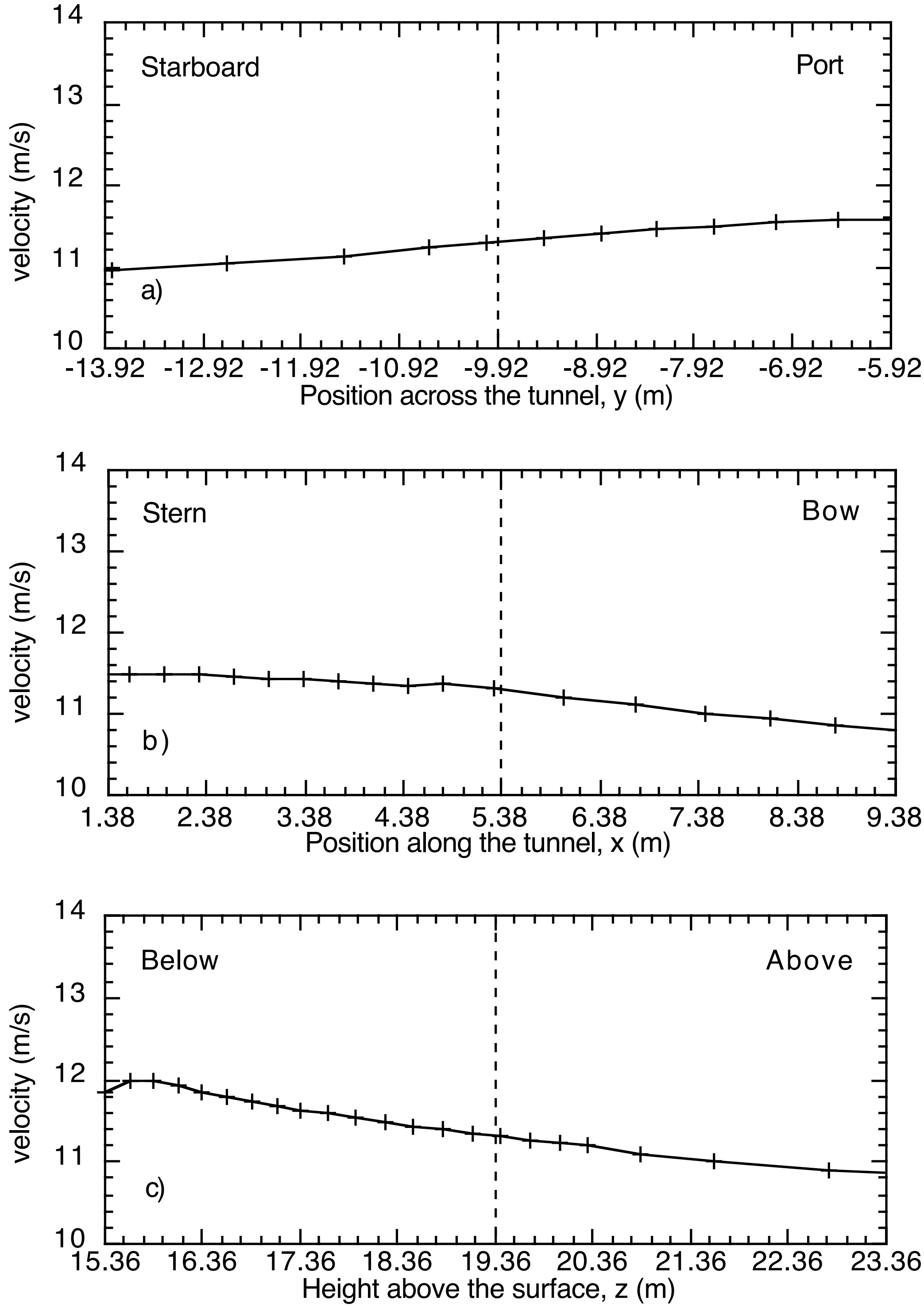

Figure 43 As for Figure 39, but for the Starlogger 3 cup anemometer. Results are from a flow 30° off the port bow.

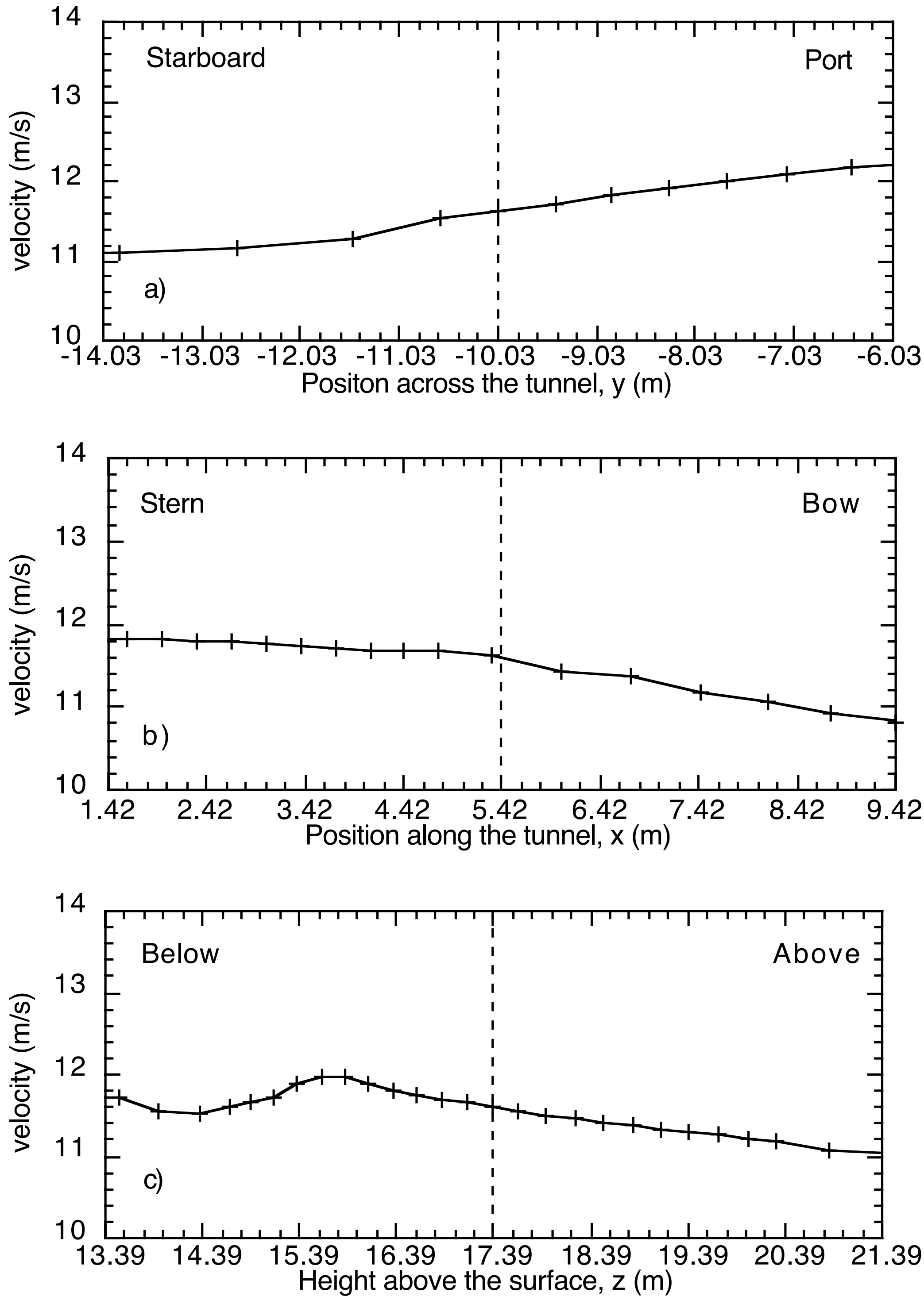

Figure 44 As for Figure 39, but for the Starlogger 4 cup anemometer. Results are from a flow 30° off the port bow.

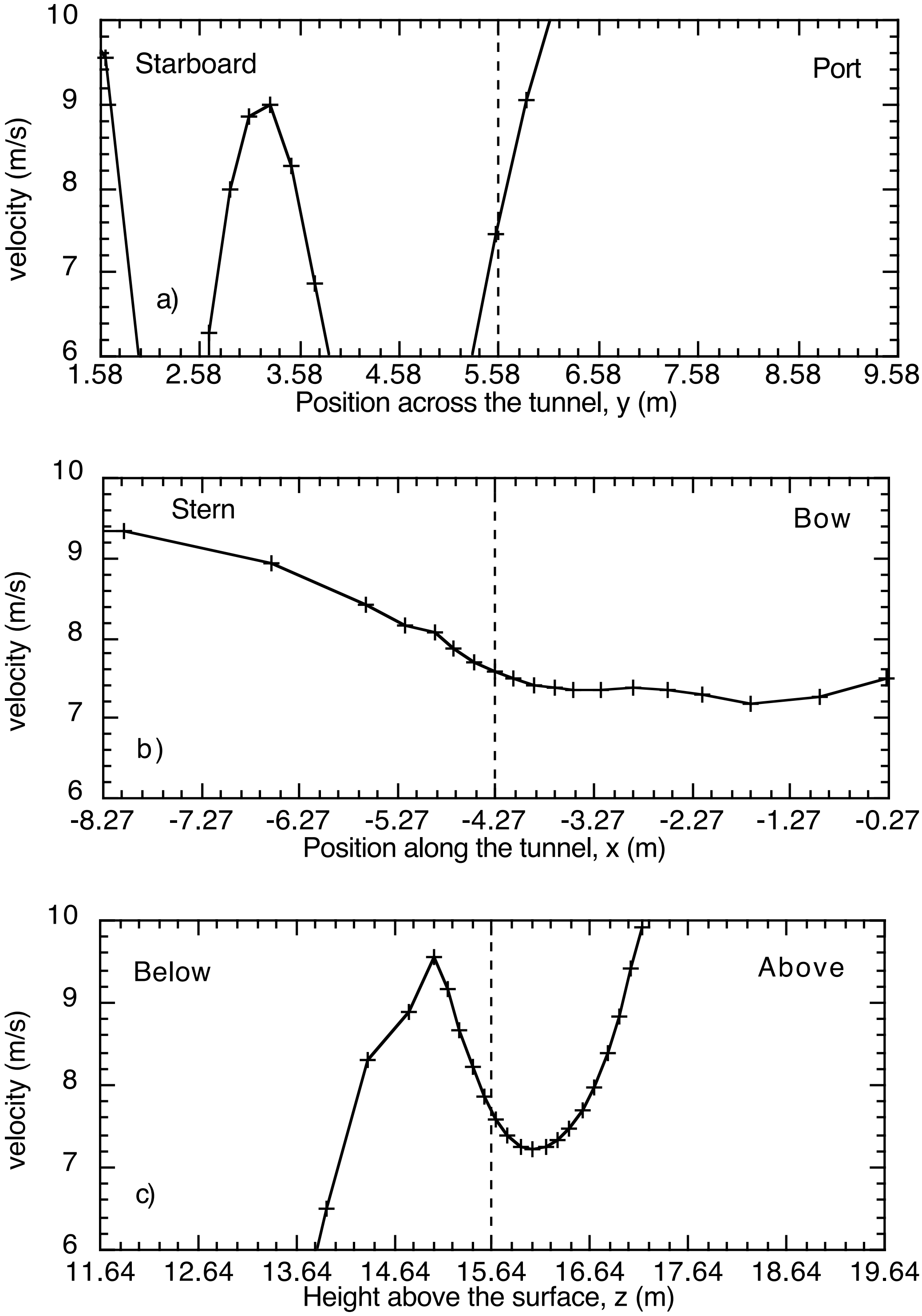

Figure 45 As for Figure 39, but for the Starlogger 5 cup anemometer. Results are from a flow 30° off the port bow.

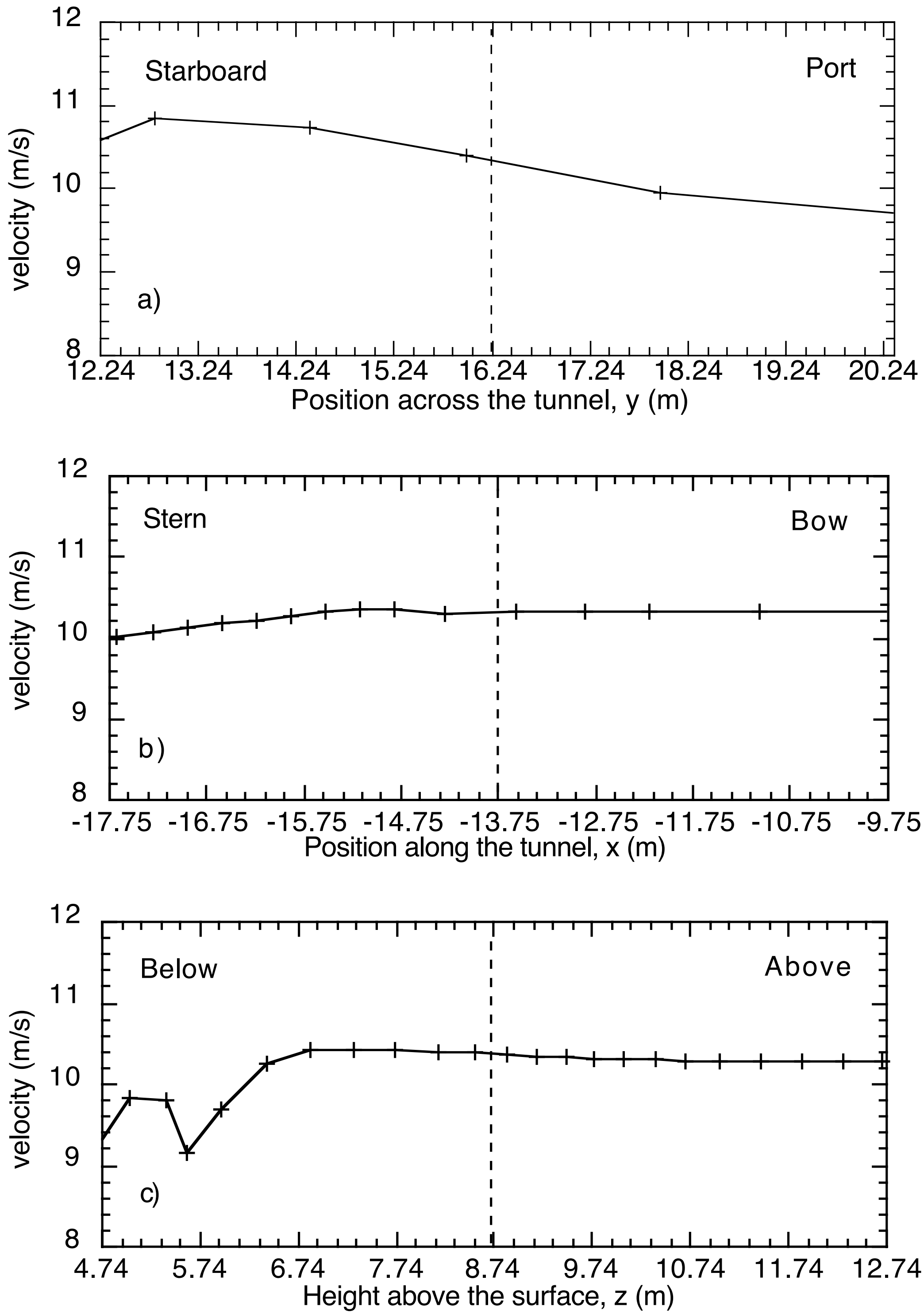

Figure 46 As for Figure 39, but for the Starlogger 6 cup anemometer. Results are from a flow 30° off the port bow.

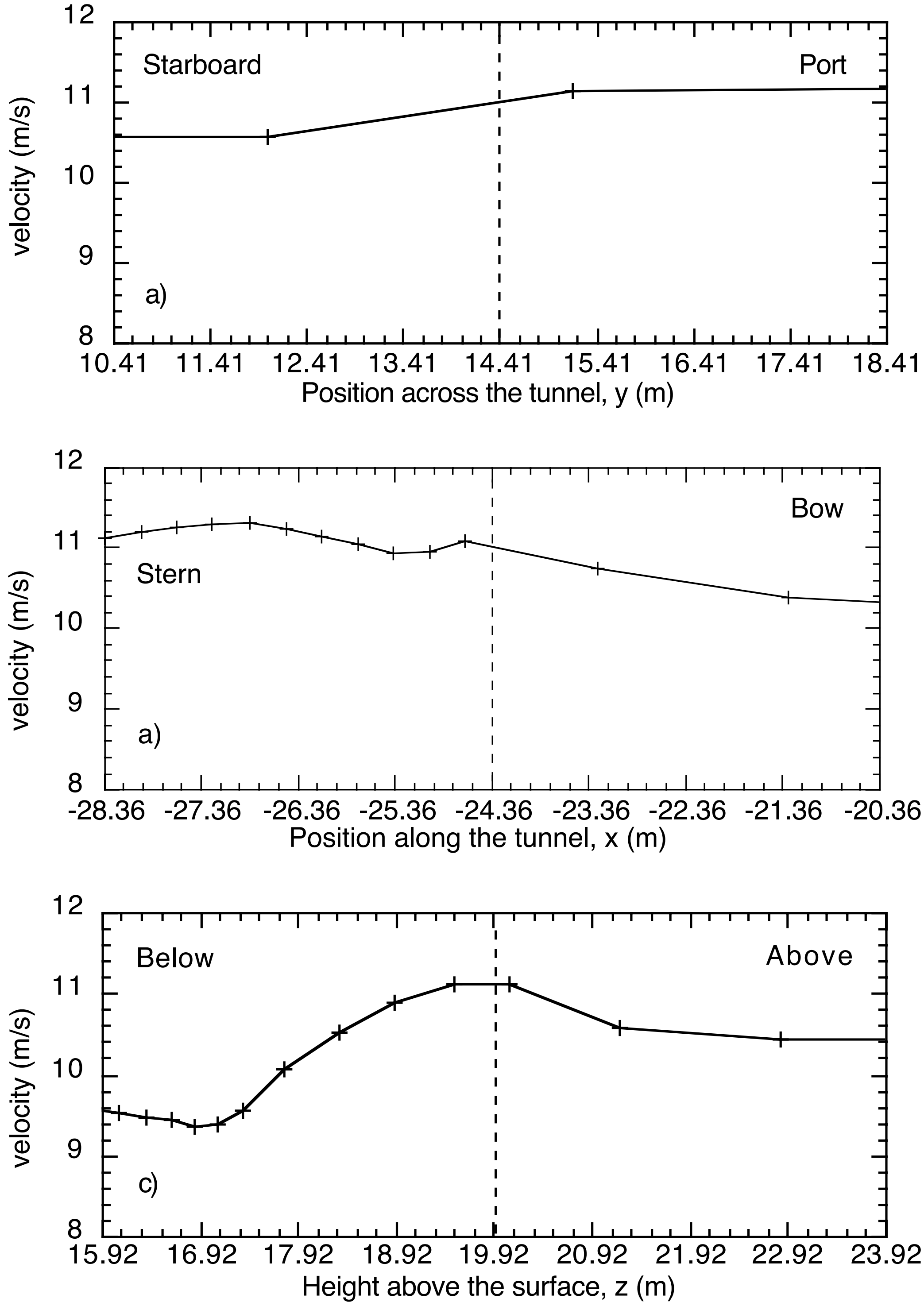

Figure 47 As for Figure 39, but for the Campbell 2 3D prop anemometer. Results are from a flow 30° off the port bow.

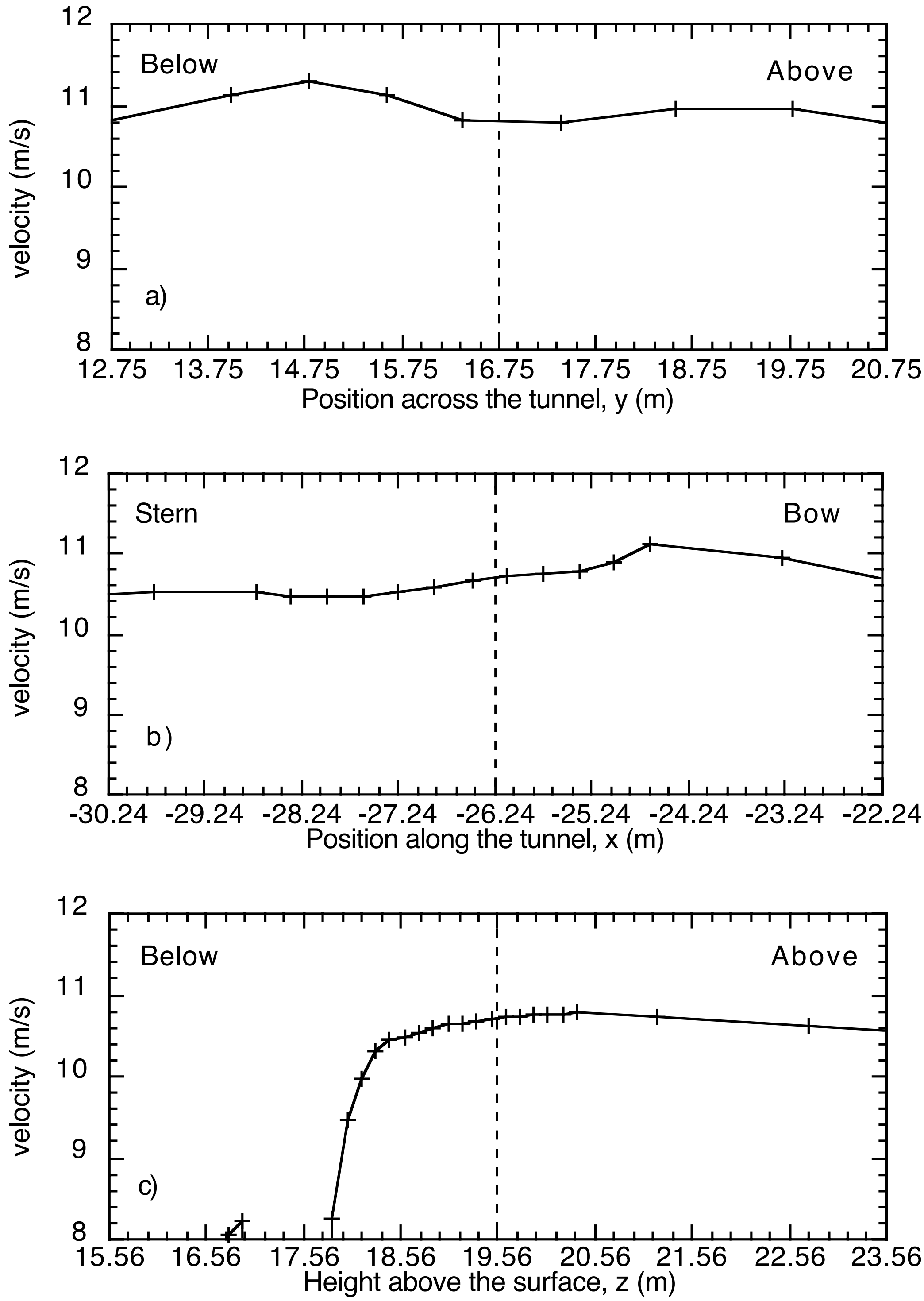

Figure 48 As for Figure 39, but for the Campbell 2 cup anemometer. Results are from a flow 30° off the port bow.

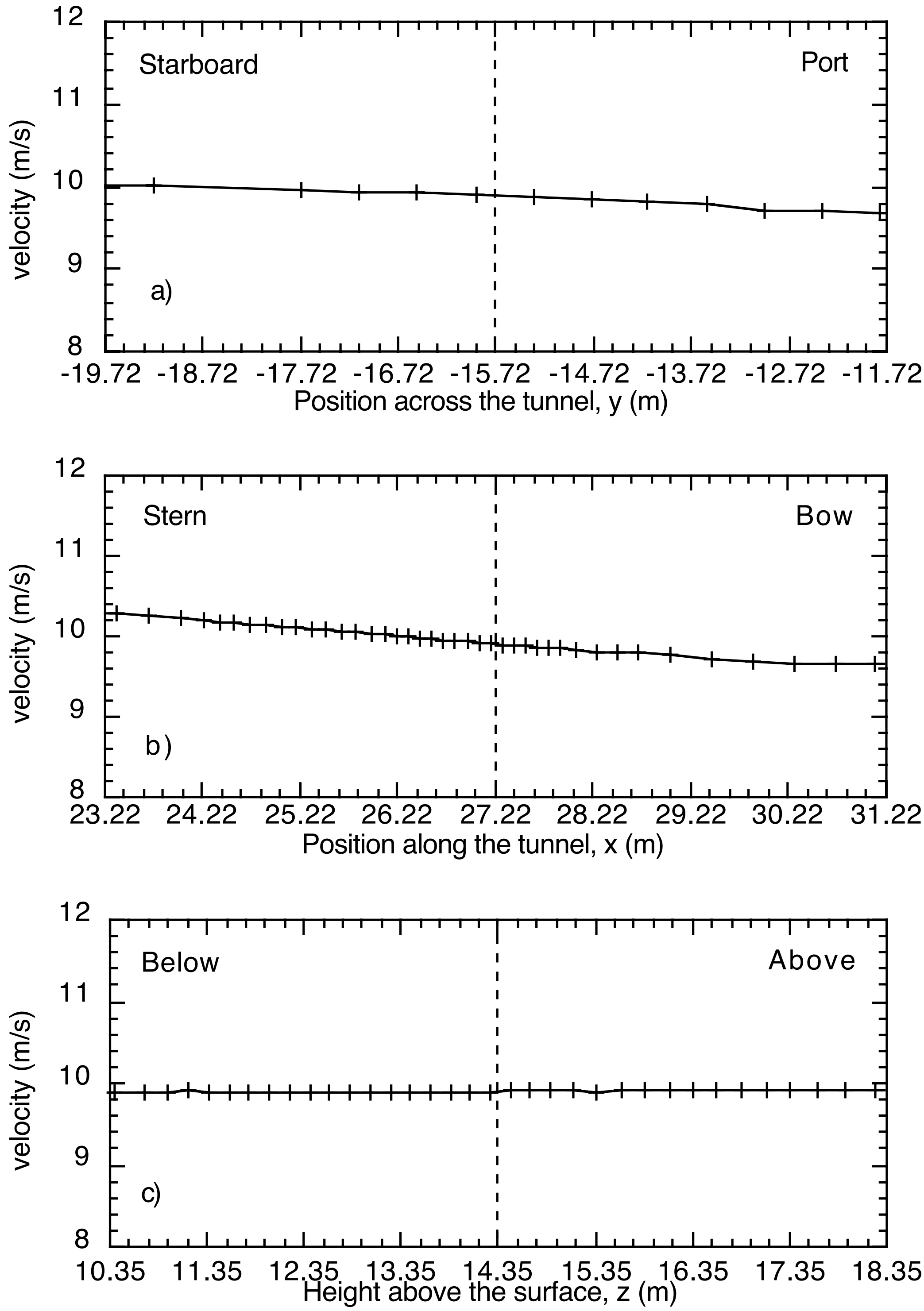

Figure 49 Lines of velocity data through the Campbell 1 3D anemometer position (indicated by the dashed line) in all three directions; a) across the tunnel (y). b) along the tunnel (x) and c) vertically (z). Results are from a flow 30° off the starboard bow.

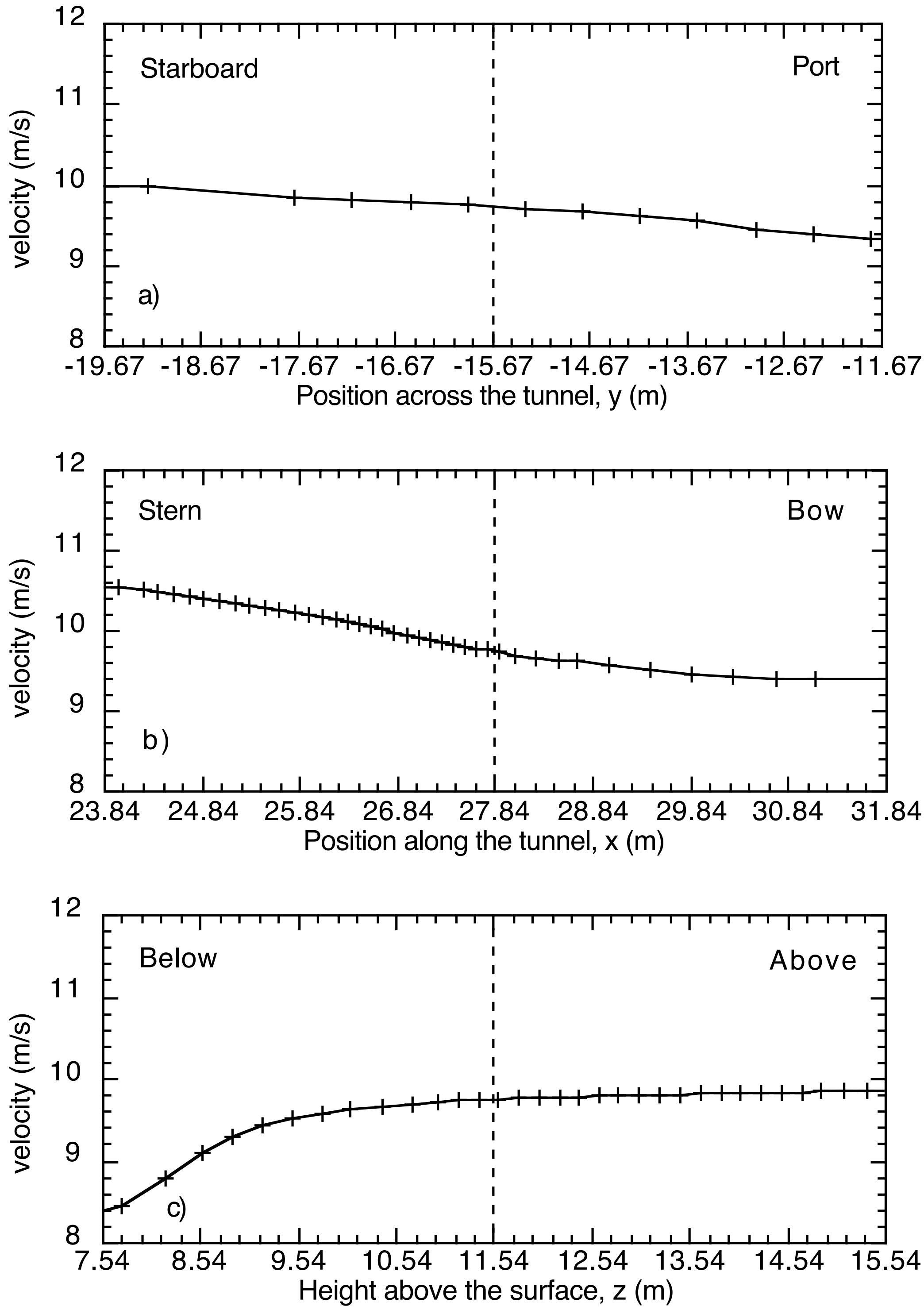

Figure 50 As for Figure 49, but for the Campbell 1 cup anemometer. Results are from a flow 30° off the starboard bow.

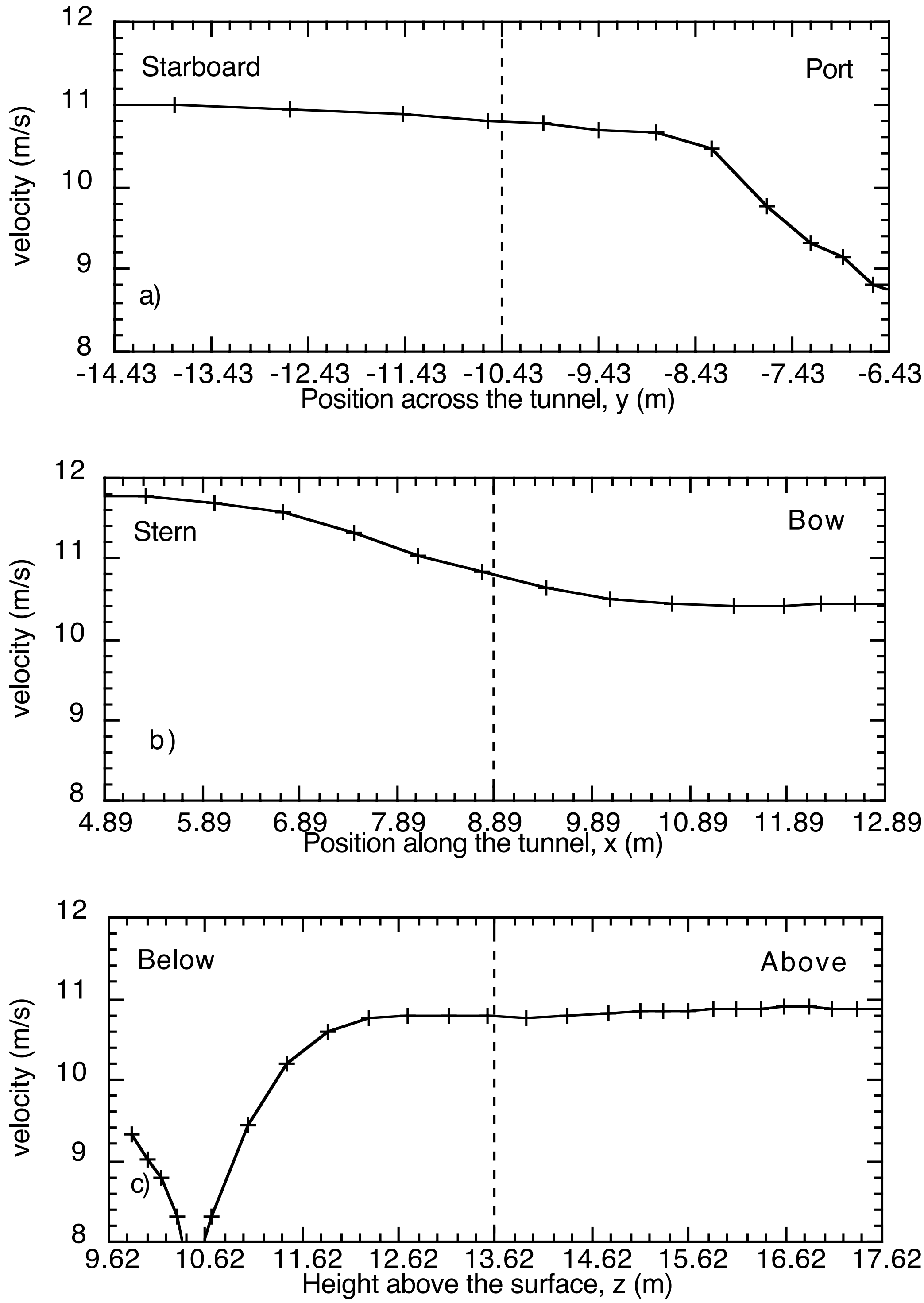

Figure 51 As for Figure 49, but for the Starlogger 1 cup anemometer. Results are from a flow 30° off the starboard bow.

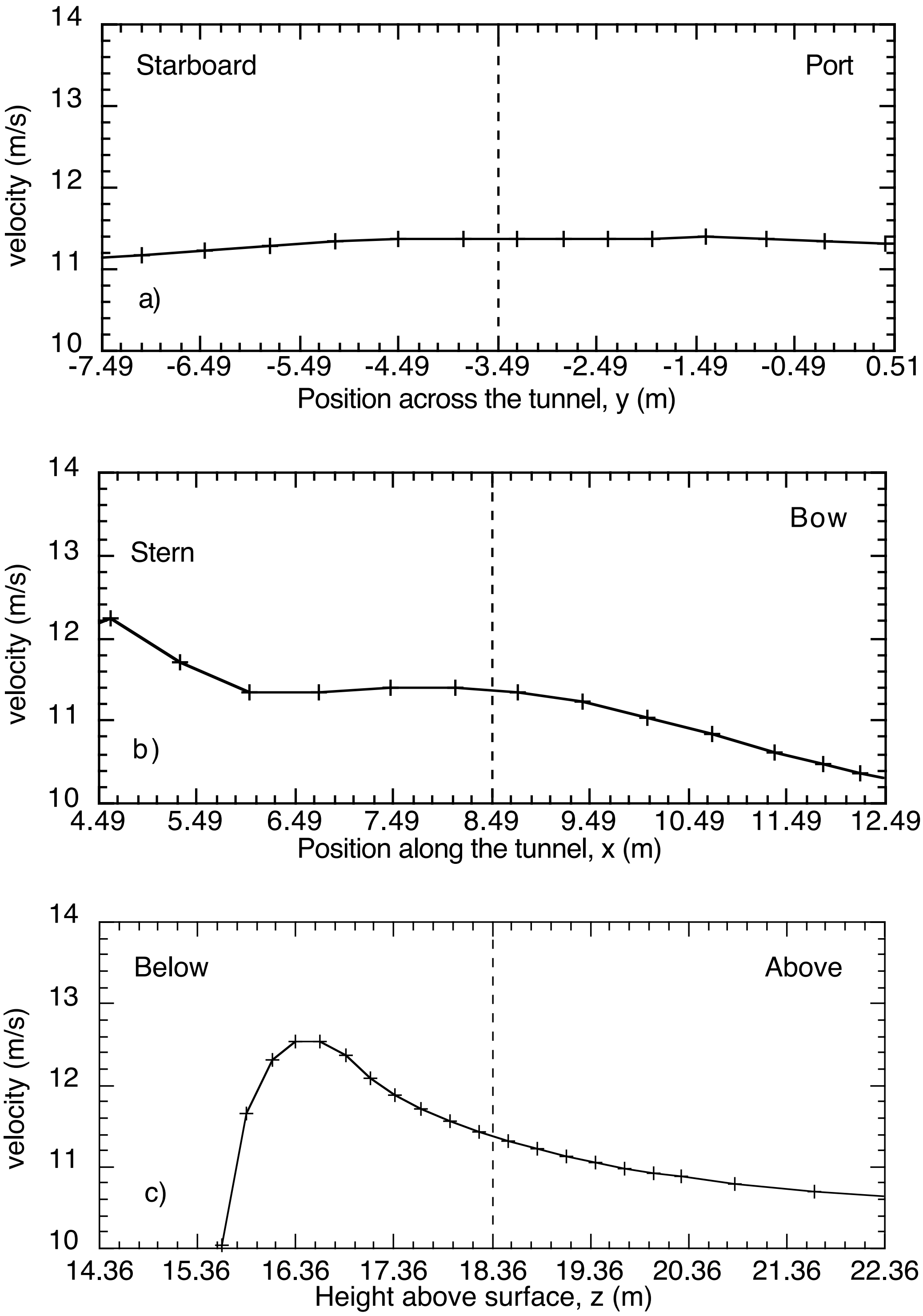

Figure 52 As for Figure 49, but for the Starlogger 2 cup anemometer. Results are from a flow 30° off the starboard bow.

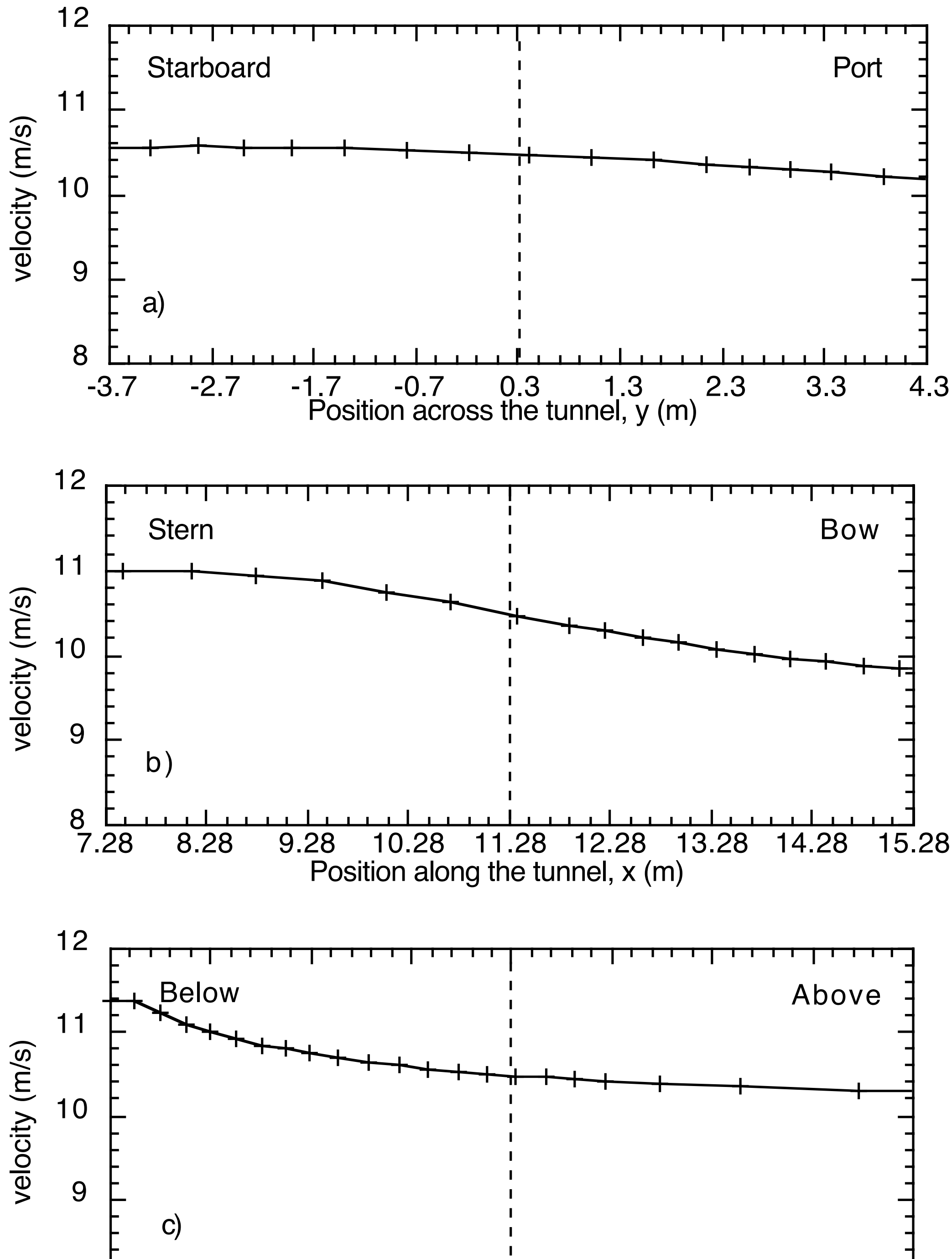

Figure 53 As for Figure 49, but for the Starlogger 3 cup anemometer. Results are from a flow 30° off the starboard bow.

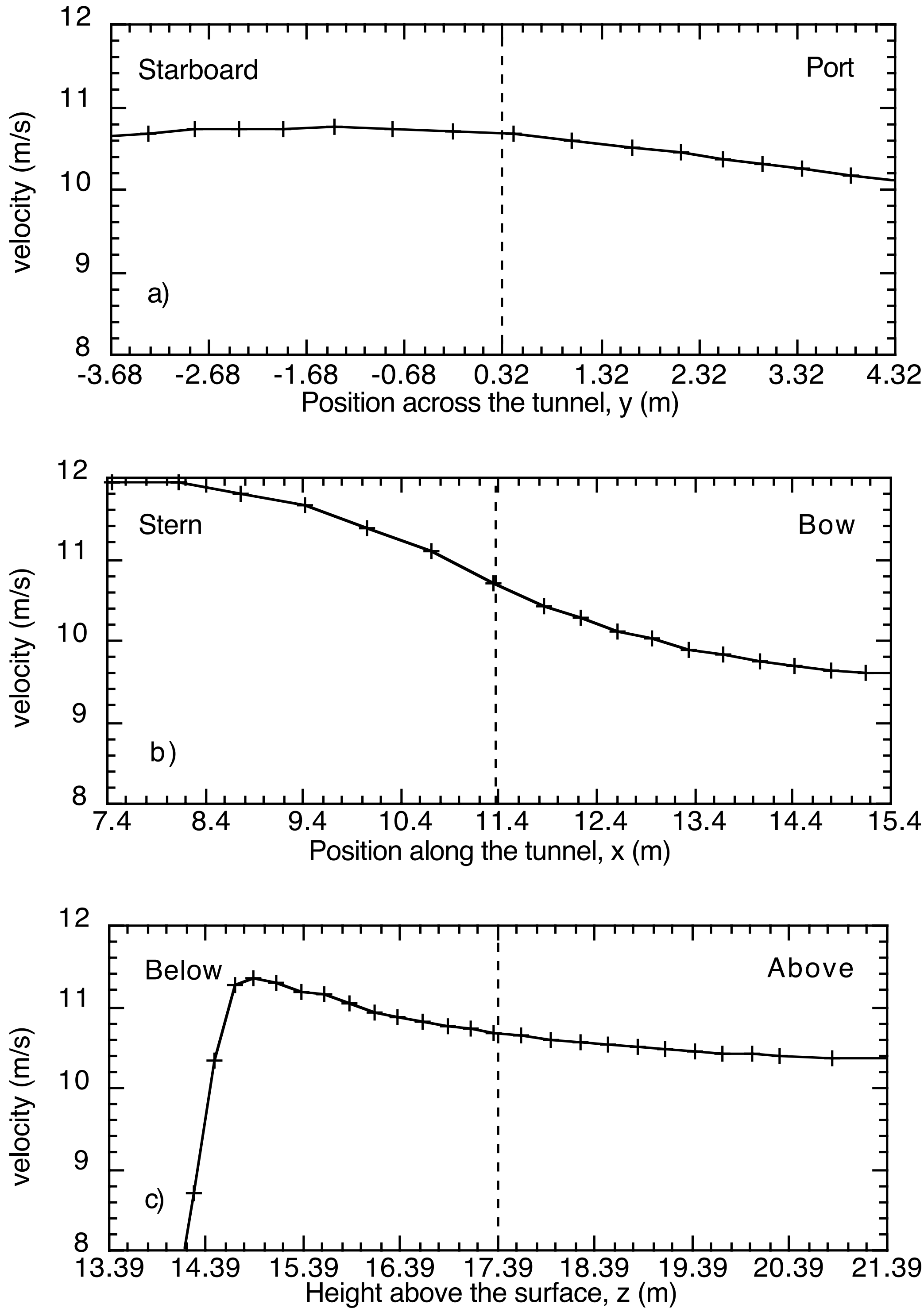

Figure 54 As for Figure 49, but for the Starlogger 4 cup anemometer. Results are from a flow 30° off the starboard bow.

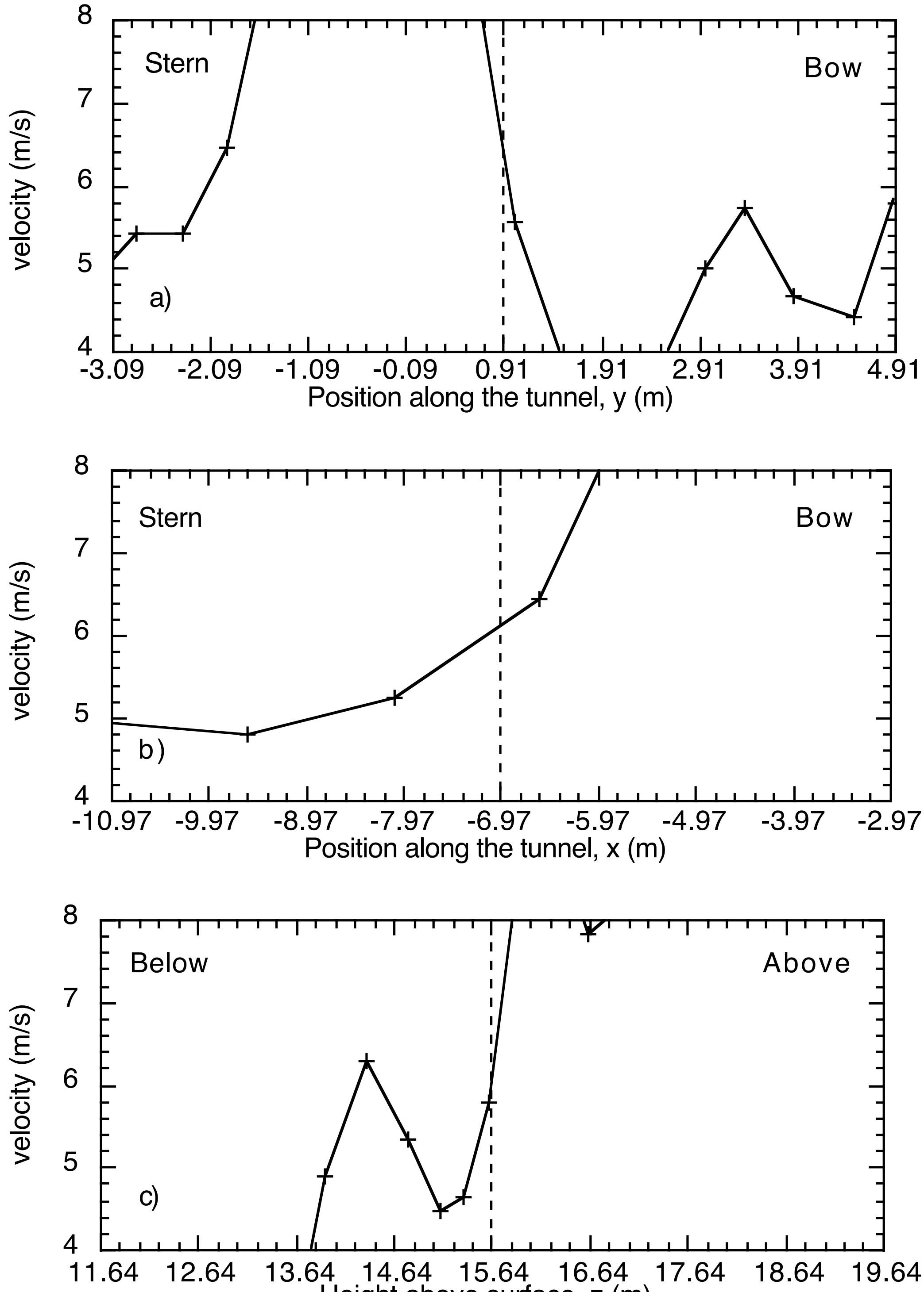

Figure 55 As for Figure 49, but for the Starlogger 5 cup anemometer. Results are from a flow 30° off the starboard bow.

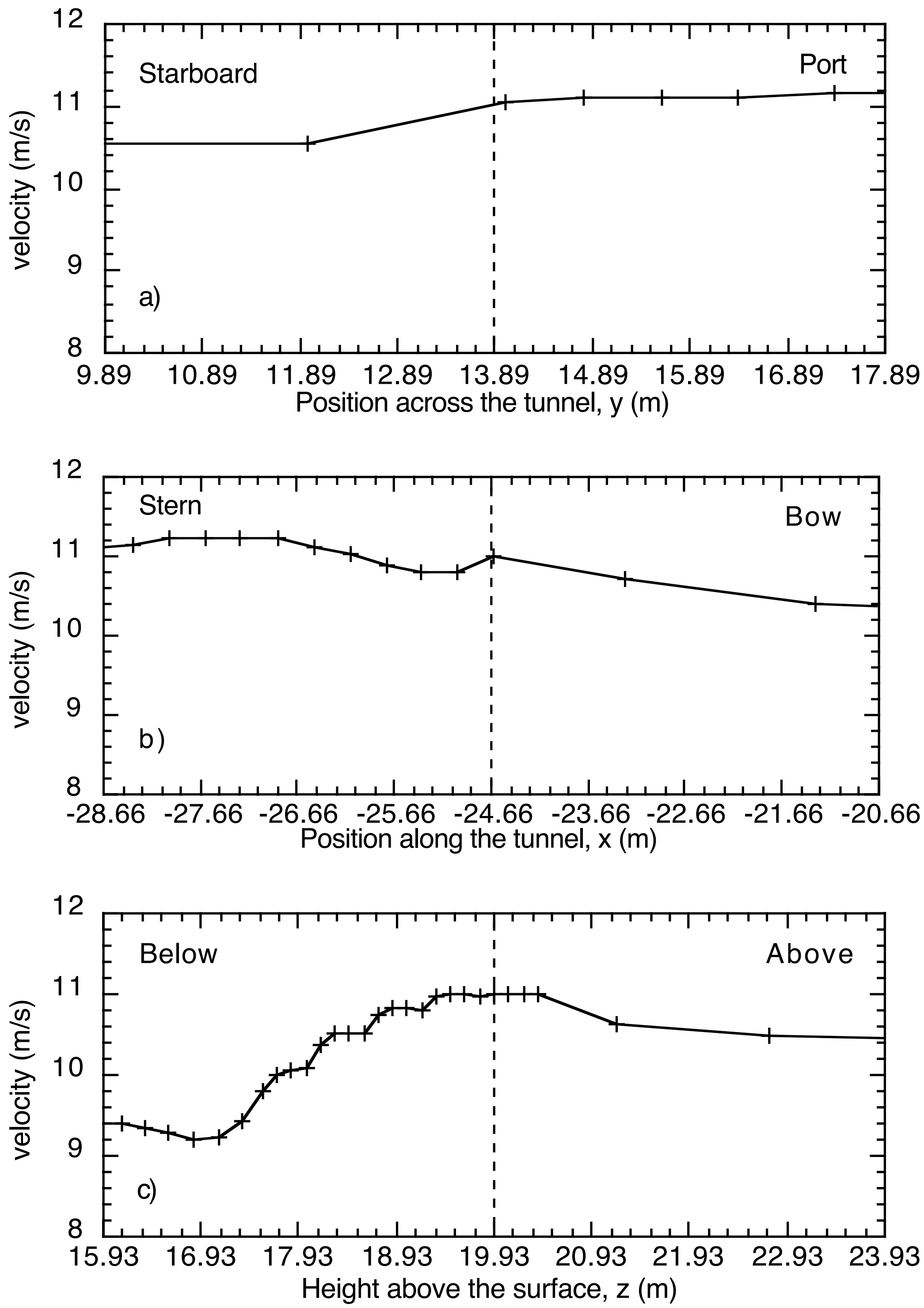

Figure 56 As for Figure 49, but for the Campbell 2 3D prop anemometer. Results are from a flow 30° off the starboard bow.

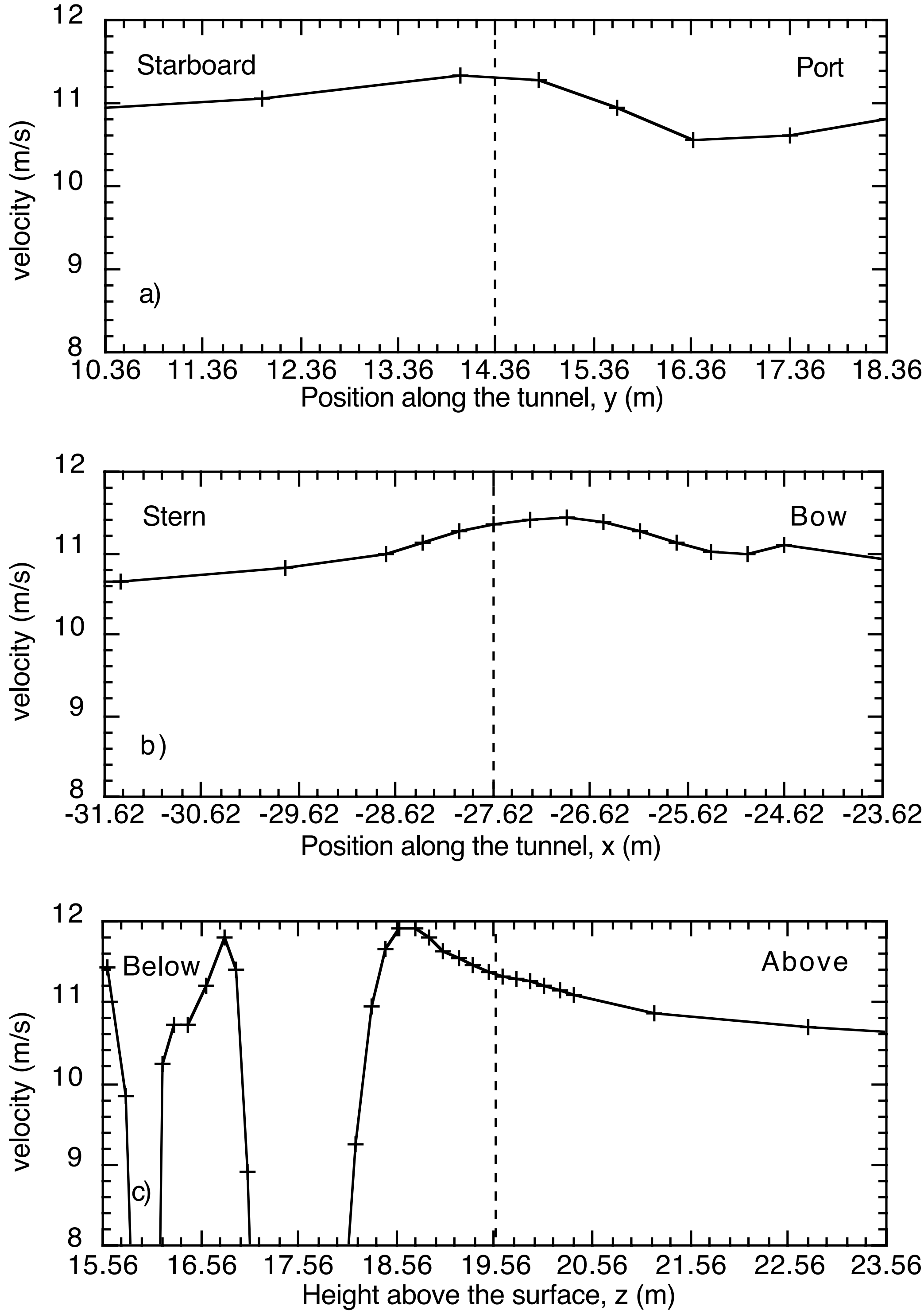

Figure 57 As for Figure 49, but for the Campbell 2 cup anemometer. Results are from a flow 30° off the starboard bow.

APPENDIX

The figures in this Appendix were generated using the VECTIS post-processing software. The variable size of the computational cells can be seen in all the Figures.

FIGURE A1 Velocity vectors on a vertical plane through the Campbell 1 3D cup anemometer site. The airflow is directly over the bow and the magnitude of the total velocity is indicated by the colour of the arrows.

FIGURE A3 As Figure A1, but for a relative wind direction of 15 degrees off the port bow.

FIGURE A3 As Figure A1, but for a relative wind direction of 30 degrees off the port bow.

FIGURE A4 Velocity vectors on a vertical plane through the Campbell 2 3D cup anemometer site. The airflow is for a relative wind direction of 15 degrees off the port bow and the magnitude of the total velocity is indicated by the colour of the arrows.

FIGURE A5 Velocity vectors on a vertical plane through the effective Starlogger 6 anemometer site. The airflow is for a relative wind direction of 15 degrees off the starboard bow and the magnitude of the total velocity is indicated by the colour of the arrows.

FIGURE A6 Velocity vectors on a vertical plane through the effective Starlogger 6 anemometer site. The airflow is for a relative wind direction of 30 degrees off the starboard bow and the magnitude of the total velocity is indicated by the colour of the arrows.

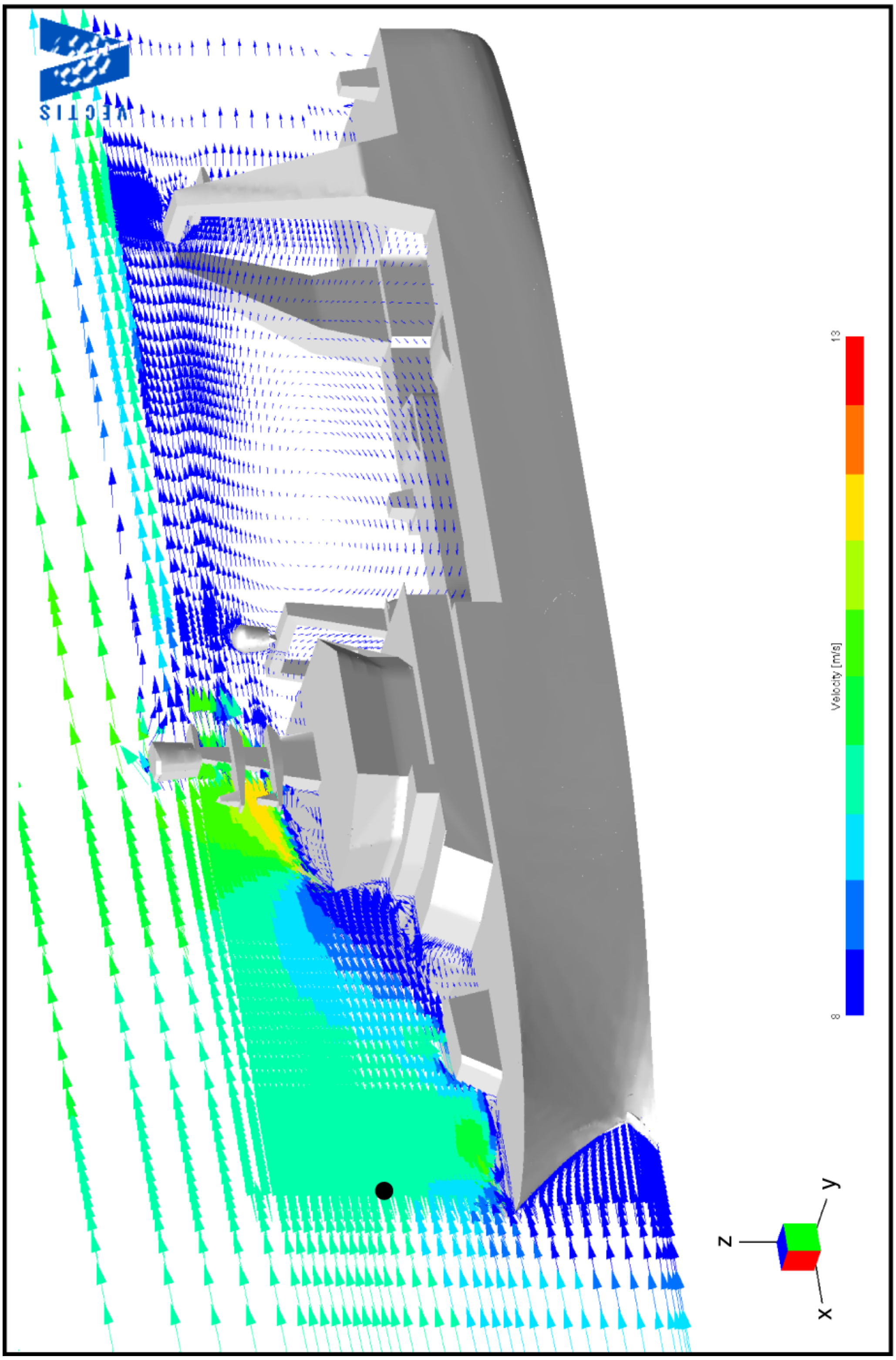

Figure A1

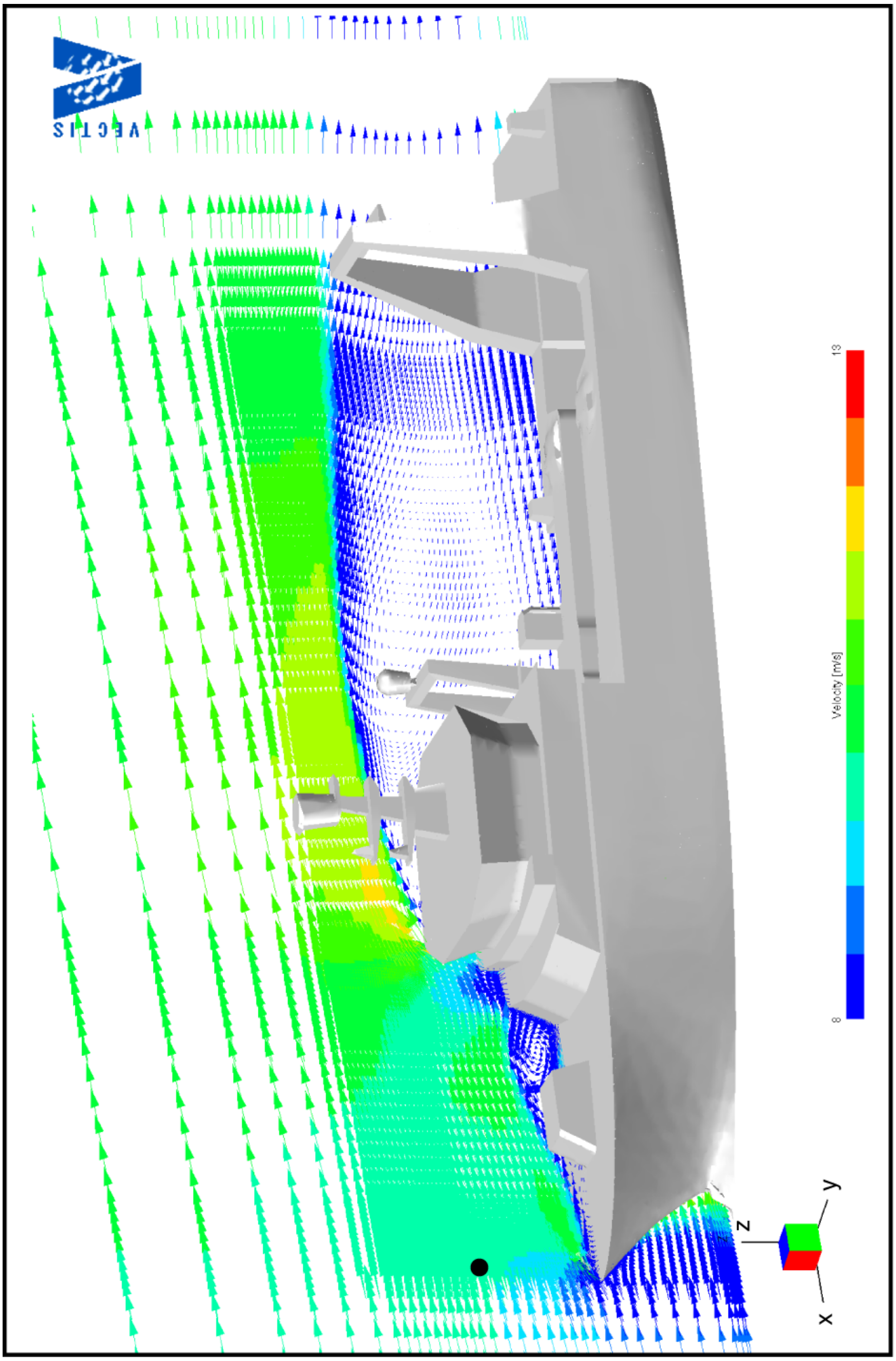

Figure A2

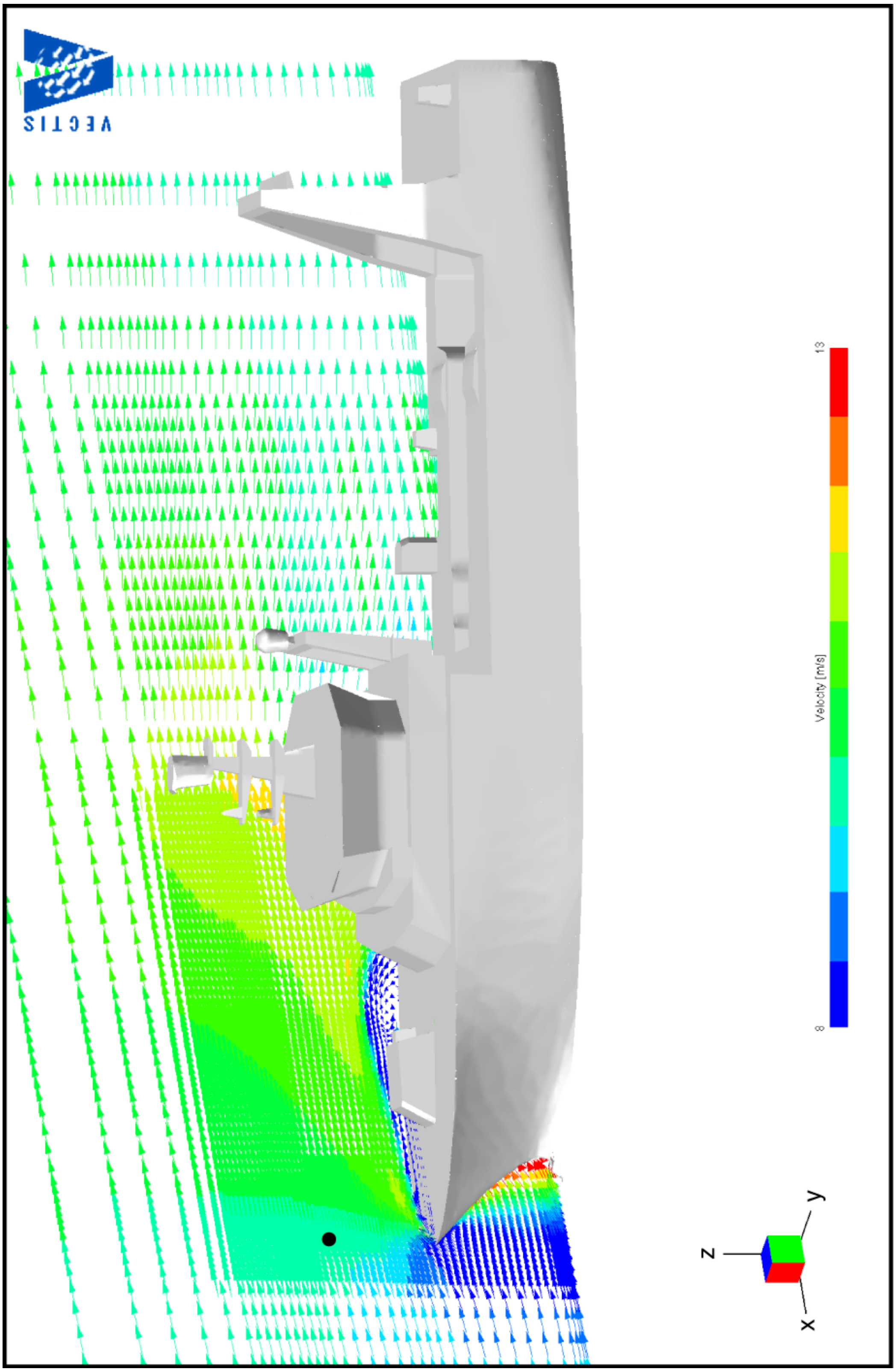

Figure A3

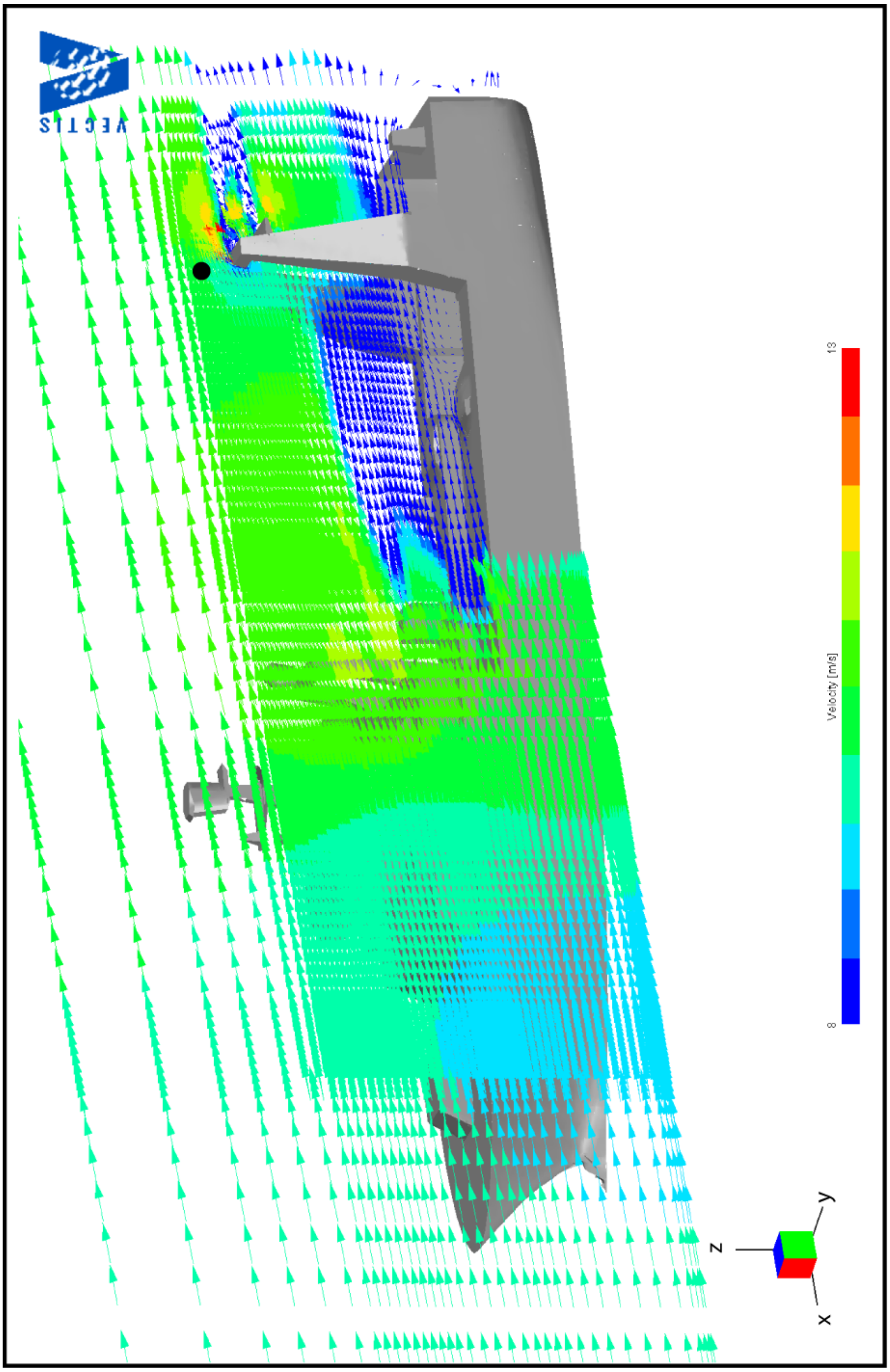

Figure A4

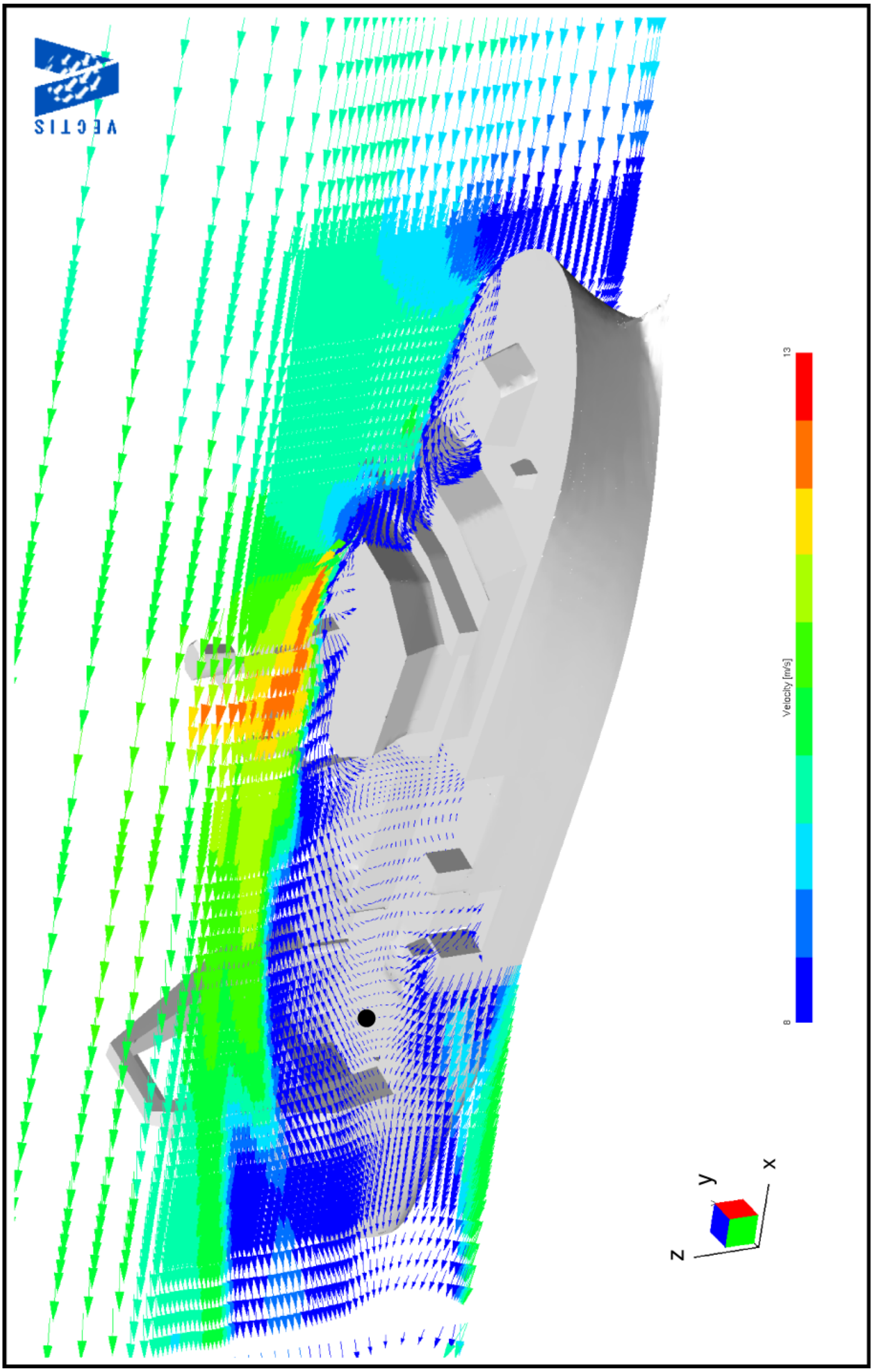

Figure A5

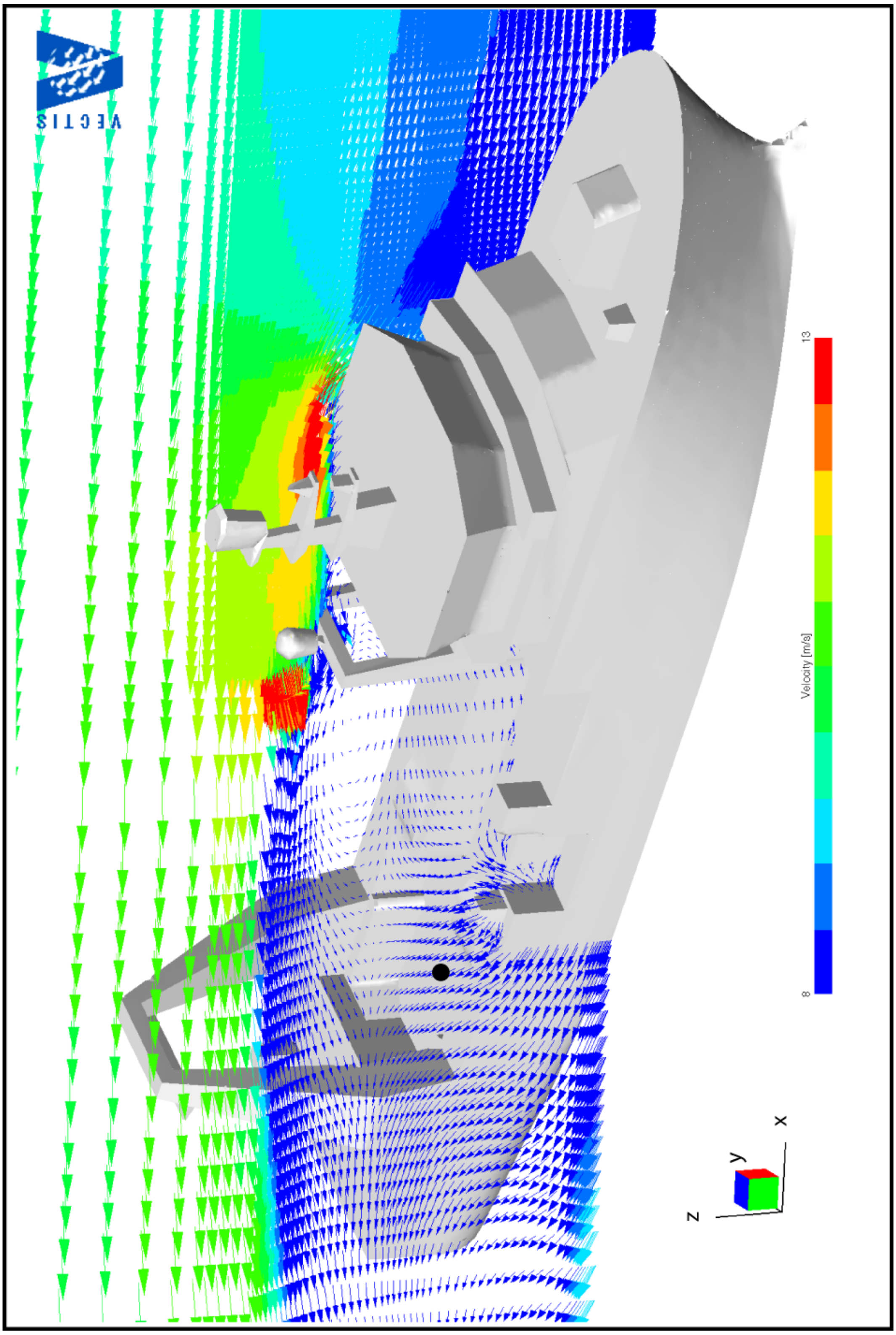

Figure A6